Gaussian Pseudopotentials with Nonlinear Core Corrections for Chemical Accuracy

Inauguraldissertation

zur
Erlangung der Würde eines Doktors der Philosophie
vorgelegt der
Philosophisch-Naturwissenschaftlichen Fakultät
der Universität Basel

von

Alexander Willand
aus Oberwil, Schweiz

Basel, 2013

Genehmigt von der Philosophisch-Naturwissenschaftlichen Fakultät

auf Antrag von

Prof. Dr. Stefan Goedecker

Prof. Dr. Jürg Hutter

Basel, den 26. Februar 2013

Prof. Dr. Jörg Schibler

Dekan

Abstract

During the last decades, density functional theory (DFT) has proven its pivotal role for computational studies in the fields of condensed matter physics and quantum chemistry. Particularly the Kohn-Sham formalism (KS) of DFT has gained enormous popularity as an *ab initio* method applicable to relatively large systems. An essential ingredient for many large scale implementations of KS-DFT are pseudopotentials which are also frequently denoted as effective core potentials. Adding a non-linear core correction (NLCC) to the well established Dual Space Gaussian type pseudopotentials, new pseudopotentials are constructed for the Perdew Burke Ernzerhof (PBE) functional. These potentials exhibit impressive features of transferability and accuracy of the results, without increasing the hardness of the pseudoatom, and they are benchmarked with respect to highly precise all-electron results of different physical and chemical quantities. The error introduced by pseudopotential approximation is sensibly lower than the one given by any small or medium size Gaussian basis sets in an all-electron calculation. Our results show that, when combined with systematic basis sets, norm-conserving pseudopotential calculations can be as accurate as all-electron calculations.

To my parents

Contents

Introduction

Pseudopotentials are a useful tool for orbital based *ab initio* methods of quantum chemistry, as they allow to exclude the core electrons from the many electron problem. Especially in the context of Kohn-Sham Density functional theory (KS-DFT), which has proven to be one of the most efficient and reliable first-principles methods, pseudopotentials are in widespread use. A well established family of pseudopotentials are dual-space Gaussian type pseudopotentials, which are in the focus of this work. The inclusion of nonlinear core corrections (NLCC) allows to systematically improve the atomization energies assessed with these pseudopotentials, which ultimately leads to chemical accuracy compared to all electron calculations for the molecules of the G2-1 test set. These and other benchmark results for a novel set of Gaussian type pseudopotentials are presented in this work, which also contains detailed notes about the construction of these pseudopotentials, and first addresses the very basic concepts needed to introduce and explain the procedure.

Therefore, the following text first aims to provide an easily accessible and perspicuous introduction into the field of pseudopotentials for KS-DFT. After an overview of the DFT methodology and the KS formalism, some practical considerations and notes about the treatment of single atoms are addressed, which are of use for the successive chapters and describe some of the work done in context of the construction of the novel pseudopotentials. Thereafter the concepts of norm conserving pseudopotentials are carefully introduced and compared with related schemes, before discussing the Gaussian type pseudopotentials in particular and the various utilities and strategies used for generating the novel NLCC-pseudopotentials. Finally, the benchmark results that confirm the high accuracy and reliability of these pseudopotentials are presented as published in the journal of chemical physics [1]. Thereafter, a short overview of future work on these pseudopotentials is followed by a brief list of applications, of which one article is presented in detail.

Chapter 1

Density functional theory - a brief outline

Density functional theory (DFT) gives the framework for a family of numerical methods to model the electronic structure of molecular systems and condensed phases from first principles of quantum chemistry. DFT based calculations have attracted much attention in the condensed matter physics community over the past decades, and they have become one of the most frequently used theoretical tools in this field.

To put DFT into context with other *ab initio* methods, one should first address the very basic formalism of computational quantum chemistry. According to the Born Oppenheimer approximation [2], the quantum mechanical description of a chemical system is formally split into an electronic and a nuclear problem. For the former, the atomic nuclei are fixed and act as an electrostatic potential that enters the electronic Schrödinger equation. In that sense, the atomic positions are just parameters of the external potential of the electronic problem. For the latter, the nuclear problem, the electronic ground state energy obtained for a given set of atomic positions acts as the potential of a Schrödinger equation that describes the quantum mechanical vibrational properties of the nuclei that are glued together by the electronic interactions.

The common starting point for most methods of electronic structure calculation is therefore the time independent many electron Schrödinger equation(1.1).

$$E\psi(x_1 \ldots x_{N_e}) = H_e\psi(x_1 \ldots x_{N_e}) \tag{1.1}$$

The Hamiltonian H_e of this many particle problem describes the interaction of N_e electrons with each other and an external potential V_{ext}, which includes the Coulomb attraction resulting from the nuclear charges.

$$H_e = \sum_{i=1}^{N_e} \left(-\frac{1}{2}\Delta_i + V_{ext}(x_i) \right) + \sum_{i<j}^{N} \frac{1}{|x_i - x_j|} \tag{1.2}$$

Here x_i denotes all degrees of freedom for the ith electron, and the Laplacian Δ_i is with respect to the electrons position. Above and all following equations are expressed in atomic units, where the electron rest mass m_e, the elementary charge e, the reduced Planck's constant $\hbar$ and the Coulomb force constant $1/(4\pi\epsilon_0)$ each take numeric values of one and are thus omitted.

For the exact quantum mechanical description of the electronic system, the ground state must be found, which diagonalizes the Hamiltonian and gives the lowest energy eigenvalue E. However, the direct solution of the Schrödinger equation of such a strongly interacting many particle system cannot be realized in practice. To deal with this problem, various assumptions and approximations can be made for the construction of both, the Hamiltonian and the wavefunctions ψ.

Another strategy for electronic structure calculations is to depart from the many particle wavefunctions and move to objects of much less complexity, that can be described in a simpler and more efficient way. DFT methods in general and the formulation of Kohn Sham theory in particular, as shortly described in the following sections, are excellent examples for the success of this approach.

1.1 Density functionals and Jacob's ladder

Density functional theory is built upon the theorems of Hohenberg and Kohn [3], which state that there exists an universal functional of the electronic density, that is minimized by the ground state density and then determines the ground states total energy. Furthermore, they demonstrate that any other ground state property may be expressed as a functional of said charge density.
In this context, we can write the total energy as an universal functional of the electronic density $E_e(\rho)$ plus some external energy terms.

$$E_{total}(\rho) = E_e(\rho) + E_{ext}(\rho) + E_{n-n} \tag{1.3}$$

This means essentially that all electron-electron interactions are rigorously described by a unique density functional, regardless of the type of electronic system studied, the external potentials or its chemical environment. In the following, the remaining terms arise from the electrostatic repulsion between N_n point charges Z_n that represent the atomic nuclei(1.5) and their attractive interaction with the electrons(1.4).

$$E_{ext}(\rho) = \sum_n^{N_n} \int \frac{\rho(\boldsymbol{r})Z_n}{|\boldsymbol{r} - R_n|} d^3\boldsymbol{r} \tag{1.4}$$

$$E_{n-n} = \sum_{n<n'}^{N_n} \frac{Z_n Z_{n'}}{|R_n - R_{n'}|} d^3\boldsymbol{r} \tag{1.5}$$

Despite intense theoretical investigations, no closed form for this universal functional has been found. In practice, the common approach is to rewrite the energy expression as the Hartree total energy plus some unknown terms that need to be approximated in some way, the exchange-correlation functionals.

$$E(\rho) = E_{kin}(\rho) + E_{ext}(\rho) + E_H(\rho) + E_{xc}(\rho) + E_{n-n} \tag{1.6}$$

Here $E_{kin}(\rho)$ stands for the kinetic energy functional and $E_H(\rho)$ reflects the classical electrostatic interaction between the electrons.

$$E_H(\rho) = \int \int \frac{1}{2} \frac{\rho(\boldsymbol{r})\rho(\boldsymbol{r'})}{|\boldsymbol{r} - \boldsymbol{r'}|} d^3\boldsymbol{r} d^3\boldsymbol{r'} \tag{1.7}$$

For the unknown exchange-correlation (XC) terms there exists an exceedingly wide variety of different approximations and parametrizations to construct a density dependence. This is exactly where the flexibility and customizability of DFT methods originates.
The numerous approximations to the XC terms are classified in different families, which are sometimes referred as the rungs of Jacob's ladder, a metaphor that was first adopted in a speech by John Perdew [4]. This emphasizes the strong wish for sophistications of the theory that ultimately lead to chemical accuracy.
The simplest and historically the most important approach is the local density approximation (LDA), the first rung of Jacob's ladder. It models the volume density of the exchange-correlation energy as a local function of the electronic density.[5]

$$E_{LDA}(\rho) = \int \epsilon_{xc}\{\rho(\boldsymbol{r})\}d^3\boldsymbol{r} \tag{1.8}$$

It should be noted that the density $\rho(\boldsymbol{r})$ is sometimes factored out when defining ϵ_{xc}, while in this work, ϵ_{xc} will always have the physical dimension of energy per volume.

Most exchange correlation functionals are formally split into separate terms for exchange and correlation, which have limited physical meaning on their own, but allow to flexibly construct functionals as arbitrary pairwise combinations.

Various parametrizations of the LDA have been proposed that have one property in common: The exchange part takes the form of the Slater or X-alpha functional(1.9).

$$\epsilon_{x-\alpha}\{\rho(\boldsymbol{r})\} = -\frac{3}{4}\left(\frac{3}{\pi}\right)^{1/3}\rho^{4/3} = -\frac{3}{4\pi r_s}\left(\frac{9\pi}{4}\right)^{1/3}\rho \tag{1.9}$$

This particular choice reproduces the analytic solution for the Fock exchange of the homogeneous electron gas, a simple, yet very useful model system for weakly interacting electrons.

The correlation term is usually some algebraic function of the Wigner-Seitz radius r_s (1.10) and also contains all dependences on the relative spin polarization, which will be readdressed in the section about spin polarized DFT.

$$r_s = \left(\frac{3}{4\pi\rho}\right)^{\frac{1}{3}} \tag{1.10}$$

In the generalized gradient approximation (GGA), the ladders second rung, local information on the gradient $\nabla\rho$ of the charge density is used for the construction of more accurate functionals. This is not in the spirit of a gradient expansion, but with the goal to refine the results of the LDA in such a way that the method remains formally very similar.

$$E_{GGA}(\rho) = \int \epsilon_{xc}\{\rho(\boldsymbol{r}), |\nabla\rho(\boldsymbol{r})|\}d^3\boldsymbol{r} \tag{1.11}$$

Furthermore, there exists a family of meta-GGA functionals that take into account second order spatial derivatives of the charge $\Delta\rho$ and possibly the kinetic energy density τ, defined by $E_{kin} = \int \tau(\boldsymbol{r})d^3\boldsymbol{r}$.

$$E_{mGGA}(\rho) = \int \epsilon_{xc}\{\rho(\boldsymbol{r}), |\nabla\rho(\boldsymbol{r})|, \Delta\rho, \tau\}d^3\boldsymbol{r} \tag{1.12}$$

Beyond this scope, hybrid functionals have been successfully constructed by including a fraction of the exact exchange energy term.(1.13)

$$E_{hybrid} = E_{GGA} + \alpha\left(E_{xx} - E_{x,GGA}\right) \tag{1.13}$$

In this notation, E_{GGA} is the linear combination of an arbitrary set of LDA and GGA functionals, and $E_{x,GGA}$ is the exchange term of E_{GGA}. The exact exchange energy is taken from the Hartree Fock energy expression and can be written in terms of single particle orbitals.(1.14)

$$E_{XX} = \sum_{i,j}\int\int\frac{1}{2}\frac{\phi_i^*(\boldsymbol{r})\phi_j^*(\boldsymbol{r})\phi_j(\boldsymbol{r}')\phi_i(\boldsymbol{r}')}{|\boldsymbol{r}-\boldsymbol{r}'|}d^3\boldsymbol{r} \tag{1.14}$$

Jacob's ladder obviously does not end here, as chemical accuracy with respect to experimental data for arbitrary systems has not been achieved yet. The ladder is sometimes drawn with potentials that depend on the (unoccupied) orbitals as the next rung, for example the DFT+U method [6], which introduces

a Hubbard-like repulsion term. At the base of the ladder one can place either Hartree Fock theory or orbital free variants of DFT, as well as the historical precursors, such as Thomas Fermi theory.

For the work presented in the following chapters, the GGA parametrization of Perdew, Burke and Ernzerhof (PBE) [7] is of particular importance, while the more complex XC families are not of further interest. The PBE functional, which is derived from physical properties and exact limits, is one of the most widely used GGA schemes. Here the exchange correlation energy takes the form of the x-alpha functional (1.9) times an enhancement factor (1.15), such that the properties of the LDA are recovered for small variations of the density.

$$E_{XC,PBE} = \int \epsilon_{x-\alpha} \ F_{xc}(r_s, \xi, s) d^3\boldsymbol{r} \qquad (1.15)$$

The enhancement factor F_{xc} incorporates the dependence on some dimensionless density gradient s (1.16) and the relative spin polarization ξ (1.17).

$$s = \frac{|\nabla\rho|}{2k_F\rho} = \frac{|\nabla\rho|}{(24\pi^2)^{1/3}} \ \rho^{-4/3} \qquad (1.16)$$

$$\xi = \frac{\rho_\uparrow - \rho_\downarrow}{\rho_\uparrow + \rho_\downarrow} = \frac{m}{\rho} \qquad (1.17)$$

1.2 An introduction to Kohn Sham theory

The Kohn-Sham (KS) formulation [8] of density functional theory (DFT) has evolved into a state of the art approach in modern electronic structure calculations. In essence, it introduces orbitals of non-interacting quasi particles as auxiliary quantities to construct the electronic charge density. One reason for this is to approximate(1.18) the functional of the kinetic energy, for which no closed form is known up to date.

$$E_{kin} = -\frac{1}{2} \sum_i \int \phi_i^*(\boldsymbol{r}) \Delta \phi_i(\boldsymbol{r}) d^3\boldsymbol{r} \qquad (1.18)$$

The kinetic energy is simply modelled as the sum over all single particle terms, that is the kinetic energy of non-interacting electrons. It can be noted that the need for corrections to this approximation is transferred to the exchange correlation potential, which was introduced in the previous section as an approximation functional to take into account all unknown energy terms.

The electronic charge density, which enters the functionals for the remaining energy terms, is obtained from the occupied single particle orbitals.(1.19)

$$\rho(\boldsymbol{r}) = \sum_{occ} \phi_i^*(\boldsymbol{r}) \phi_i(\boldsymbol{r}) \qquad (1.19)$$

As will be addressed in a following section, the above connection between the charge and the orbitals leads to a requirement of self consistency.

For closed shell systems, paired electrons of opposite spin states are considered to occupy each spatial orbital. In this approach, no further spin effects are treated. For N_e electrons this gives $N_e/2$ orbitals of occupation 2. In general, each occupied orbital may be assigned an occupation number q_i, which equals one for all orbitals in equations (1.18) and (1.19) or two for closed shell shell systems. In certain cases, it can be useful to allow fractional occupation numbers that sum up to the total number of electrons, as shown in equations (1.20) and (1.21). Fractional occupation numbers are employed in finite temperature schemes or to obtain certain symmetry constraints, as will be discussed in a later chapter.

$$\rho(\boldsymbol{r}) = \sum_i q_i \phi_i^*(\boldsymbol{r})\phi_i(\boldsymbol{r}) \tag{1.20}$$

$$E_{kin} = -\sum_i \frac{q_i}{2} \int \phi_i^*(\boldsymbol{r})\Delta\phi_i(\boldsymbol{r})d^3\boldsymbol{r} \tag{1.21}$$

To find the charge density that minimizes the energy in the Kohn-Sham scheme, the variation of the total energy with respect to the single particle orbitals must vanish. In the context of density functionals, this implies functional derivatives with respect to either the total charge $\rho(\boldsymbol{r})$ or the orbitals $\phi_i(\boldsymbol{r})$, which are related by the chain rule (1.22).

$$\frac{\delta E(\rho)}{\delta\phi_i(\boldsymbol{r})} = \frac{\delta E(\rho)}{\delta\rho}\frac{\delta\rho}{\delta\phi_i(\boldsymbol{r})} = \frac{\delta E}{\delta\rho}2q_i\phi_i(\boldsymbol{r}) \tag{1.22}$$

The functional derivative of $E(\rho)$ can be defined via its scalar product with an arbitrary normalized test function $\theta(\boldsymbol{r})$, which is related to a simple partial derivative(1.23).

$$\left\langle \theta(r) \left| \frac{\delta E}{\delta\rho(\boldsymbol{r})} \right. \right\rangle = \frac{\partial}{\partial\alpha}E(\rho + \alpha\theta)\Big|_{\alpha=0} \quad \forall \ \langle\theta \mid \theta\rangle = 1 \tag{1.23}$$

To illustrate the concept, let us denote the derivative of some arbitrary density functional $E(\rho)$ by a potential function $V(\boldsymbol{r})$ (1.24).

$$\frac{\delta E}{\delta\rho(\boldsymbol{r})} = V(\boldsymbol{r}) \tag{1.24}$$

The functional derivative can be understood as a linear approximation of the functional $E(\rho)$ in terms of the scalar product with a function (1.25).

$$E(\rho) \approx \langle V \mid \rho \rangle = \int V(\boldsymbol{r})\rho(\boldsymbol{r})d^3\boldsymbol{r} \tag{1.25}$$

This concept applies to all density functionals related to potential energy terms. For the single particle kinetic energy (1.21) the functional derivative(1.26) is straightforward to obtain.

$$\frac{\delta E_{kin}}{\delta\phi_i(\boldsymbol{r})} = -q_i\Delta\phi_i(\boldsymbol{r}) \tag{1.26}$$

The derivatives of the remaining terms with respect to the density are the external (1.27), the Hartree- (1.28) and exchange-correlation potential (1.29), respectively.

$$V_{ext}(\boldsymbol{r}) = \frac{\delta E_{ext}(\rho)}{\delta\rho(\boldsymbol{r})} = \sum_n^{N_n} \frac{Z_n}{|\boldsymbol{r} - R_n|} \tag{1.27}$$

$$V_H(\boldsymbol{r}) = \frac{\delta E_H(\rho)}{\delta\rho(\boldsymbol{r})} = \int \frac{\rho(\boldsymbol{r}')}{|\boldsymbol{r} - \boldsymbol{r}'|}d^3\boldsymbol{r}' \tag{1.28}$$

$$V_{xc}(\boldsymbol{r}) = \frac{\delta E_{xc}(\rho)}{\delta\rho(\boldsymbol{r})} \tag{1.29}$$

The analytic form of the exchange correlation potential (1.29) depends on the family and implementation of the chosen approximation scheme for the XC-functionals. It can be considered given as some real space parametrization of the density, which is evaluated on the fly while the exchange correlation energy is computed.

The integral form of the Hartree potential (1.28) is equivalent to Poisson's equation (1.30), for which highly efficient numerical methods can be exploited to obtain the potential $V_H(\boldsymbol{r})$ associated with a given charge distribution $\rho(\boldsymbol{r})$.

$$-\Delta V_H(\boldsymbol{r}) = \rho(\boldsymbol{r}) \tag{1.30}$$

We can substitute the potentials of equations (1.26), (1.28), (1.27) and (1.29) by a single particle effective potential H_{KS} (1.31) to write down the variation of the energy (1.22). The minimal DFT energy (1.6) is obtained at the stationary point where this variation is zero for all occupied orbitals, so the factor of $2q_i$ for the occupancies can be discarded (1.32).

$$H_{KS} = -\frac{1}{2}\Delta + V_{ext}(\rho) + V_H(\rho) + V_{xc}(\rho) \tag{1.31}$$

$$H_{KS}\phi_i(\boldsymbol{r}) = \boldsymbol{0} \tag{1.32}$$

This problem has to be solved under the constraint of orthogonal states, i.e. the orbitals have to form a set of orthonormal functions(1.33).

$$\langle \phi_j \mid \phi_k \rangle = \delta_{j,k} \ \forall j, k \tag{1.33}$$

A constrained minimization problem can be addressed with the method of Lagrange multipliers.(1.34).

$$\nabla f(x) - \sum_k \Lambda_k \nabla g_k(x) = 0 \tag{1.34}$$

In this simple notation, some function $f(x)$ is minimized under the set of constraints $g_k(x) = 0$. The same methodology is translated to our problem by replacing the scalar x with the set of orbitals ϕ_i and the nabla operator ∇ with the functional derivative, using two indices to count the constraints $g_{j,k}$ of orthonormality.(1.35)

$$g_{j,k} = \langle \phi_j \mid \phi_k \rangle - \delta_{j,k} \tag{1.35}$$

The double sum over the corresponding functional derivatives boils down to a weighted sum of orbitals.(1.36)

$$\sum_{j,k} \Lambda_{j,k} \frac{\delta g_{j,k}}{\delta \phi_i} = 2 \sum_j \Lambda_{i,j} \delta \phi_j \tag{1.36}$$

The Euler Lagrange equations for the set of orthogonal orbitals that minimize the energy expression is then given by a set of inhomogeneous differential equations (1.37).

$$H_{KS}\phi_i(\boldsymbol{r}) - \sum_j \Lambda_{i,j}\phi_j(\boldsymbol{r}) = \boldsymbol{0} \tag{1.37}$$

The Lagrange multipliers $\Lambda_{i,j}$ suffice the same symmetry relation as the constraints $g_{i,j}$ and can be understood as a matrix that is multiplied with the vector of orbitals ϕ in equation (1.37). Since the matrix Λ is hermitian we can choose the set of orbitals ϕ_i that diagonalize Λ, the canonical orbitals (1.38).

$$\sum_j \Lambda_{i,j}\phi_j(\boldsymbol{r}) = \epsilon_i\phi_i(\boldsymbol{r}) \tag{1.38}$$

This is possible without restriction because the Kohn Sham energy and the charge density are invariant under unitary transformations (1.39) of the set of single particle orbitals.

$$\sum_i \phi_i^* \phi_i = \sum_{i,j} (\phi_j^* U_{i,j}^\dagger)(U_{i,j}\phi_j) \quad \forall \; U^\dagger = U^{-1} \tag{1.39}$$

When expressed for the canonical orbitals, the Euler Lagrange equations (1.37) take the much simpler form of a set of single particle Schrödinger equations (1.40).

$$H_{KS}\phi_i(\boldsymbol{r}) = \epsilon_i \phi_i(\boldsymbol{r}) \tag{1.40}$$

This is the commonly used formulation of the Kohn equations (1.40) and explains the notation of the Kohn Sham Hamiltonian H_{KS}, which was introduced earlier as a single particle effective potential (1.31). In this sense, the details of the interactions between the electrons are transferred to the Kohn Sham Hamiltonian while the orbitals formally appear as independent entities. This reflects the fundamental approach of Kohn Sham methods to model the electrons as fictitious non-interacting particles that move in an effective potential, such that the density of the interacting electrons is recovered. In contrast to the theoretical foundations of DFT, the existence of such a potential for any given system of electrons is not proven, so the Kohn Sham theory relies on an assumption that is not certain. This theoretical problem is known as the non-interacting V-representability condition. As emphasized before, the potential depends on the total charge density, which is related to the orbitals by equation (1.19). This means the Kohn Sham equations must be solved self consistently, so the orbitals have to diagonalize the Kohn Sham Hamiltonian resulting from their own total charge density. Before addressing this problem in some of the next sections, let us relate the total energy expression to the eigenvalue problem of equation (1.40).

The sum of the Kohn Sham eigenvalues ϵ_i, possibly weighted by fractional occupation numbers q_i, gives the band-structure energy, which in general describes the energetics of non-interacting electrons moving in a mean field potential.

$$E_{BS} = \sum_i q_i \epsilon_i = \sum_i q_i \int \phi_i^*(\boldsymbol{r}) H_{KS}\phi_i(\boldsymbol{r})d^3\boldsymbol{r} \tag{1.41}$$

The band-structure energy can be rearranged (1.42) for comparison with the total energy expression (1.6), which takes the form of equation (1.43).

$$E_{BS} = -\sum_i \frac{q_i}{2} \int \phi_i^*(\boldsymbol{r})\Delta\phi_i(\boldsymbol{r})d^3\boldsymbol{r} + \int \left(V_{ext}(\boldsymbol{r}) + V_{xc}(\boldsymbol{r}) + V_H(\boldsymbol{r})\right)\rho(\boldsymbol{r})d^3\boldsymbol{r} \tag{1.42}$$

$$E_{KS} = E_{kin} + E_{ext}(\rho) + E_{xc}(\rho) + E_{n-n} + \frac{1}{2}\int V_H(\boldsymbol{r})\rho(\boldsymbol{r})d^3r \tag{1.43}$$

The kinetic energy term in the total energy can thus be eliminated using the Kohn Sham eigenvalues. This is in practice the preferable way to express the Kohn Sham energy.(1.44)

$$E_{KS} = \sum_i q_i \epsilon_i + E_{xc}(\rho) + E_{n-n} - \int \left(V_{xc}(\boldsymbol{r}) + \frac{1}{2}V_H(\boldsymbol{r})\right)\rho(\boldsymbol{r})d^3\boldsymbol{r} \tag{1.44}$$

1.3 Periodic systems and Bloch's Theorem

The work to be presented in the following chapters will focus on systems with free boundary conditions, in particular isolated atoms and small molecules. The basic concepts for solving the Kohn Sham equations of periodic systems are therefore addressed only very briefly.

Blochs theorem states that for a lattice potential that shows translational invariance (1.45) with respect to the direct lattice vectors R_L, the eigenstates $\phi_{i,k}$ must fulfil a boundary condition (1.46) that conserves the crystal momentum $\boldsymbol{k}$.

$$V_{ext}(\boldsymbol{r} + \boldsymbol{R}_L) = V_{ext}(\boldsymbol{r}) \quad \forall \boldsymbol{R}_L \tag{1.45}$$

$$\phi_{i,k}(\boldsymbol{r} + \boldsymbol{R}_L) = e^{\imath \boldsymbol{k} \cdot \boldsymbol{r}} \phi_{i,k}(\boldsymbol{r}) \tag{1.46}$$

The general solution for this boundary condition is equivalent to a planewave expansion of the wavefunction.

$$\phi_{i,k}(\boldsymbol{r}) = \sum_G c_{G,i}(\boldsymbol{k}) \; e^{\imath(\boldsymbol{G}+\boldsymbol{k}) \cdot \boldsymbol{r}} \tag{1.47}$$

Here $\boldsymbol{G}$ stands for the reciprocal lattice vectors, i.e. the Fourrier transform of $\boldsymbol{R}_L$, and $c_{G,i}$ are the coefficients of the planewave expansion for a given lattice vector and $\boldsymbol{k}$-point. In practice, the $\boldsymbol{k}$-points of the irreducible Brilloin zone, that is the region of irreducible symmetry in the reciprocal lattice, are sampled on a grid, and the Kohn Sham equations are solved for each sample. The resulting energy spectrum with respect to the crystal momentum $\boldsymbol{k}$ then describes the band structure of the solid state system.

Without going into the details of $\boldsymbol{k}$-point sampling and the Kohn Sham equations of crystalline systems, it can be noted that planewaves are the natural choice for a basis set to describe nearly free electrons of periodic systems, such as the conduction bands of solids. This is in contrast to the sharply localized states of single atoms, as described in the next chapter, and gives a strong motivation for the concept of pseudopotentials, which are the topic of the following chapters.

1.4 Discretization of the Kohn Sham equations

As briefly derived in a previous section, the Kohn Sham (KS) scheme of density functional theory (DFT) leads to a set of single particle Schrödinger equations that are to be solved self consistently, the Kohn Sham equations(1.48), where the charge density is constructed from fictitious single particle orbitals (1.49).

$$\left(-\frac{1}{2}\Delta + V_{ext}(\rho) + V_H(\rho) + V_{xc}(\rho) \right) \phi_i = \epsilon_i \phi_i \tag{1.48}$$

$$\rho(\boldsymbol{r}) = \sum_{occ} \phi_j^*(\boldsymbol{r})\phi_j(\boldsymbol{r}) \tag{1.49}$$

The goal is to find a set of Kohn Sham orbitals ϕ_i that give the lowest DFT energy, such that the electronic charge density $\rho(\boldsymbol{r})$ of the ground state is obtained. These orbitals are then the eigenstates of the Kohn Sham Hamiltonian, which in return depends explicitly on the charge density and thus on the occupied orbitals. This is commonly referred as the self consistency requirement of KS-DFT and will be addressed in a subsequent section. Apart from this difficulty, finding a numerical solution for the eigenstates of a given Hamiltonian imposes some general technical problems that need to be discussed first.

In order to employ numerical techniques to the Kohn Sham equations, it is inevitable to discretize the problem in some way. One possibility is to solve the partial differential equations on a real space grid, but this strategy can get highly impractical from a technical point of view. While real space integration on grids can be useful to address parts of the problem related to the evaluation of the exchange correlation and Hartree terms, it is typically not well suited to obtain the Kohn Sham orbitals. This is usually done rather by expanding the orbitals in a finite set of basis functions, in order to address the Kohn Shamn equations by means of linear algebra. The choice of the basis set is an important feature to classify the technical aspects of a DFT calculation, and indeed the computational implementation of the problem

can be strongly connected to the types of basis set it is designed to support. To illustrate the concept, an orthonormal basis set is considered, for which the overlap matrix S (1.50) equals the identity matrix per definition.

$$S_{j,k} = \langle b_j(\boldsymbol{r}) \mid b_k(\boldsymbol{r}) \rangle = \delta_{j,k} \tag{1.50}$$

Given a system of orthonormal functions $b_j(\boldsymbol{r})$, any function in the space spanned by $b_j(\boldsymbol{r})$ can be expressed with a set of coefficients $c_{i,j}$.(1.51).

$$\phi_i(\boldsymbol{r}) = \sum_j c_{i,j} b_j(\boldsymbol{r}) \; ; \; c_{i,j} = \langle b_j(\boldsymbol{r}) \mid \phi_i(\boldsymbol{r}) \rangle \tag{1.51}$$

In the same sense, the action of a linear operator A can be discretized and expressed using the matrix elements with respect to the basis set(1.52).

$$\langle b_j(\boldsymbol{r}) \mid A\phi_i(\boldsymbol{r}) \rangle = \sum_k A_{j,k} c_{i,k} \; ; \; A_{j,k} = \langle b_j(\boldsymbol{r}) \mid A b_k(\boldsymbol{r}) \rangle \tag{1.52}$$

In this context, a minimization or eigenvalue problem is expressed in the subspace of the basis functions, the free variables are simply scalars and numerical standard methods can be employed. For an orthonormal basis set, the discretization of the Kohn Sham equations (1.48) results in a ordinary eigenvalue problem, while for an arbitrary basis set, a general eigenvalue problem must be solved.(1.53).

$$\sum_k H_{j,k} c_{i,k} = \epsilon_i \sum_k S_{j,k} c_{i,k} \tag{1.53}$$

Here $H_{j,k}$ are the matrix elements of the Kohn Sham Hamiltonian (1.54) and $S_{j,k}$ stands for the elements of the overlap matrix(1.50).

$$H_{j,k} = \left\langle b_j(\boldsymbol{r}) \middle| -\frac{1}{2}\Delta + V_{ext}(\rho) + V_H(\rho) + V_{xc}(\rho) \middle| b_k(\boldsymbol{r}) \right\rangle \tag{1.54}$$

To determine the eigenvectors of equation (1.53) one may either employ standard matrix techniques using efficient libraries such as LAPACK, or one may solve the associated optimization problem, that is to minimize the Rayleigh quotient(1.55).

$$\epsilon = \frac{\boldsymbol{c}^T H \boldsymbol{c}}{\boldsymbol{c}^T S \boldsymbol{c}} \tag{1.55}$$

This equivalence of solving an eigenvalue or minimization problem will be readopted in the section about the self consistency requirement.

As already stressed, the actual choice of the basis set is a key feature for the implementation of a DFT code. For instance, a basis set of non-orthogonal functions requires considerations of the overlap matrix. Furthermore, orthogonality is a key property of most systematic and complete basis sets. These terms reflect the convergence of the total energy with respect to the size of the basis set and are explained as follows.

As mentioned earlier, the Hohenberg-Kohn Theorem states that the total energy is variational, so finding the ground state charge density implies a minimization of the DFT energy expression (1.6), which is done with respect to orthogonalized orbitals by solving the Kohn Sham equations (1.48) in a discretized form (1.53) or (1.55). According to the variational properties of DFT, the choice of the basis set leads to discretization errors. Such errors are a consequence of the fact that the true Kohn Sham orbitals cannot be represented exactly in a finite basis set, unless there is some a priori information about the solution. As a result, exploiting the variational principle in a given basis set will give the lowest energy value accessible in the orbital space spanned by that basis set, and lower DFT energy values are expected

in a systematically enlarged basis set. It is important to note that a systematic improvement is not possible in all cases and a property of the basis set. Only a systematic basis set can be enlarged in such way that the discretization errors are reduced. If the DFT ground state energy can be approximated with arbitrary precision the basis said to be complete. Furthermore, if the energy convergences quickly with respect to the number of basis functions, the term efficiency is commonly used. These are not only desirable properties of the basis set in a strict sense, but that qualities may rather depend on the entire DFT method and its particular implementation.

Apart from the variational properties just discussed, one should be aware of the fact that intrinsic approximations are made in DFT based calculations due to the choice of the exchange correlation functionals. In contrast to discretization errors resulting from systematic basis sets, there is no guarantee that the DFT energy resulting from a calculation with approximate functionals is higher than the ground state DFT energy. Since no closed form of the exchange correlation functionals is known, there is no way to tell what the exact DFT ground state density is, and the quality of different parametrizations of the exchange correlation terms can only be judged by comparison of experimentally accessible observables or results obtained with other *ab initio* methods of presumably higher reliability.

1.5 The self consistency requirement of KS-DFT

In the previous discussion, Kohn Sham theory was introduced as an efficient approach to density functional theory. The orbital scheme implies a description of the electrons as noninteracting particles moving in an effective potential. This potential in return depends explicitly on the electronic charge distribution given by the orbitals. Moreover, the problem must be solved in such a way that the total charge is the same as that of the interacting electrons. This aspect of the problem was put aside in the previous section, were the solution of the single particle equations was addressed for a given Hamiltonian. It was noted that the eigenvalue problem can be solved with either standard minimization schemes or methods of linear algebra when the orbitals are expanded in a finite basis set.

One approach to meet the requirements of self consistency is to address the optimization of the charge density and the orbitals in a hierarchical way. This is done in the standard self consistency cycle, where the charge density is refined iteratively. At each step the input charge density is considered constant while solving the eigenvalue problem for the Kohn Sham orbitals. The orbitals yield an output charge density, which is compared with the input charge to define a convergence criterion for the self consistency cycle. The input charge density is then updated, for instance by mixing it with a fraction of the output charge density. This sort of straight mixing (1.56) is the simplest kind of mixing scheme.

$$\rho_{in} = (1 - \alpha) \, \rho_{in} + \alpha \rho_{out} \qquad (1.56)$$

Here the scalar α is the mixing parameter which must be chosen sufficiently small to ensure convergence. There exists a variety of more sophisticated mixing schemes with improved convergence rates, such as Broyden's method [9] or Pulay mixing [10]. The self consistency cycle coupled with some diagonalization scheme is a very common approach for small basis sets.

Another strategy for finding a self consistent solution of the Kohn Sham equations are direct minimization schemes. As soon as the action of the Kohn Sham Hamiltonian on the orbitals is accessible, it can be used as a search direction to alter the vector of orbital coefficients, such that the DFT energy (or Rayleigh quotient) is minimized efficiently. At each step of the direct minimization, the charge density is recomputed and the Hamiltonian is adopted to the evolution of the orbitals. Furthermore, it must be ensured that the Kohn Sham orbitals remain orthonormal, for instance with standard orthogonalization schemes. Direct minimization is the method of choice when the number of basis functions is large and setting up all the matrix elements gets expensive or practically impossible. On the other hand, the minimization problem with respect to a large number of coefficients, typically many thousand of them,

can be very complicated, so it is important to have a systematic basis set, where good convergence acceleration can be achieved. If the action of the Kohn Sham Hamiltonian on the vector of orbital coefficients is available in an operator form, it can be used on the fly to optimize the orbitals without setting up any matrix elements. Furthermore, the convergence rate of a minimization scheme can be improved considerably when good preconditioners for the Hamiltonian are available.

1.6 Spin polarized DFT

Whenever the total electron count is odd-numbered, or if systems are addressed where spin polarization effects play an important role, the closed shell description of density functional is not applicable. To resolve these limitations and for the quantitative description of magnetic effects, DFT can be generalized to the spin polarized case [11], where the charge distribution is augmented by a vectorial magnetization density $m(\boldsymbol{r})$. The energy dependence on this quantity shall be transferred to the exchange correlation term, so in analogy to equation (1.6) we can define a density functional for the total energy.

$$E(\rho, m) = E_{kin} + E_{ext}(\rho) + E_H(\rho) + E_{xc}(\rho, m) + E_{n-n} \tag{1.57}$$

In the non-collinear case, the variation of the exchange-correlation energy then needs additional derivatives with respect to each component of m. This gives the exchange-correlation magnetization b_{xc}.

$$b_{xc,k}(\boldsymbol{r}) = -\frac{\delta E_{xc}(\rho, m)}{\delta m_k(\boldsymbol{r})} \tag{1.58}$$

The Kohn Sham orbitals can be expressed as spinors that construct the charge density ρ and magnetization m.

$$\phi_i = \begin{pmatrix} \phi_{i,\uparrow} \\ \phi_{i,\downarrow} \end{pmatrix} \tag{1.59}$$

$$\rho(\boldsymbol{r}) = \sum_i \phi_j^\dagger(\boldsymbol{r})\phi_i(\boldsymbol{r}) \tag{1.60}$$

$$m(\boldsymbol{r}) = \sum_i \phi_i^\dagger(\boldsymbol{r})\sigma\phi_i(\boldsymbol{r}) \tag{1.61}$$

Here σ denotes the Pauli spin matrix vector, and the Kohn Sham equations take a spinor form.

$$\left(-\frac{1}{2}\Delta + V_{ext}(\rho) + V_H(\rho) + V_{xc}(\rho) - b_{xc}\,\sigma\right)\phi_i = \epsilon_i\phi_i \tag{1.62}$$

In nature, magnetic phenomena are often collinear, which means that all magnetization vectors m are either parallel or anti-parallel. In this particular case, the spin polarized formulation of Kohn Sham DFT becomes much more intuitive. The variation of the magnetization is nonzero in only one direction, for instance along the z-axis, and the exchange-correlation magnetization no longer couples different spin states.

$$(-b_{xc}\,\sigma)\begin{pmatrix} \phi_{i,\uparrow} \\ \phi_{i,\downarrow} \end{pmatrix} = b_{xc}\begin{pmatrix} -\phi_{i,\uparrow} \\ \phi_{i,\downarrow} \end{pmatrix} \tag{1.63}$$

It is then convenient to split the electronic charge into two spin channels.

$$\rho_\uparrow(\boldsymbol{r}) = \rho(\boldsymbol{r}) + \frac{m_z(\boldsymbol{r})}{2} = \sum_i \phi_{i,\uparrow}^*(\boldsymbol{r})\phi_{i,\uparrow}(\boldsymbol{r}) \tag{1.64}$$

$$\rho_\downarrow(\boldsymbol{r}) = \rho(\boldsymbol{r}) - \frac{m_z(\boldsymbol{r})}{2} = \sum_i \phi_{i,\downarrow}^*(\boldsymbol{r})\phi_{i,\downarrow}(\boldsymbol{r}) \qquad (1.65)$$

The exchange-correlation potential is the only term in the Kohn-Sham Hamiltonian that depends on the spin state.

$$V_{xc,\uparrow}(\boldsymbol{r}) = \frac{\delta E_{xc}(\rho_\uparrow, \rho_\downarrow)}{\delta \rho_\uparrow(\boldsymbol{r})} \qquad (1.66)$$

$$V_{xc,\downarrow}(\boldsymbol{r}) = \frac{\delta E_{xc}(\rho_\uparrow, \rho_\downarrow)}{\delta \rho_\downarrow(\boldsymbol{r})} \qquad (1.67)$$

The Kohn Sham equations decouple for spin up and down orbitals.

$$\left(-\frac{1}{2}\Delta + V_{ext}(\rho) + V_H(\rho) + V_{xc,\uparrow}(\boldsymbol{r}) \right) \phi_{i,\uparrow} = \epsilon_{i,\uparrow}\phi_{i,\uparrow} \qquad (1.68)$$

$$\left(-\frac{1}{2}\Delta + V_{ext}(\rho) + V_H(\rho) + V_{xc,\downarrow}(\boldsymbol{r}) \right) \phi_{i,\downarrow} = \epsilon_{i,\downarrow}\phi_{i,\downarrow} \qquad (1.69)$$

The sum of the eigenvalues over all occupied Kohn Sham orbitals gives the band-structure energy.

$$E_{BS} = \sum_i^{N_\uparrow} \epsilon_{i,\uparrow} + \sum_i^{N_\downarrow} \epsilon_{i,\downarrow} \qquad (1.70)$$

In analogy to equation (1.44), the total energy can be expressed with the Kohn Sham eigenvalues to avoid the kinetic energy term(1.71).

$$E_{KS} = E_{BS} + E_{xc} + E_{n-n} - \int \left(V_{xc,\uparrow}\ \rho_\uparrow + V_{xc,\downarrow}\ \rho_\downarrow + \frac{1}{2}V_H\ \rho \right) d^3\boldsymbol{r} \qquad (1.71)$$

In this formulation of spin polarized Kohn Sham-DFT, there are independent orbitals for the spin up and spin down states. In this sense, the theory uses an unrestricted open shell formalism. For self consistent field (SCF) methods, for example the Hartree Fock (HF) method, it is important to distinguish between spin restricted and unrestricted calculations. In a restricted open shell scheme, where the spatial parts of the corresponding up and down spin orbitals are not allowed to differ, effects of spin contamination can be avoided. Such contamination can be considered an undesired mixing of electronic spin states that results from exploiting too much variational freedom. In the Kohn Sham scheme, however, effects of spin contamination are not observed in the same manner, as the physical quantities are the spin densities, while the orbitals are only a tool to construct these densitites from fictitious, independent particles. In this sense, and due to the approximate nature of the exchange correlation functionals spin dependence, one can argue that spin contamination plays only a minor role in KS-DFT.

1.7 Relativistic effects

In the following section, a very brief overview is given for the relativistic description of an atomic system. The results of this introduction will be needful in a later chapter about pseudopotentials that approximate such effects in a very simple and computationally efficient manner.

For an accurate description of the heavier chemical elements it becomes necessary to either take into account relativistic corrections or to depart from a non-relativistic formalism. First of all, this can be seen with a very simple estimate based on the Bohr model(1.72), comparing the electron velocity (1.73) with the relativistic relation of the electrons mass m_v and rest mass m_e (1.74).

$$r_0 = \frac{4\pi\epsilon_0\hbar^2}{Ze^2m_v} \tag{1.72}$$

$$v = \sqrt{\frac{4\pi\epsilon_0}{m_e r_0}} = \frac{Ze^2}{4\pi\epsilon_0} \tag{1.73}$$

$$m_v = \frac{m}{\sqrt{1-(v/c)^2}} \tag{1.74}$$

Going back to atomic units and inserting the relativistic mass m_v into the equation for the Bohr radius (1.72), a contraction of the radius is observed and related to the nuclear mass Z (1.75).

$$r_v = \frac{1}{Zm_v} = \frac{\sqrt{1-(Z/c)^2}}{Z} \approx r_0\sqrt{1-(Z/137)^2} \tag{1.75}$$

With this very rough estimate, an error of less than 5% is expected for up to $Z < 43$, so for light elements, these effects should be negligible. To discuss the issue in a less heuristic manner, a more complicated formalism is needed that extends the Schrödinger equation in the sense of the relativistic energy-momentum equation.(1.76)

$$E = \sqrt{p^2c^2 + m^2c^4} \approx mc^2 + \frac{p^2}{2m} + \frac{p^4}{8m^3c^2} + \dots \tag{1.76}$$

In order to obtain a combined description of both quantum mechanical and relativistic effects, a formal description with Dirac's equation is necessary. For simplicity, the time independent Dirac equation (1.77) is given below for a single electron moving in the scalar potential V_{ext}.

$$(c\alpha \cdot \boldsymbol{p} + \beta mc^2 + V_{ext})\Psi = E\Psi \tag{1.77}$$

In this notation, $\boldsymbol{p}$ is the momentum operator in three dimensional space, β is a 4×4 matrix and α a three component vector of such matrices. The wavefunction is described by a four component spinor, which can be split into a two component major Φ_A and a two component minor Φ_B.

$$\Psi = \begin{pmatrix} \Psi_1 \\ \Psi_2 \\ \Psi_3 \\ \Psi_4 \end{pmatrix} = \begin{pmatrix} \Phi_A \\ \Phi_B \end{pmatrix} \tag{1.78}$$

Expressing equation (1.77) in terns of the major and minor gives a coupled pair of equations, where the components of α are replaced with the Pauli spin matrix vector σ.

$$c\sigma \cdot \boldsymbol{p}\Phi_B + (mc^2 + V_{ext} - E)\Phi_A = 0 \tag{1.79}$$

$$c\sigma \cdot \boldsymbol{p}\Phi_A - (mc^2 - V_{ext} + E)\Phi_B = 0 \tag{1.80}$$

In the non-relativistic limit, where the energy term of the rest mass is preferably subtracted out (1.81), the minor Φ_B becomes negligible and the equations can be decoupled. This is shown by first solving equation (1.80) for the minor.

$$E' = E - mc^2 \tag{1.81}$$

$$\Phi_B = \frac{c\sigma \cdot \boldsymbol{p}\Phi_A}{E' + 2mc^2 - V_{ext}} \tag{1.82}$$

This expression (1.82) is approximated using a Taylor series (1.83) for a term (1.84) which is small in the non-relativistic limit.

$$\frac{1}{1+x} \approx 1 - x + 2x^2 \dots \tag{1.83}$$

$$x = \frac{E' - V_{ext}}{2mc^2} \approx \frac{E_{kin}}{2mc^2} \approx \left(\frac{v}{2c}\right)^2 \tag{1.84}$$

The expression for the minor Φ_B neglecting terms of order $\left(\frac{v}{c}\right)^2$ has a small amplitude compared to the major.(1.85)

$$\Phi_B \approx \frac{\sigma \cdot \boldsymbol{p}}{2mc} \Phi_A \tag{1.85}$$

Eliminating the minor by insertion into equation (1.79) gives the Pauli equation (1.86), which is the spinor equivalent of the Schrödinger equation if no external magnetic field is present.

$$\left(\frac{1}{2m}(\sigma \cdot \boldsymbol{p})(\sigma \cdot \boldsymbol{p}) + V - E'\right)\Phi_A = H_P\Phi_A = 0 \tag{1.86}$$

Keeping the terms in the order of $\left(\frac{v}{c}\right)^2$, i.e. the linear term of the Taylor expansion, the Hamiltonian of equation (1.86) gains three additional terms, which are the mass-velocity energy as already present in equation(1.76), the Darwin term and the spin-orbit coupling.

$$H = H_P - \left(\frac{p^4}{8m^3c^2}\right) + \left(\frac{\hbar^2}{8m^2c^2}\nabla \cdot \nabla V\right) - \left(\frac{\hbar}{4m^2c^2}\sigma \cdot (\boldsymbol{p} \times \nabla V)\right) \tag{1.87}$$

The operators for the mass-velocity and Darwin term do not depend on the spin state of the wavefunction, so a description with scalar orbitals is possible and the correction terms are thus classified as scalar relativistic effects. The qualitative effect of these terms is a contraction and stabilization of the s- and p-orbitals, while orbitals of larger angular momentum are expanded due to a better screening of the nuclear charge. In contrast, the spin orbit term lifts the spin degeneracy of all orbitals with a nonzero angular momentum numbers ℓ. This effect is therefore known as the spin-orbit splitting and will play an important role for relativistic effects in the chapter about pseudopotentials.

1.8 Semi-empirical dispersion corrections

One of the major limitations in density functional theory (DFT) is the description of long-range electronic correlation phenomena, which are the source of dispersion interactions or van der Waals forces. This class of intermolecular long range interactions plays a pivotal role for the structure prediction of supramolecular systems. Such interactions are not only essential for the description of biological macromolecules, such as DNA or protein complexes, but also for the packing of crystals, the study of self assembly on surfaces or the description of molecular films and aggregates.

While long range electronic interactions are formally accessible by means of many body perturbation theory, such as second order Møller Plesset perturbation theory (MP-2) or coupled cluster methods (CC), such methods are computationally demanding and in practice not applicable to large scale systems. For this reason, several methods have been proposed to incorporate approximate dispersions correction terms into DFT calculations. As a part of the work presented in a later chapter, the semiempirical dispersion corrections by Grimme [12, 13] have been applied in conjunction with novel pseudopotentials, and the reliability of this strategy has been verified for a benchmark system of various molecular complexes.

The energy in the original DFT-D scheme by Grimme [14] is given by the Kohn Sham DFT energy E_{DFT} plus a semiempirical correction term (1.88), which is simply a sum over dispersion terms over all diatomic distances $R_{i,j}$.

$$E_{DFT-D} = E_{DFT} - s_6 \sum_{i<j} C_6^{i,j} \ (R_{i,j})^{-6} \ f_{dmp}(R_{i,j}) \tag{1.88}$$

The dispersion pair coefficients $C_6^{i,j}$ depend only on the chemical species of each atom pair and are scaled with a global factor s_6. A damping function f_{dmp} ensures that the dispersion terms are avoided for short distances $R_{i,j}$ compared to the sum of the two atoms Van der Waals radii. This is essential to avoid problems with the short range interaction covered by the XC functionals. Once a set of coefficients has been derived for a given XC functional and range of atomic species, the semiempirical energy corrections and the corresponding derivatives for the forces can be added in a DFT calculation with practically no extra computational effort.

The method was extensively tested and gradually refined. In the DFT-D2 scheme [12], the dispersion pair coefficient $C_6^{i,j}$ is defined as the geometric mean (1.89) of two atom specific constants C_6^i, which are derived via the London formula for dispersion.

$$C_6^{i,j} = \sqrt{C_6^i \ C_6^j} \tag{1.89}$$

Here the C_6^i are proportional to the atomic ionization potential times the static dipole polarizability, which are both obtained from DFT calculations.

The DFT-D2 method has been further refined and sophisticated with the goal to use less empiricism and to derive most coefficients and parameters from *Ab Initio* calculations. The DFT-D3 scheme [13] makes use of more complicated form of the energy correction, which contains two body terms that extend equation (1.88) from $R_{i,j}^6$ to $R_{i,j}^8$ summands, and three body terms (1.90) that add more geometry information of the system, including interatomic angles θ.

$$E_{A,B,C} = C_6^{A,B,C} \frac{3 \ \theta_A \theta_B \theta_C - 1}{(R_{A,B} R_{B,C} R_{A,C})^3} \ ; \ C_6^{A,B,C} = \sqrt{C_6^{A,B} C_6^{B,C} C_6^{A,C}} \tag{1.90}$$

The most notable difference is that the dispersion pair coefficients $C_6^{A,B}$ are interpolated from the C_6^A via a Gaussian distance weighted average, which takes into account the environment of each atom based on a concept of fractional coordination numbers. The eighth order coefficients $C_8^{A,B}$ are derived from the $C_6^{A,B}$ using recursion relations. These sophistications lead to a higher accuracy and a broader range of applicability compared to the DFT-D2 method.

1.9 Unoccupied Kohn Sham orbitals

One of the drawbacks of density functional theory (DFT) is its failure to accurately predict band gaps of solids or HOMO-LUMO gaps of molecules, i.e. the energy differences between eigenvalues of occupied and unoccupied electronic states. This is not surprising, since the DFT formalism is designed to accurately describe electronic densities, total energies and forces, while the orbitals introduced in the Kohn Sham (KS) scheme are purely fictitious quantities. Thus the question is justified whether unoccupied KS orbitals and their eigenvalues have a physical meaning and whether they are suitable at all to describe band gaps. Because the electronic density in the KS formalism and therefore the total energy depends only on the occupied KS orbitals, the unoccupied orbitals have limited importance for the variational problem of finding the minimal DFT energy. Thus a more complicated formalism is actually needed for the accurate description of unoccupied states and band gaps, for example the DFT+U scheme [6]. Regardless of these problems, it may be desirable to visualize the lowest unoccupied KS orbitals, and estimates for band gaps

based on GGA calculations are not uncommon, as the gaps tend to be underestimated by a factor that is fairly constant for some materials.

If the KS equations are discretized in a basis set with few coefficients, for example a Gaussian basis set, the problem may be solved via diagonalization schemes, so at least some of the lowest unoccupied KS orbitals and their eigenvalues are directly accessible. However, in most systematic basis sets, for instance with planewaves, there are typically thousands of coefficients per orbital, so the KS equations are solved by means of minimization, and only the occupied KS orbitals are computed.

In that case, the only feasible way to obtain the lowest unoccupied KS orbitals is to employ a subspace diagonalization method, where the dimensionality of the eigenvalue problem is reduced greatly, and orthogonality to the previously found occupied orbitals is ensured. For this purpose, several iterative subspace schemes are available in the *BigDFT* package, including the Davidson method [15]. This method is presented in some detail here, because it was originally implemented in *BigDFT* by the author of this work. However, the following section is not of further relevance for the remaining chapters about pseudopotentials and related topics.

The basic idea of the Davidson method is to use a small set of N_virt approximate eigenvectors to span a subspace for iterative diagonalization, and to append to that subspace the corresponding residues (1.91) during each iteration.

$$g_i = H_{KS}\phi_i + \sum_j \Lambda_{i,j}\phi_j \tag{1.91}$$

Setting the residues (1.91) to zero corresponds to the Euler Lagrange equation (1.37) of the second section, where the Lagrange multipliers ensure only orthogonality to the occupied orbitals. Solving the general eigenvalue problem (1.53) associated with the overlap matrix and matrix elements of H_{KS} in the subspace spanned by the set of ϕ_i and g_i yields a unitary transform that constructs an improved guess for the eigenstates ϕ_i of the next iteration, and the procedure is repeated until the residues are converged.

In *BigDFT*, an initial guess for the N_{virt} unoccupied eigenvalues ϕ_i and eigenvalues ϵ_i of the KS Hamiltonian H_{KS} is obtained from the subspace diagonalization in a minimal atomic basis set that is also used to generate the input guess for the occupied orbitals. For any given set of virtual orbitals, the residues are then calculated (1.91) and preconditioned.

A subspace diagonalization is then done in the space spanned by the present set of approximate eigenvectors and their preconditioned gradients. In the original Davidson method the dimension of the subspace is increased in each iteration since one keeps all the previous preconditioned gradients in the subspace. To save memory the dimension of the subspace is limited in each iteration to $2\,N_{virt}$ using only the present set of approximate eigenvectors together with their preconditioned gradients. Even though the number of requested unoccupied orbitals is typically small (frequently only the lowest unoccupied molecular orbital), a larger set of vectors N_{virt} is considered in our method (in a parallel calculation at least one per processor), but only the gradients of the desired number of orbitals are taken into account for the convergence criterion for the norm of the gradients. This, together with the fact that the preconditioner in *BigDFT* is rather good, allows to achieve fast convergence rates comparable to the ones achieved in the calculation of the occupied orbitals. Some 20 iterations are typically needed.

Chapter 2

Practical considerations for atomic DFT

In contrast to the previous chapter, where some general concepts of Kohn Sham density functional theory (KS-DFT) were introduced, the following sections will focus on some particular problems that arise when implementing or modifying an atomic DFT program. DFT calculations on single atoms are of particular interest in this work for two reasons: First of all, the treatment of isolated atoms with spherical symmetry is essential for the construction of pseudopotentials, as will be discussed in the following chapter. Second, the accurate computation of the single atoms DFT energy is crucial for the evaluation of atomization energies, which will play an important role for benchmarking the pseudopotentials. Both of these aspects are directly related to the work presented in the later chapters, for which several atomic DFT codes had to be modified.

2.1   Spherical symmetry and radial Kohn Sham equations

The hydrogen atom is one of the few model systems of quantum mechanics with an analytic solution of the Schrödinger equation. More precisely, the electronic problem describes a single particle moving in a radially symmetric potential, so the eigenstates can be decomposed (2.1) into radial functions $\varphi_{n,\ell}$ and spherical harmonics $Y_{l,m}$.

$$\phi_{n,\ell,m}(\boldsymbol{r}) = \frac{1}{r}\ \varphi_{n,\ell}(r)Y_{l,m} \tag{2.1}$$

In this notation, r stands for the distance to the atomic nucleus and equals the norm of the position vector $\boldsymbol{r}$. The dependence on the angular coordinates is given by $Y_{l,m}$, for which the arguments are omitted.
The radial part $\varphi_{n,\ell}$ of the atomic orbitals is then the solution of a one-dimensional Schrödinger equation with an effective potential (2.2), and the eigenstates are characterized by the atomic quantum numbers n, ℓ and m.

$$\left(-\frac{1}{2}\frac{\partial^2}{\partial r^2} + \frac{l(l+1)}{2r^2} + V_{ext}(r)\right)\ \varphi_{n,\ell}(r) = \epsilon_n\ \varphi_{n,\ell}(r) \tag{2.2}$$

For other neutral atoms than hydrogen, there are obviously several electrons that interact with each other, but the characteristics of the atomic orbitals remain similar, i.e. the assignment of s-, p- and d- orbitals corresponding to $\ell = 0$, 1 and 2 is possible, respectively. However, the concept of a radial

mean field equation is only justified for atoms that are spherically symmetric, which corresponds to equal occupancies for each set of orbitals with equal principal and angular quantum numbers n, ℓ. This is for example the case for atoms of chemical elements with filled s or p shells, like alkaline earths or rare gases. Nevertheless, fractional occupation numbers can be used to obtain a spherically symmetric electronic configuration for any other atom. The resulting radial problem can then be addressed, for example using the Kohn Sham (KS) formalism, but one should keep in mind that the atoms ground state differs from the spherical configuration. The Kohn Sham Hamiltonian (2.3) then only contains radially symmetric terms, and the KS equations (3.11) are simplified to a purely one dimensional problem.

$$H_{KS_r} = -\frac{1}{2}\frac{\partial^2}{\partial r^2} + \frac{l(l+1)}{2r^2} + V_H(r) + V_{xc}(r) + V_{ext}(r) \tag{2.3}$$

$$H_{KS_r}\ \varphi_{n,\ell}(r) = \epsilon_{n,\ell}\ \varphi_{n,\ell}(r) \tag{2.4}$$

The Kohn Sham eigenvalues with equal n, ℓ are degenerate in $m = -\ell \ldots \ell$, so the index m of the radial part $\varphi_{n,\ell,m}$ is omitted (2.5). The occupation numbers thus take values in the range from zero to $(2\ell + 1)$.

$$\sum_{m=-\ell}^{\ell} \phi_{n,\ell,m}(\boldsymbol{r}) = \frac{1}{r}\ \varphi_{n,\ell}(r) \sum_{m=-\ell}^{l} Y_{l,m} \tag{2.5}$$

In the following two sections, some practical considerations for the implementation of the generalized gradient approximation (GGA) in an atomic density functional theory (DFT) code are briefly discussed, neglecting the aspects of spin polarization, which are addressed thereafter.

2.2 Density gradients on radial grids

In order to implement a scheme for the generalized gradient approximation (GGA), the real space gradient of the charge density is required. For the case of a spherically symmetric atom, where the radial Kohn Sham equations are solved, this simply implies a partial derivative in the radial direction (2.6).

$$\nabla\rho(r) = \frac{\partial\rho}{\partial r}\ \nabla \mid \boldsymbol{r} \mid = \frac{\partial\rho}{\partial r}\ \frac{\boldsymbol{r}}{r} \tag{2.6}$$

For any given point in space, the gradient of a radial function is parallel (or antiparallel) to the radial direction - obviously, the problem has to remain one dimensional also in the GGA.
The radial orbitals $\varphi_{n,\ell}$ and charge density ρ can be represented on a real space grid (2.7).

$$\rho(r_j) = \rho_j\ ;\ \varphi_{n,\ell}(r_j) = \varphi_{j,n,\ell} \tag{2.7}$$

Usually, this representation is chosen for the evaluation of the exchange correlation terms, while a discretization with respect to the basis set is used for other portions of the code, as will be discussed during the next section of this chapter.
For the radial grid points r_j, a simple logarithmic form is chosen (2.8).

$$r_j = r_0\ e^{\alpha\ j} - s \tag{2.8}$$

The logarithmic grid can be mapped to a uniform grid u_j to derive approximations for integrals and derivatives. For simplicity, but without any restriction, the grid spacing h is chosen to be one (2.9).

$$u_j = h\ j = j \tag{2.9}$$

On the uniform grid, integrals are then approximated by sums over u_j (2.10) and derivatives are well described by finite differences (2.11).

$$\int \rho(u)du \approx \sum_j \rho(u_j); \tag{2.10}$$

$$\frac{\partial \rho}{\partial u} \approx \sum_i \rho(u_{j+i})C_i \tag{2.11}$$

The derivatives of the mapping from r_j to u_j and vice versa thus serve as integration weights w_j (2.12) and differential factors d_j (2.13), respectively.

$$\left(\frac{\partial r}{\partial u}\right)_j = (\alpha r_0 \ e^{\alpha u} - s)_j = w_j \tag{2.12}$$

$$\left(\frac{\partial u}{\partial r}\right)_j = \left(\frac{1}{\alpha r}\right)_j = d_j \tag{2.13}$$

Volume integrals are evaluated using the precomputed weights w_j.

$$\int \rho(r)dr = \int \left(\frac{\partial r}{\partial u}\rho(u)\right) du \approx \sum_j w_j \rho_j \tag{2.14}$$

$$\int \rho(r)d^3\boldsymbol{r} \approx 4\pi \sum_j r_j^2 w_j \rho_j \tag{2.15}$$

To find the radial derivative of the charge density on each grid point, finite differences are used along with the differential factors d_j.

$$\left(\frac{\partial \rho}{\partial r}\right)_j = \left(\frac{\partial \rho}{\partial u}\frac{\partial u}{\partial r}\right)_j \approx d_j \sum_i \rho(u_{j+i})C_i \tag{2.16}$$

2.3 A Gaussian basis set for the pseudo-atom

For the atomic DFT code that solves the radial Kohn Sham (KS) equations in presence of a pseudopotential, a Gaussian basis set is employed. As will be discussed in the following chapter, the pseudopotential method results in smooth wavefunctions, such that the discretization of the KS orbitals with some twenty to thirty Gaussians (2.17) centered on the atom is perfectly accurate. In contrast, this is not feasible for the all electron problem, where for instance radial grids and interpolating splines are used to obtain highly accurate results. For the example of the pseudo-atomic code used in this work, the key parameters of the Gaussian basis set are ng and rij, the number of Gaussians and a scaling factor for the spatial resolution, respectively (2.17).

$$g_k(r) = e^{-\frac{1}{2}\left(\frac{r}{\sigma_k}\right)^2} \ ; \ \sigma_k = \lambda^k \ \frac{r_{loc}}{rij} \ ; \ k \in \{1, ng\} \tag{2.17}$$

The parameter r_{loc} will be readdressed later in detail and ensures proper scaling for different pseudo-atoms. Furthermore, the input flag *denbas*, an abbreviation for *denser basis set*, controls the recursion factor λ for the width of the Gaussians, which takes one of two predefined values (2.18).

$$\lambda = \begin{cases} 2^{3/10} \approx 1.23 & default \\ 2^{1/4} \approx 1.19 & denbas \end{cases} \tag{2.18}$$

The use of the Gaussian basis set allows to tackle a general eigenvalue problem (1.53) of conveniently low dimensionality. This has to be done iteratively to solve the KS equations self consistently. The matrix elements of the KS Hamiltonian with respect to the Gaussian basis functions and the overlap matrix(2.19) are readily evaluated, as most integrals are expressed analytically, including the kinetic energy term (2.20), the external potential and the pseudopotential terms to be introduced in the successive chapters.

$$S_{i,j} = \left\langle exp\left(-\frac{1}{2}\frac{r^2}{\sigma_i^2}\right)\middle| exp\left(-\frac{1}{2}\frac{r^2}{\sigma_j^2}\right)\right\rangle = \sqrt{\frac{2\pi\sigma_i^2\sigma_j^2}{\sigma_i^2+\sigma_j^2}} \tag{2.19}$$

$$\left\langle exp\left(-\frac{1}{2}\frac{r^2}{\sigma_i^2}\right)\middle| -\frac{\Delta}{2}\middle| exp\left(-\frac{1}{2}\frac{r^2}{\sigma_j^2}\right)\right\rangle = -\frac{\sigma_i\sigma_j\sqrt{2\pi(\sigma_i^2\sigma_j^2)}}{2(2\sigma_i^2\sigma_j^2+\sigma_i^4+\sigma_j^4)} \tag{2.20}$$

The remaining terms for those quantities to be defined later are very similar to the examples in equations (2.19) and (2.20). After each diagonalization, the electronic charge density is updated with a straight mixing scheme (1.56) and a linear transformation is then used to switch from the Gaussian representation to a real space grid. This transformation matrix, the overlap and the matrix elements of the external potentials are precomputed once and for all. The exchange correlation (XC) and Hartree potentials, however, need to be recomputed from the current charge density during each step of the self consistency loop. It is the efficient evaluation of these terms that requires a real space representation of the charge density. The matrix elements of the new potential terms are then updated and the procedure is repeated until self consistency is achieved. Thereafter the total energy and other quantities for further analysis are computed.

In the following sections, modifications to this and other atomic DFT codes are discussed with a focus on accessing the XC terms and the inclusion of collinear spin polarization. One of the codes that was modified in this regard solves the atomic problem without symmetry constraints, which leads to further difficulties addressed in the next section.

2.4 Atomic DFT beyond spherical symmetry

In the following section, the concept of a radial grid for an atom of spherical symmetry is generalized to an atomic DFT program that utilizes an angular grid and spherical harmonics. The angular component of each Kohn Sham orbital $\phi_k(\boldsymbol{r})$ is no longer treated implicitly by assignment of angular momenta l, but expanded explicitly in spherical harmonics. To evaluate the exchange correlation terms in real space, the total charge density is also represented on a real space grid with a radial index j and an angular index k. Let us consider the multipole expansion $\rho_{l,m}$ of the charge density ρ (2.21) in spherical harmonics Y_{lm} up to an angular momentum of l_{max}.

$$\rho(\boldsymbol{r}) = \sum_{l=1}^{l_{max}}\sum_{m=-l}^{l}\rho_{l,m}(r)Y_{l,m}(\boldsymbol{r}) \tag{2.21}$$

Further we assume an angular integration grid is utilized, with a logarithmic radial part r_j and some choice of normalized vectors a_k, such that integrals (2.22) are well approximated as weighted sums with radial and angular weights rw_j and aw_k, respectively.

$$\int \rho(\boldsymbol{r})d^3\boldsymbol{r} = \sum_{k,j}\rho_{l,m}(r_j\boldsymbol{a_k})\ rw_j\ aw_k \tag{2.22}$$

This gives the charge distribution on the angular grid points $r_j\boldsymbol{a_k}$ from the radial points of the multipole expansion (2.23) and vice versa (2.24).

$$\rho(r_j \boldsymbol{a_k}) = \sum_{l=1}^{l_{max}} \sum_{m=-l}^{l} \rho_{l,m}(r_j) Y_{l,m}(\boldsymbol{a_k}) = \rho_{j,k} \tag{2.23}$$

$$\rho_{l,m}(\boldsymbol{r_j}) = \sum_{k} \rho(r_j \boldsymbol{a_k}) Y_{l,m}(\boldsymbol{a_k}) a w_k = \rho_{j,\ell,m} \tag{2.24}$$

For this setup, we need to compute the gradient of the charge density $\rho(\boldsymbol{r})$ (2.25).

$$\nabla \rho = \sum_{l,m} \rho_{l,m}(r) \nabla Y_{l,m} + Y_{l,m} \nabla \rho_{l,m}(r) \tag{2.25}$$

We will need the actual values on each point of the angular grid to evaluate the exchange correlation terms in real space, inserting equation (2.25) in equation (2.23).

$$(\nabla \rho)_{j,k} = \sum_{l,m} \rho_{j,\ell,m} \nabla Y_{l,m}(r_j \boldsymbol{a_k}) + Y_{l,m}(\boldsymbol{a_k}) \nabla \rho_{l,m}(r_j \boldsymbol{a_k}) \tag{2.26}$$

Since $\rho_{l,m}$ is a radial quantity, its gradient requires the derivative in the radial direction.

$$\nabla \rho_{l,m}(r) = \frac{\partial \rho_{l,m}}{\partial r} \frac{\boldsymbol{r}}{r} \tag{2.27}$$

For each grid point, this equals the angular grid direction $\boldsymbol{a_k}$ times the differential discussed earlier (2.6).

$$(\nabla \rho_{l,m})_j = \boldsymbol{a_k} \nabla_r \rho_{j,\ell,m} \tag{2.28}$$

We may simplify the gradient of equation (2.26), inserting above equation (2.27) and the multipole expansion (2.23).

$$(\nabla \rho)_{j,k} = \boldsymbol{a_k} \nabla_r \rho_{j,k} + \sum_{l,m} \rho_{j,\ell,m} \nabla Y_{l,m}(\boldsymbol{a_k}) \tag{2.29}$$

The only remaining problem is that the gradient of the spherical harmonics $\nabla Y_{l,m}$ in each angular direction $\boldsymbol{a_k}$ needs to be precomputed. The values of the spherical harmonics on the grid points $r_j \boldsymbol{a_k}$ are evaluated using some polynomials $P_{l,m}$ in Cartesian coordinates.

$$P_{l,m}(u(\boldsymbol{r})) = Y_{l,m} \; ; \; u(\boldsymbol{r}) = \frac{\boldsymbol{r}}{|\boldsymbol{r}|} \tag{2.30}$$

$$Y_{l,m}(\boldsymbol{a_k}) = P_{l,m}(\boldsymbol{a_k}) = y_{k,\ell,m} \tag{2.31}$$

Each component of the gradient $\nabla Y_{l,m}$ then requires partial derivatives of $P_{l,m}$ in all three directions.

$$\nabla_r Y_{l,m} = (\nabla_r \otimes u) \nabla_u P_{l,m} \tag{2.32}$$

The tensor derivative of the normalized vector u is derived with the quotient rule.

$$\nabla \otimes \left(\frac{\boldsymbol{r}}{r} \right) = \frac{I r - \boldsymbol{r} \otimes \boldsymbol{r}/r}{r^2} = \frac{I - u \otimes u}{r} \tag{2.33}$$

Inserting equation (2.33) into the matrix product of equation (2.32) yields the component of the polynomials gradient $\nabla_u P_{l,m}$ that is orthogonal to the radial direction, divided by the distance to the origin r.

$$\nabla Y_{l,m} = \frac{\nabla_u P_{l,m} - u \left(u \cdot \nabla_u P_{l,m} \right)}{r} \tag{2.34}$$

21

It is thus easy to precompute a vectorial quantity $d_{k,\ell,m}$ which equals the gradient of the spherical harmonics $\nabla Y_{l,m}$ on the grid point $r_j \boldsymbol{a_k}$, scaled by r_j.

$$r_j \left(\nabla Y_{l,m}(r_j \boldsymbol{a_k}) \right) = \nabla_u P_{l,m} - \boldsymbol{a_k} \left(\boldsymbol{a_k} \cdot \nabla_u P_{l,m} \right) = d_{k,\ell,m} \tag{2.35}$$

2.5 Towards the spin polarized atom

The next problem that needs to be addressed in this context is the inclusion of collinear spin polarization into an existing program, which solves the Kohn Sham equations of a closed shell atom. This type of modification was a necessity for the results that are discussed in the following chapters, and has been incorporated by the author in three different codes. Two of these programs are restricted to spherically symmetric atoms and pseudo-atoms, respectively, while the third one allows to treat the all electron problem for an atom with arbitrary fractional occupation numbers.

As shown in the previous chapter, the transition from closed shell equations to collinear spin polarization requires to replace the electronic charge density by two spin densities, which are explicit arguments of the exchange-correlation functionals, while the other energy terms depend only on the sum of both spin densities, i. e. the electronic charge distribution. For this reason, the total charge density is usually stored as a redundant, third (sub-)array. The radial Kohn Sham equations (2.3), (3.11) are then written in the manner of equations (1.68) and (1.69) from the previous chapter, introducing the atomic quantum number s for the spin index.

$$H_{KS}(r,s) = \frac{1}{2} \frac{\partial^2}{\partial r^2} + \frac{l(l+1)}{2r^2} + V_H(r) + V_{xc}(r,s) + V_{ext}(r) \tag{2.36}$$

$$H_{KS}(r,s)\, \varphi_{n,\ell,s}(r) = \epsilon_{n,\ell,s}\, \varphi_{n,\ell,s}(r) \tag{2.37}$$

Accordingly, the set of orbitals φ, KS eigenvalues ϵ and occupation numbers q is doubled, as indicated by the index convention n, ℓ, s, where s stands for either spin up or spin down orbitals. The band energy (2.38) and total energy (2.39) for two spin densities and fractional occupation numbers are straightforward to asses.

$$E_{BS} = \sum_{i}^{N_\uparrow} q_{i,\uparrow}\epsilon_{i,\uparrow} + \sum_{i}^{N_\downarrow} q_{i,\downarrow}\epsilon_{i,\downarrow} \tag{2.38}$$

$$E_{KS} = E_{BS} + E_{xc} + E_{n-n} - \int \left(V_{xc,\uparrow}\, \rho_\uparrow + V_{xc,\downarrow}\, \rho_\downarrow + \frac{1}{2}V_H\, \rho \right) dr^3 \tag{2.39}$$

While for most segments of the code, only the sum of the two spin densities is used, special care must be taken when evaluating the exchange correlation functionals in context of the general gradient approximation (GGA). Some general considerations and a more practical view on this problem are given in the following two sections, respectively.

2.6 Evaluation of spin polarized XC functionals

In the introductory chapter about the Kohn Sham formalism of density functional theory (DFT), the exchange correlation potential V_{xc} was defined as the functional derivative of the exchange correlation energy E_{xc}. Both quantities were considered given as some parametrization of the electronic charge density $\rho(\boldsymbol{r})$. In the following section, practical considerations of the general gradient approximation (GGA) for the exchange correlation functionals are discussed briefly, which is typically defined for the

case of collinear spin polarization, as it was described in the previous section. For simplicity, let us first address the local density approximation (LDA). Here, the volume density $\epsilon(\rho)$ of the energy E_{xc} is just a parametrization of the local charge ρ. The functional derivative of E_{LDA} from equation (1.8) is equal to the partial derivative of that parametrization.

$$V_{LDA}(\boldsymbol{r}) = \frac{\delta}{\delta\rho(\boldsymbol{r})}\left(\int \epsilon_{xc}(\rho)d^3\boldsymbol{r}\right) = \frac{\partial\epsilon_{xc}(\rho)}{\partial\rho(\boldsymbol{r})} \tag{2.40}$$

This is easy to see with the definition of the functional derivative in equation (1.23).

$$\int \theta(\boldsymbol{r})V_{LDA}(\boldsymbol{r})d^3\boldsymbol{r} = \left(\frac{\partial}{\partial\alpha}\int \epsilon_{xc}(\rho + \alpha\theta)d^3x\right)|\alpha = 0 \; ; \; \forall\theta(\boldsymbol{r}) \tag{2.41}$$

The generalization to the case of collinear spin polarization is straightforward, and referred as the local spin density approximation (LSDA).

$$E_{LSDA} = \int \epsilon_{xc}(\rho_\uparrow, \rho_\downarrow)d^3r \tag{2.42}$$

Here we may consider the two spin density channels as independent variables and again construct the exchange correlation potentials as partial derivatives.

$$V_{LSDA_\uparrow}(\boldsymbol{r}) = \frac{\partial\epsilon_{xc}(\rho_\uparrow, \rho_\downarrow)}{\partial\rho_\uparrow(\boldsymbol{r})} \tag{2.43}$$

$$V_{LSDA_\downarrow}(\boldsymbol{r}) = \frac{\partial\epsilon_{xc}(\rho_\uparrow, \rho_\downarrow)}{\partial\rho_\downarrow(\boldsymbol{r})} \tag{2.44}$$

However, this is no longer true if we move to the generalized gradient approximation (GGA), where ϵ_{xc} also depends on some local information on the gradient $\nabla\rho$ of the charge density. Let us begin with a representation that depends on the vectorial density gradient, without spin polarization, and write down the integral equation (1.23) for the functional derivative V_{GGA}.

$$\int \theta(\boldsymbol{r})V_{GGA}(\boldsymbol{r})d^3\boldsymbol{r} = \left(\frac{\partial}{\partial\alpha}\int \epsilon_{xc}(\rho + \alpha\theta, \nabla\rho + \alpha\nabla\theta)d^3x\right)|\alpha = 0 \; ; \; \forall\theta(\boldsymbol{r}) \tag{2.45}$$

The partial derivative with respect to the scalar α is derived with the chain rule, treating ρ and the three components of $\nabla\rho$ as independent variables.

$$\int \theta(\boldsymbol{r})V_{GGA}(\boldsymbol{r})d^3\boldsymbol{r} = \int \left(\frac{\partial\epsilon_{xc}}{\partial\rho}\theta + \left\langle\frac{\partial\epsilon_{xc}}{\partial\nabla\rho}\middle|\nabla\theta\right\rangle\right)d^3\boldsymbol{r} \tag{2.46}$$

The second summand is rearranged using integration by parts and the requirement that the normalized test function θ does vanish at the integration boundaries.

$$\int \left(\frac{\partial\epsilon_{xc}}{\partial\nabla\rho}\cdot\nabla\theta\right)d^3r = \left\langle\mathbf{0}\middle|\frac{\partial\epsilon_{xc}}{\partial\nabla\rho}\right\rangle - \int \left\langle\theta\nabla\middle|\frac{\partial\epsilon_{xc}}{\partial\nabla\rho}\right\rangle d^3r \tag{2.47}$$

The general expression for the GGA exchange correlation potential V_{GGA} therefore includes terms with partial derivatives of ϵ_{xc} with respect to each component of the density gradient.

$$V_{GGA} = \frac{\partial\epsilon_{xc}(\rho, \nabla\rho)}{\partial\rho} - \left\langle\nabla\middle|\frac{\partial\epsilon_{xc}(\rho, \nabla\rho)}{\partial\nabla\rho}\right\rangle \tag{2.48}$$

The second summand in expression (2.48), which can be thought of as a correction term, is named after White and Bird [16], who discussed its importance and efficient computation in Fourier space. The actual evaluation of these terms when accessing the exchange correlation routines trough a standard library is described in the following section.

2.7 Accessing libXC with interfaces from ABINIT

For the actual inclusion of spin polarized exchange correlation functionals in the atomic and pseudo-atomic DFT codes, the *libXC* package [17] is utilized. The *libXC* code forms a large and portable library of subroutines that implement an extensive and still growing collection of XC functionals. Since the package is supported by more than a dozen of independently developed DFT codes, it is also considered well tested and reliable.

In order to use the same input parameters and conventions for choosing an XC functional as in the *BigDFT* code, which is available as a module to the *Abinit* package, the routines to initialize and interface *libXC* are widely taken from the *Abinit* code. When negative, the *Abinit* input variable *ixc* determines the XC functional through a six digit code, where the first three digits stand for the exchange and the last three digits stand for the correlation part. Together with *nspol*, the number of spin densities, which takes a value of either one or two, *ixc* is passed to the routines that initialize *libXC*. It is noteworthy that initialization may take place more than once, as an LDA functional is typically used for the input guess, such that the program switches to the user defined XC functional during a later stage of the calculation. When passing information of the spin density gradient to the *libXC* exchange correlation libraries, it is needful to introduce a three component vector σ, which holds the scalar products of the two spin density gradients with themselves (2.49, 2.51) and each other (2.50).

$$\sigma_1 = \langle \nabla\rho_\uparrow | \nabla\rho_\uparrow \rangle = |\nabla\rho_\uparrow|^2 \tag{2.49}$$

$$\sigma_2 = \langle \nabla\rho_\downarrow | \nabla\rho_\uparrow \rangle \tag{2.50}$$

$$\sigma_3 = \langle \nabla\rho_\downarrow | \nabla\rho_\downarrow \rangle = |\nabla\rho_\downarrow|^2 \tag{2.51}$$

Care must be taken when porting the corresponding routines, as the conventions in *Abinit* are slightly different.

For each point, the *libXC* routines return the energy density ϵ_{xc} (2.52) and its partial derivatives with respect to the spin densities (2.53) and the components of the σ vector (2.54).

$$\epsilon_{xc}(\rho_\uparrow, \rho_\downarrow, \sigma_1, \sigma_2, \sigma_3) \tag{2.52}$$

$$V_{\rho_\uparrow} = \frac{\partial\epsilon_{xc}}{\partial\rho_\uparrow} \; ; \; V_{\rho_\downarrow} = \frac{\partial\epsilon_{xc}}{\partial\rho_\downarrow} \tag{2.53}$$

$$V_{\sigma_k} = \frac{\partial\epsilon_{xc}}{\partial\sigma_k} \tag{2.54}$$

The exchange correlation potential in the sense of equation (2.48) is related to the above partial derivatives via the chain rule. First, the derivative with respect to the Cartesian components of the gradient (2.55) and (2.56) are expressed with the quantities returned by *libXC*.

$$\frac{\partial\epsilon_{xc}}{\partial\nabla\rho_\uparrow} = V_{\sigma_1} 2\nabla\rho_\uparrow + V_{\sigma_2}\nabla\rho_\downarrow \tag{2.55}$$

$$\frac{\partial\epsilon_{xc}}{\partial\nabla\rho_\downarrow} = V_{\sigma_3} 2\nabla\rho_\downarrow + V_{\sigma_2}\nabla\rho_\uparrow \tag{2.56}$$

In this form, it is straightforward to add the White-Bird correction terms as defined in equation (2.48). The two spin channels of the potential (2.57) and (2.58) are thus easily accessible.

$$V_{xc\uparrow} = V_{\rho_\uparrow} - \left\langle \nabla \left| \frac{\partial \epsilon_{xc}}{\partial \nabla \rho_\uparrow} \right. \right\rangle \tag{2.57}$$

$$V_{xc\downarrow} = V_{\rho_\downarrow} - \left\langle \nabla \left| \frac{\partial \epsilon_{xc}}{\partial \nabla \rho_\downarrow} \right. \right\rangle \tag{2.58}$$

As pointed out in an earlier section of this chapter, the treatment of an atom with spherically symmetric occupancy leads to a one dimensional problem with a radial coordinate only. For this special case, only partial derivatives with respect to the radial coordinate are needed, since the gradients point in the radial direction as well. Thus products of the radial derivatives are the only arguments needed for the exchange correlation routines as defined in equations (2.49) to (2.51) and for the White-Bird correction in equations (2.57) and (2.58).

2.8 Relativistic atomic calculations

In the previous chapter, it was mentioned that relativistic effects play an important role when heavier chemical elements are present in some atomistic simulation. In the context of an *ab initio* calculation, this implies that the underlying formalism is no longer based on the Schrödinger equation, but on its relativistic counterpart, the Dirac equation. As will be discussed in the next chapter, pseudopotentials can be constructed from relativistic atomic calculations, such that simple and efficient relativistic corrections can be included in large scale calculations. Such a pseudopotential is then applied in a non-relativistic formalism but reproduces some relativistic properties of the atoms. To obtain reference data for these properties, a relativistic formulation of KS-DFT for a single atom is of particular interest. The starting point for this is to write the Dirac equations for a radial potential in the form of equation (2.59) and (2.60), which corresponds to equations (1.79) and (1.80) of the previous chapter, expressed in atomic units and with spherical coordinates.

$$\frac{\partial P}{\partial r} + \frac{\kappa}{r} P - \left(2c^2 + E - V(r) \right) \frac{Q}{c} = 0 \tag{2.59}$$

$$\frac{\partial Q}{\partial r} - \frac{\kappa}{r} P \left(E - V(r) \right) \frac{P}{c} = 0 \tag{2.60}$$

For this notation, a new quantum number κ was introduced(2.61), which is related to the angular momentum number.

$$\kappa = \begin{cases} \ell & \text{if } j = \ell - \frac{1}{2} \\ -(\ell+1) & \text{if } j = \ell + \frac{1}{2} \end{cases} \tag{2.61}$$

The solutions of this formulation of Dirac's equation are separated into a radial part times a spin angle function.

$$\Psi(\boldsymbol{r}) = \frac{1}{r} \begin{pmatrix} P(r) Y_{j,\ell,m_j} \\ \imath Q(r) Y_{j,\ell,m_j} \end{pmatrix} \tag{2.62}$$

The scalar radial functions $P(r)$ and $Q(r)$ correspond to the major and minor of the spinor wavefunction, respectively. The spin angle functions are a generalization of the spherical harmonics to two component spinors (2.63), (2.64).

$$Y_{\ell,j,m_j} = \begin{pmatrix} \sqrt{\frac{\ell+m+1}{2\ell+1}} \, Y_{\ell,m} \\ \sqrt{\frac{\ell-m}{2\ell+1}} \, Y_{\ell,m+1} \end{pmatrix} \quad \text{where} \quad \begin{matrix} j = \ell + 1/2 \\ m_j = m + 1/2 \end{matrix} \quad \text{or } \kappa < 0 \tag{2.63}$$

$$Y_{\ell,j,m_j} = \begin{pmatrix} \sqrt{\frac{\ell-m+1}{2\ell+1}} \; Y_{\ell,m-1} \\ -\sqrt{\frac{\ell+m}{2\ell+1}} \; Y_{\ell,m+1} \end{pmatrix} \quad \text{where} \quad \begin{array}{l} j = \ell - 1/2 \\ m_j = m - 1/2 \end{array} \quad \text{or} \; \kappa > 0 \qquad (2.64)$$

These functions are sometimes referred as the spin spherical harmonics and form a set of eigenstates of the total angular momentum operator, that is the square modulus(2.65) and z-component (2.66) of $J = L + S$.

$$J^2 Y_{\ell,j,m_j} = \hbar^2 j(j+1) Y_{\ell,j,m_j} \qquad (2.65)$$

$$J_z Y_{\ell,j,m_j} = \hbar m_j Y_{\ell,j,m_j} \qquad (2.66)$$

While the Dirac equation for the central potential provides the exact description of a single electron, one can argue that the many body problem can be treated with a relativistic generalization of density functional theory, and that the corresponding formulation of the Kohn Sham equations for an atom should condense to the same kind of single particle equations. The generalization of the Hohenberg Kohn theorem using the covariant form of the electromagnetic potential and the four-current as the density is technically possible, as shown by Rajagopal and Callaway [?], but this approach has not been fruitful for practical applications so far. It is much more convenient to include some relativistic corrections into a calculation that is otherwise following a non-relativistic formalism. The radial orbital equations are therefore approximated in the limit of small energies, in analogy to equations (1.85) and (1.86).

$$Q = \frac{1}{2c} \left(\frac{\partial P}{\partial r} + \frac{\kappa}{r} \right) P \qquad (2.67)$$

Doing so by inserting the corresponding approximation for the minor (2.67) yields a radial effective Schrödinger equation for the major P.

$$\frac{1}{2} \left(\frac{\partial^2 P}{\partial r^2} + \frac{\kappa(\kappa+1)}{r} \right) + (V(r) - E)) P = 0 \qquad (2.68)$$

The connection to the non-relativistic formalism(2.68) will be interesting in the chapter about pseudopotentials, where the focus is on the description of the valence orbitals in a region where the interactions are relatively weak.

In analogy to equation (1.87) the approximation of the order $(v/c)^2$ can be derived to rewrite the scalar relativistic correction terms and the spin orbit coupling.(2.69).

$$H = H_{KS} - \left(\frac{p^4}{8m^3} \right) + \left(\frac{\Delta V}{8c^2} \right) - \left(\frac{1}{2c^2} \frac{1}{r} \frac{\partial V}{\partial r} \boldsymbol{l} \cdot \boldsymbol{s} \right) \qquad (2.69)$$

It will turn out that the last term, the spin orbit splitting, can be approximated by a pseudopotential, even though the construction of such a potential relies on the matching of the solution of the Dirac equation (2.59),(2.60) in the limit of an (effective core) Schrödinger equation (2.68). This gives access to an efficient treatment of relativistic effects for larger atomistic systems.

Chapter 3

Introduction to pseudopotential methods

The goal of the following part is to give a perspicuous and simple introduction to the field of pseudopotentials. In essence, these are empirical potentials that allow to exclude the core states from the many electron problem, which reduces the computational effort greatly. The pseudopotentials, which are called effective core potentials in the quantum chemistry community, mimic the interaction of the remaining valence electrons with both, the lower lying core electrons and the shielded atomic nucleus. Starting from the basic concepts and some historical approaches, the methodology is explained, technical aspects are addressed and pseudopotentials are briefly compared with related methods.

3.1 The concept of pseudization

The basic idea that motivates the use of pseudopotentials is that mostly the valence electrons govern the chemical and physical properties of a molecular or crystalline systems. The lower lying core electrons, however, are often in good approximation rigid and chemically inert, which is typically described as the frozen core approximation. This implies that the low energy electronic states are insensitive to the chemical environment, i.e. to neighbouring atoms, and that they closely resemble the core orbitals of an isolated atom. Such atomic orbitals are known to have a highly oscillatory shape due to the strong interaction with the atomic nucleus, which makes them highly unsuitable to expand in a finite basis set of limited spatial resolution. As a consequence, it would be convenient to exclude the core states from the many electron problem, subtracting out core-core and core-nucleus energy terms. This is done by replacing the nuclear potential by a pseudopotential that models the core-valence and valence-nucleus interactions. As a result, there are no orbitals needed for the core states, and the valence is replaced by the so called pseudovalence, which diagonalizes the pseudo-Hamiltonian, i.e. the Hamiltonian that contains the pseudopotential. Since the nucleus is electrostatically shielded by the core states implied via the pseudopotential, the attractive interaction resulting from the pseudopotential is much weaker than the bare nuclear potential with its singularity. This is one reason why the pseudovalence is expected to be much smoother and easier to resolve near the nucleus than the true valence orbitals. Another way of looking at the same effect is to conclude that the nodal structure of the valence orbitals results from orthogonality constraints to the underlying core states, and since these orbitals are no longer present, the pseudized valence can relax to form much smoother orbitals, which is energetically favorable.

The concept of pseudization is illustrated in figure 3.1. The upper two curves show the radial density distribution of a valence orbital $\phi(r)$ and its pseudovalence counterpart $\phi^{PS}(r)$, which is smoother near
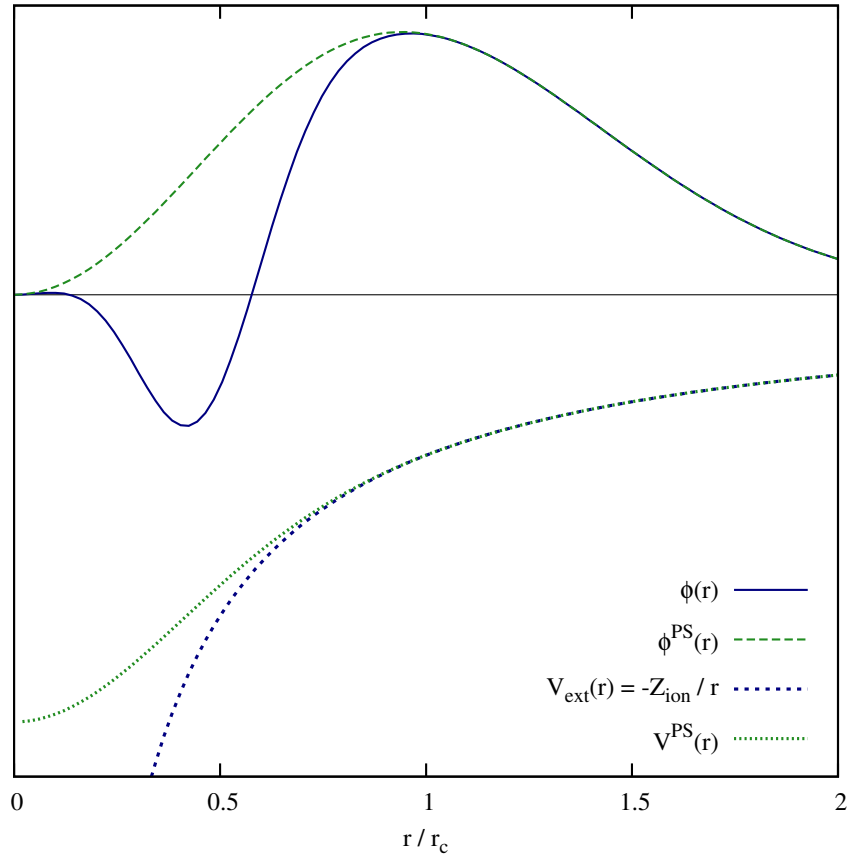
Figure 3.1: Schematic of pseudization: The central potential $V_{ext}(r)$ is replaced with a pseudopotential $V^{PS}(r)$ to obtain a smooth pseudovalence $\phi^{PS}(r)$.

the nucleus. The pseudopotential $V^{PS}(r)$ reproduces the central potential $V(r)$ outside of the core region r_c, but the singularity in the origin is smoothened out.

With the pseudopotential method, the computational effort is decreased significantly, not only since the number of orbitals is lowered, but mainly because smaller basis sets can be employed. It can be noted that pseudopotential methods have played a crucial role for the development of planewave methods in Kohn Sham density functional theory, which have been the historically dominant approach of DFT.

3.2 Phillips Kleinman construction

The historical origins of the pseudopotential method are closely related to the orthogonalized planewave method (OPW). In this early approach, the electronic core states are projected out from a planewave basis set, which is then used to discretize the valence orbitals. Nowadays, a scheme for constructing a pseudopotential in this framework is of little relevance, but it gives some simple, yet clear insights into the nature of pseudopotentials.

Let us consider a homo-atomic molecular system, where the orbitals are formally separated into valence states that form bands, labelled by index v, and core states that are chemically inert and assigned to single atoms. Thus there are composite indices c and a for core energy levels and atoms labels, respectively. A set of pseudovalence orbitals may be constructed from the solution of the all electron problem. The intention is to make the pseudovalence smoother than the valence, and this is accomplished by adding a linear combination of core orbitals.

$$| \phi_v^{PS} \rangle = | \phi_v \rangle + \sum_{a,c} C_{v,a,c} | \phi_{a,c} \rangle \tag{3.1}$$

$$\langle \phi_v^{PS} | \phi_{a,c} \rangle = C_{v,a,c} \tag{3.2}$$

Applying the all electron Hamiltonian H yields the valence and core eigenvalues ϵ_v and ϵ_c. We may require that the former are accurately reproduced by the pseudovalence, and that the latter are the same for equivalent core states c on all atoms a.

$$H | \phi_v^{PS} \rangle = \epsilon_v | \phi_v \rangle + \sum_{a,c} C_{v,a,c} \, \epsilon_c | \phi_{a,c} \rangle \tag{3.3}$$

Inserting equation (3.1) into equation (3.3) eliminates the all electron valence orbitals.

$$H | \phi_v^{PS} \rangle = \epsilon_v | \phi_v^{PS} \rangle + \sum_{a,c} C_{v,a,c} \{ \epsilon_c - \epsilon_v \} | \phi_{a,c} \rangle \tag{3.4}$$

Equation (3.4) takes the form of a Schrödinger equation for the pseudovalence, where the Hamiltonian has an additional potential term V_{PK}.

$$\{ H + V_{PK} \} | \phi_v^{PS} \rangle = \epsilon_v | \phi_v^{PS} \rangle \tag{3.5}$$

This potential consists of projectors to atomic core states, weighted by energy differences of the eigenvalues.

$$V_{PK} = \sum_{a,c} \{ \epsilon_v - \epsilon_c \} | \phi_{a,c} \rangle \langle \phi_{a,c} | \tag{3.6}$$

Equation (3.6) gives the Philips Kleinman scheme of pseudopotential construction [18], and as previously noted, its relevance is of a historical nature and related to the OPW method. However, there are some points which are common with most other schemes of pseudopotential construction. First of all, it is a very common approach to generate the pseudopotential based on an all electron calculation of a single atom. The pseudovalence of the isolated atom is typically required to match the all electron valence in some sense, while it should be as smooth as possible close to the nucleus. This typically leads to a formal description of the pseudopotential with projectors related to atomic quantum numbers. It should be noted that outside of a core region, where the core orbitals have exponentially decayed, the Philips Kleinmain potential (3.6) vanishes, so there the all electron valence is indeed matched. Near the nucleus, however, there are repulsive terms due to the projectors, so the attractive interaction resulting from the pseudopotential will be much weaker than that of the bare nucleus. This screening of the nuclear potentials singularity is another important requirement to obtain a smooth pseudovalence.

3.3 Norm Conserving pseudopotentials

In general, the use of a pseudopotential should result in smooth pseudovalence orbitals which reproduce the chemistry of the valence as reliably as possible, also when we move to different electronic configurations

and environments. These desired key properties of a pseudopotential are commonly referred as softness, accuracy and transferability. The softer the pseudopotential is, the smoother the resulting pseudovalence will get. Consequently, a smaller basis set can be employed to expand the orbitals, which results in a fast and efficient calculation. The accuracy and transferability of a pseudopotential can be assessed by its ability to reproduce quantities from all electron calculations over a wide range of different chemical compounds or other test systems. During the process of generating a pseudopotential based on atomic reference data, there is no guarantee to meet these requirements, but there are strategies that tend to improve the conflicting properties of softness and transferability.

A general concept that has contributed greatly to the sophistication of the pseudopotential method in this context is the construction of norm conserving pseudopotentials. Beyond a chosen core region of radius r_c the pseudovalence ϕ^{PS} is required to rapidly converge to or match exactly the all electron valence ϕ (3.7).

$$\phi^{PS}(r) = \phi(r) \quad \forall r \geq r_c \tag{3.7}$$

Within the core radius, the pseudovalence ϕ^{PS} is allowed to be as smooth as possible to eliminating nodes and wiggles, but the charge integral over the core region must be equal to that of the true valence (3.8).

$$\int_0^{r_c} r^2 \phi^{PS*}(r)\phi^{PS}(r)dr = \int_0^{r_c} r^2 \phi^*(r)\phi(r)dr \tag{3.8}$$

Almost redundantly, the eigenvalues of the valence orbitals have to be reproduced by the pseudovalence: If the eigenvalues are matched precisely with a norm conserving(3.8) pseudopotential, the deviation to the valence beyond the core region is expected to be very small and vice versa. If all of these requirements are met, the pseudopotential is of the norm conserving type.

As a result of the norm conservation (3.8) and matching criterion (3.7), the logarithmic derivative evaluated at the core radius r_c must be the same for the valence and the pseudovalence orbitals with equal eigenvalues (3.9).

$$\frac{\partial ln\left(\phi(r)\right)}{\partial r}\bigg|_{r=r_c} = \frac{1}{\phi(r_c)}\frac{\partial \phi}{\partial r}(r_c) = \frac{1}{\phi^{PS}(r_c)}\frac{\partial \phi^{PS}}{\partial r}(r_c) \tag{3.9}$$

This property is essential for the pseudovalence to reproduce the scattering properties of the true valence, e.g. the phase shift felt by plane waves scattered at the core region of the atomic site.

Furthermore, the energy range for which the logarithmic derivative matches is an important measure for the transferability of the pseudopotential. The energy derivative of said logarithmic derivatives can be related to the charge integral over the core region (3.10).

$$-\frac{\partial}{\partial E}\frac{\partial}{\partial r}ln(\phi(r_c,E)) = \frac{1}{r_c^2\phi^*(r_c,E)\phi(r_c,E)}\int_0^{r_c} r^2\phi^*(r,E)\phi(r,E)dr \tag{3.10}$$

As a result of the relationship in equation (3.10) and the norm conservation requirement (3.8), the errors in the logarithmic derivative over a range of different energy eigenvalues are second order in the deviation from the reference energy. This is a strong indication that norm conserving pseudopotentials have intrinsically good transferability properties. In the following section, a general procedure will be described for generating a norm conserving pseudopotential based on an all electron calculation of a spherically symmetric atom.

To close this section, a simple derivation of equation (3.10) is shown for real valued orbitals in the one dimensional case. For this purpose, the logarithmic derivative of the orbital (3.9) can be substituted (3.11) to obtain a partial differential equation (3.12) that is equivalent to the radial Schrödinger equation (3.13).

$$x(E, r) = \frac{\partial ln\,(\phi(r))}{\partial r} \tag{3.11}$$

$$\frac{\partial x(E, r)}{\partial r} + x^2(E, r) = 2\Big(V_{eff}(r) - E\Big) \tag{3.12}$$

$$\frac{\partial^2 \phi(r)}{\partial r^2} = 2\Big(V_{eff}(r) - E\Big)\phi(r) \tag{3.13}$$

Here the dependence of the logarithmic derivative $x(E, r)$ on the eigenvalue E indicates that the orbital ϕ matches for that eigenvalue. The energy derivative of equation (3.12) is then derived with the chain rule (3.14).

$$\frac{\partial^2 x(E, r)}{\partial r \partial E} + 2x(E, r)\frac{\partial x(E, r)}{\partial E} = -2 \tag{3.14}$$

For any function $f(r)$ the relation (3.16) holds true due to the product rule (3.15).

$$\frac{\partial(\phi^2 f)}{\partial r} = \phi^2(r)\left(\frac{2f(r)}{\phi(r)}\frac{\partial \phi}{\partial r} + \frac{\partial f}{\partial r}\right) \tag{3.15}$$

$$\frac{\partial f}{\partial r} + 2x(E, r)f(r) = \frac{1}{\phi^2(r)}\frac{\partial}{\partial r}\left(\phi^2(r)f(r)\right) \tag{3.16}$$

Substituting equation (3.16) into equation (3.14) gives a term (3.17) that can be integrated over the radial coordinate to obtain the relation to be shown (3.18).

$$\frac{1}{\phi^2(r)}\frac{\partial}{\partial r}\left(\phi^2(r)\frac{\partial x(E, r)}{\partial E}\right) = -2 \tag{3.17}$$

$$-\phi^2(r_c)\frac{\partial x(E, r)}{\partial E}(r_c) = 2\int_0^{r_c} \phi^2(r)dr \tag{3.18}$$

Integration over the spherical core region instead ($d^3\boldsymbol{r} = 4\pi r^2 dr$) leads to equation (3.10).

3.4 Bachelet Haman Schlüter construction

The scheme proposed by Bachelet, Haman and Schlüter[19] for the construction of norm conserving pseudopotentials has lead to some major advances of the pseudopotential method, as it provides a systematic, standardized and clear recipe to generate reliable pseudopotentials, a process that was previously often entangled with the actual method to employ the potential.

First a spherically symmetric atomic reference configuration is chosen and the radial all electron problem is solved with an atomic DFT calculation. Then core radii are assigned, one for each angular momentum quantum number ℓ of the valence orbitals. These will directly affect the pseudopotentials softness and should be chosen between the valences outermost node and extremum. This is because a trial potential is constructed from the nuclear potential in such a way that the singularity is continuously cut away within that given core radius. Furthermore, the trial potential should be designed to yield a lowest eigenvalue that matches the corresponding valence state. One way to accomplish these two properties is shown in equation (3.19), where a cutting function that rapidly decays from one to zero beyond the core radius is used to remove the singularity and to adjust the depth of the potential well accordingly.

$$V_t = -\frac{Z_{ion}}{r}\left(1 - f(r/r_{c,\ell})\right) + V_{0,\ell}f(r/r_{c,\ell}) \tag{3.19}$$

In this notation, Z_{ion} is the ionic charge, that is the nuclear charge minus the total charge of the core electrons, f stands for the cutting function, $r_{c,\ell}$ is a core radius and $V_{0,\ell}$ is the depth of the trial potential. The norm conservation property is then imposed on the eigenorbitals of the Hamiltonian that includes the trial potential. This is done by adding a correction function that rapidly decays beyond the core radius, in order to obtain the desired pseudovalence. Using numerical inversion of the radial Schrödinger equation (3.20), the screened pseudopotential (3.21) is obtained which gives the desired pseudovalence orbitals.

$$\left(-\frac{\partial^2}{\partial r^2} + \frac{l(l+1)}{2r^2} + V_\ell(r) \right) \phi_\ell = \epsilon_\ell \phi_\ell \tag{3.20}$$

$$V_\ell(r) = \epsilon_\ell - \frac{l(l+1)}{2r^2} + \frac{1}{2\phi_\ell} \frac{\partial^2 \phi_\ell}{\partial r^2} \tag{3.21}$$

Finally, this potential must be unscreened, that is the Hartree and exchange correlation energy terms resulting from the pseudovalence charge density are to be subtracted out.

$$V_\ell^{PS}(r) = V_\ell(r) - \int \frac{\rho_v(\boldsymbol{r'})}{\mid r - r' \mid} d\boldsymbol{r'} - V_{xc}(\rho_v(r)) \tag{3.22}$$

In summary, the BHS constructions consists of the following steps:

- Solve the radial all electron problem to obtain the eigenvalues and charge integrals.
- Construct a trial potential for the chosen core radii and given valence eigenvalues.
- Impose norm conservation on the pseudovalence orbitals to match the charge integrals.
- Invert the radial Schrödinger equation to obtain the screened potential.
- Subtract the Hartree and XC terms of the pseudovalence charge to unscreen the potential.

As stated previously, the BHS construction and related schemes result in pseudopotentials which depend explicitly on the angular momentum channels ℓ. While the implication is straightforward in the case of a spherically symmetric atomic calculation as used for the construction scheme, it implies in the general case the use of an angular momentum projection operator.(3.23)

$$\hat{P}_\ell \phi(r) = \sum_{m=-\ell}^{\ell} Y_{\ell,m}(r) \int Y_{\ell,m}^*(r') \phi(r') dr = \sum_{m=-\ell}^{\ell} \mid Y_{\ell,m} \rangle \langle Y_{\ell,m} \mid \phi \rangle \tag{3.23}$$

$$V_{PP} \phi(r) = \sum_\ell V_\ell^{PS}(r) \hat{P}_\ell \phi(r) \tag{3.24}$$

In this sense, we are back to the projector formalism introduced in section about the PK-construction.

3.5 Kleinman Bylander separation

In the previous sections, it was shown that norm conserving pseudopotentials do explicitly impose some dependence on the angular momentum number. Using the angular momentum projection operator $\hat{P}_\ell$, the potential may be written as a sum over different angular momentum channels $\hat{V}_\ell$, which is commonly referred as a nonlocal form.(3.25)

$$V_{PP}(\boldsymbol{r}) = \sum_\ell \hat{V}_\ell(\boldsymbol{r}) \hat{P}_\ell \tag{3.25}$$

If the local part common among and independent of the channels $\hat{V}_\ell$ is subtracted out, the pseudopotential takes a semilocal form, that is local in the radial, but nonlocal in the angular coordinates. Since the higher order summands are dominantly local, this is needful to truncate the angular momentum projector expansion at some small value ℓ_{max}.

$$V_\ell(\boldsymbol{r}) = \hat{V}_\ell(\boldsymbol{r}) - V_{loc}(\boldsymbol{r}) \ \forall \ell \tag{3.26}$$

$$V_{SL}(\boldsymbol{r}) = \sum_{\ell=0}^{\ell_{max}} V_\ell(\boldsymbol{r})\hat{P}_\ell \tag{3.27}$$

$$V_{PP}(\boldsymbol{r}) = V_{loc} + V_{SL} \tag{3.28}$$

In other words, for distances far from the core region, all ℓ-components must converge rapidly to the unscreened potential, so it is convenient to subtract out some local part and keep the dependency on the ℓ-channels only for the short ranged difference function.

The semilocal representation of a pseudopotential is rather impractical, because the effort to compute and store the matrix elements per ℓ channel still scales quadratically with the number of basis functions. Writing down the matrix elements of the semilocal part in bra-ket notation (3.29), we see that the radial function V_ℓ brakes the symmetry in the sense that we cannot separate the left hand from the right hand side.

$$\langle b_i \mid V_{SL} \mid b_j \rangle = \sum_{\ell,m} \langle b_i \mid \left(\mid \hat{P}_{\ell,m} \rangle V_\ell \langle \hat{P}_{\ell,m} \mid \right) \mid b_j \rangle \tag{3.29}$$

The equivalent expression using volume integrals gives a different term for each pair of basis functions $b_i(\boldsymbol{r})$ and $b_j(\boldsymbol{r'})$.

$$\int b_i(\boldsymbol{r})V_{SL}b_j(\boldsymbol{r'})d\boldsymbol{r}d\boldsymbol{r'} = \sum_{\ell,m} \int b_i(\boldsymbol{r})Y_{\ell,m}(\hat{\boldsymbol{r}})V_\ell(r)\delta(\boldsymbol{r},\boldsymbol{r'})Y_{\ell,m}(\hat{\boldsymbol{r}'})b_j(\boldsymbol{r'})d\boldsymbol{r}d\boldsymbol{r'} \tag{3.30}$$

It would be convenient to factorize the problem into a separable form, such that the left hand term and right hand term in the bra-ket notation can be precomputed separately, which results in a linear scaling with respect to the basis set size.

$$\langle b_i \mid V_{sep} \mid b_j \rangle = \sum_{\ell,m} \langle b_i \mid \hat{P}_{\ell,m}V_\ell \rangle \langle V_\ell \hat{P}_{\ell,m} \mid b_j \rangle \tag{3.31}$$

In other words, the corresponding integral terms are then factored into products of lower dimensional integrals.

$$\int b_i(\boldsymbol{r})V_{sep}b_j(\boldsymbol{r'})d\boldsymbol{r}d\boldsymbol{r'} = \sum_{\ell,m} \int b_i(\boldsymbol{r})Y_{\ell,m}(\hat{\boldsymbol{r}})V_\ell(r)d\boldsymbol{r} \int Y_{\ell,m}(\hat{\boldsymbol{r}'})V_\ell(r')b_j(\boldsymbol{r'})d\boldsymbol{r'} \tag{3.32}$$

Kleinman and Bylander were the first to propose such a separable form for the nonlocal part of a pseudopotential [20]. The starting point for this is to add an arbitrary, local potential $V_K(\boldsymbol{r})$ to the local part and to subtract the same potential from the semilocal part.

$$V_{PP} = (V_{loc} + V_K) + \sum_{\ell=1}^{\ell_{max}} (V_\ell - V_K)\hat{P}_\ell = V'_{loc} + V'_{SL} \tag{3.33}$$

$$V'_{SL} = \sum_{\ell=1}^{\ell_{max}} (\delta V_\ell)\hat{P}_\ell \tag{3.34}$$

The goal is to replace the new semilocal part V'_{SL} with some separable form. This is done with projectors on the atomic eigenstates $\Phi_{n,l,m}$ associated with the pseudopotential.

$$V_{sep} = \sum_{n,\ell,m} \frac{|\delta V_\ell \, \Phi_{n,\ell,m}\rangle\langle\Phi_{n,\ell,m} \, \delta V_\ell|}{\langle\Phi_{n,\ell,m}|\delta V_\ell|\Phi_{n,\ell,m}\rangle} \tag{3.35}$$

As a consequence of this choice, the action of the separable part V_{sep} and the semilocal form δV_ℓ on the atomic reference states $\Phi_{n,\ell,m}$ are the same, as the orbitals form an orthonormal set.

$$V_{sep}|\Phi_{n,l,m}\rangle = \delta V_l|\Phi_{n,l,m}\rangle \tag{3.36}$$

If the pseudopotential was constructed by inversion of the Schrödinger equation, these orbitals are the radial pseudovalence functions $\phi_{n,l}$ used to obtain each nonlocal term V_l, including the angular dependence in form of spherical harmonics $Y_{l,m}$.

$$\Phi_{n,\ell,m}(\boldsymbol{r}) = \frac{1}{r} \, \varphi_{n,\ell}(r)Y_{\ell,m}(\boldsymbol{r}) \tag{3.37}$$

Noting that the projectors of the semilocal part (3.34) can be expressed with spherical harmonics as well, it is readily shown that the separable form is indeed equivalent for the description of the reference states.

$$V'_{SL} = \sum_{\ell,m} |Y_{\ell,m}\rangle\delta V_\ell\langle Y_{\ell,m} | \tag{3.38}$$

$$V'_{SL}|\Phi_{n,\ell,m}\rangle = |Y_{\ell,m}\rangle\delta V_\ell\phi_{\ell,m} = \delta V_\ell|\Phi_{n,\ell,m}\rangle \tag{3.39}$$

Thus the pseudopotential takes a numerically efficient separable form, while the usual requirements for generating a norm conserving pseudopotential persist, as the action of the pseudopotential in the atomic reference configuration remains the very same. Of course, the separable and semilocal forms are no longer equivalent when the pseudopotential is employed in a calculation where the pseudovalence is subject to different chemical environments. As a result, the Kleinman Bailander form can lead to problems in certain cases, such as the emergence of ghost states. These are somewhat unphysical eigenstates with an undesired number of nodes and no clear all electron valence counterpart.

3.6 Limitations of the pseudopotential method

So far, some basic concepts and formal aspects of the pseudopotential method have been introduced briefly. In the following sections, some important limitations of the method will be addressed, as well as the common strategies to adapt the pseudopotentials in such a way that these issues can be resolved.

The pseudopotential method basically relies on two assumptions, the frozen core approximation and a decoupling of the core and valence charges in the exchange correlation terms. As stated in the introductory section of this chapter, the former assumption implies that the low lying electronic states are rigid. The second statement is a consequence of the fact that the pseudopotential method linearizes all electronic core-valence interactions, as they are transferred to an effective core potential. The exchange correlation functionals, however, are nonlinear per definition, so there may exist cases where this leads to fundamental problems. In other words, if there are pronounced exchange correlation terms for interactions between the core and the valence electrons, it is problematic to linearize and subtract out these terms, so special care must be taken. One prominent example for difficult systems in this regard are those containing chemical elements with semicore states, as explained in the next section.

Another important class of systems where nonlinear effects play an important role are spin polarized molecules or atoms. In the presence of magnetic moments, a spin polarized DFT formulation is needed.
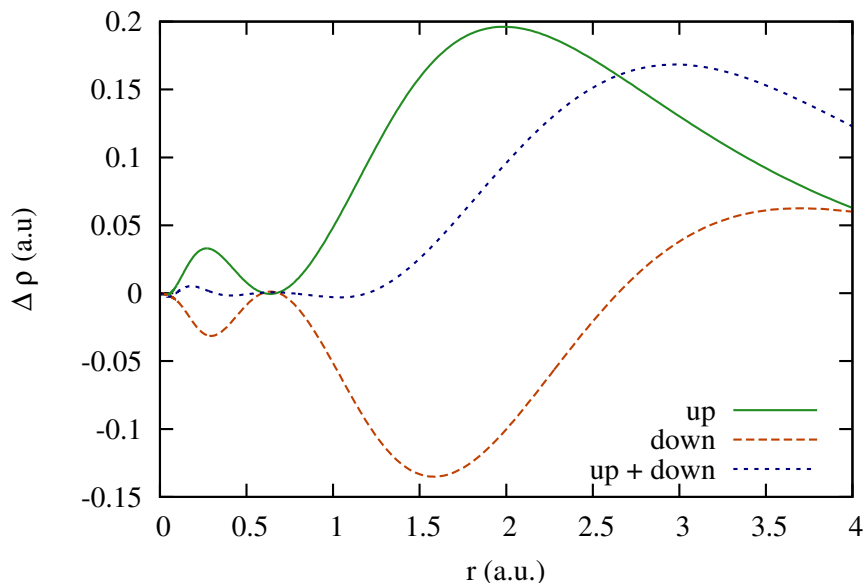
Figure 3.2: Inert core region: When half an electron is added to a phosphorus atom ($[Ne]3s^23p^{3.5}$), the valence charge distribution hardly changes within a certain core region. In contrast, changes in the individual spin densities of the valence are observed much closer to the ionic center.

The problems due to the linearization of the core valence interactions are then much more pronounced even for light elements. This is due to the fact that the nonlinearities in the XC terms are enhanced when the functionals are generalized to include a dependence on the relative spin polarization (3.40).

$$\xi = \frac{\rho_\uparrow - \rho_\downarrow}{\rho_\uparrow + \rho_\downarrow} = \frac{m}{\rho} \tag{3.40}$$

It turns out that in common implementations of the general gradient approximation (GGA), the dependence on the total charge is usually much less complicated than the correction terms that take into account the spin effects. As a result, relatively small coupling effects between core and valence spin densities can lead to strong nonlinearities and thus to rather large errors in pseudopotential based calculation.

Another explanation for difficulties arising from spin polarized calculations with pseudopotentials is the assignment of an actual core radius r_c in the sense of equations (3.7) or (3.19), which implies a region near the nucleus where the charge distribution is rigid. For example, one can compare different electronic configurations of an atom and plot the change of the radial valence charge distribution. For a closed shell atom, it is typically easy to identify an inert core region in which the valence distribution will not significantly change, as shown in in figure 3.2.

When a pseudopotential is constructed, the matching to the valence orbitals should take place within this inert region. Otherwise, the smoothening of the central potential and valence may take place outside of the inert region, and poor transferability properties are to be expected, as the pseudopotential is rigid in a region where the valence needs to be adaptive. As can be seen in figure 3.2, an inert core region is no longer observed if one takes a look at the individual spin densities. Apparently, the changes in the spin densities are widely cancelled in the core region, but only if their sum is considered, i.e. the total

charge distribution. However, if a spin polarized formulation of the exchange correlation functionals is evaluated, the assessment of an inert core region is problematic.

Strategies and corrections to circumvent these problems are not only addressed in the following sections, they are in fact an essential part of the work presented in the successive chapters.

3.7 A note about semicore states

While the pseudopotential approach is surprisingly reliable when the valence and core orbitals are well separated in real space and momentum, it imposes a serious source of errors for atoms with so called semicore states: Orbitals that are neither valence nor core states, as they have lower eigenvalues than the valence, but are weakly bound and poorly localized. In that case, there is some overlap between the semicore and valence orbitals, and their exchange correlation interactions no longer decouple. Problematic in particular are alkali metals, rare earths and those transition metals with partially filled d orbitals. For instance, the $3d$ orbital of titanium is rather compact due to the lack of lower lying d states and therefore it overlaps significantly with the filled $3p$ and $3s$ orbitals.

The straightforward idea to circumvent problems arising from the semicore states is to treat them en par with the valence states. In other words, the semicores are not frozen and eliminated as the other core electrons, but pseudized like the valence states. As a consequence, the computational effort for the calculation increases significantly, not only because the number of orbitals (valence plus semicores) is raised, but mainly because the semicores require a denser basis set and lead to overall harder pseudopotentials. This strategy is not only possible for the mentioned transition or alkali metals, where it clearly is necessary, but for any atomic system where the distinction between core and valence states is delicate. In that sense, pseudopotentials that explicitly include semicore states can be seen as a compromise between the accuracy of an all electron calculation and the efficiency of a pseudopotential with only few valence electrons. While it may be desirable to trade off some accuracy for higher speed using a pseudopotential with fewer electrons, there is usually not much room for different choices of assigning the core orbitals. This is because the addition of lower lying states to the pseudovalence, for example the $2s$ orbitals of elements with a partially filled $3p$ valence, leads to pseudopotentials that are far too hard to be of practical use.

For the work presented in the following chapters, only light chemical elements were considered, yet the inclusion of semicore states plays an important role for the accurate description of alkali and alkaline earth metals.

3.8 Pseudopotentials for spin polarized calculations

As just noted in the previous two sections, the employment of a pseudopotential implies a linearization of the electronic core-valence interactions. Since there are nonlinear terms arising from the exchange correlation (XC) functionals, an overlap between core and valence states can lead to significant errors, especially when semicore states are present. However, even if the core and valence orbitals are well separated, there can be major problems with the pseudopotential method if spin polarized systems are considered, for which the nonlinearities of the XC potential are much more pronounced.

Historically one of the first approaches to solve this problem is to introduce a spin dependence in the pseudopotential as proposed by Zunger [21]. The nonlocal part then has different components for each angular momentum channel ℓ of the two spin densities. The major drawback with pseudopotentials that are explicitly spin dependent is that the transferability is not necessarily improved with this strategy. While a certain spin polarized configuration of the single atom can be matched perfectly with a given pseudopotential, other polarized occupancies may be described rather poorly, and there is a trade-off for the accuracy of the closed shell atom as well. To resolve this problem, Zunger also proposed the

interpolation of the pseudopotential with respect to the atoms magnetic moment. This basically means that several spin dependent pseudopotentials are generated for different magnetic configurations of the atom and then averaged in some way to match the relative spin polarization on the atomic site, a strategy that has not proven to be very successful. Further efforts have been made to construct more accurate and reliable spin dependent pseudopotentials, for example by E. A. Carter and S. C. Watson [22]. Here the pseudopotential is no longer explicitly spin-dependent, but it rather includes a correction term that is linear in the local spin polarization 3.40.

A more convenient solution to circumvent the problems with spin polarized systems is the inclusion of nonlinear core corrections (NLCC), a simple modification to the evaluation of the XC functionals.

In essence, the NLCC scheme proposed by Louie and coauthors [23] tackles the problems of nonlinearities by adding a partial core charge density ρ_c. The valence charge density ρ is superposed with this model core charge if and only if the XC functionals need to be accessed (3.41).

$$E_{xc} = \int \varepsilon_{xc}(\rho + \rho_c) d^3\boldsymbol{r} \tag{3.41}$$

For all remaining energy terms, only the valence charge ρ is taken into account, so the partial core density ρ_c is merely a quantity to correct the nonlinear XC terms. ρ_c equals the frozen core charge in the valence region and neglects most of the core charge near the nucleus, where it usually takes a smooth and simple form. The motivation for this is that nonlinear corrections are needed mainly where the pseudovalence and frozen core charges are of similar amplitude. The variation of the XC energy (3.41) with respect to the orbitals in the sense of equation (1.22) remains formally the same (3.42), since the partial core density ρ_c is constant.

$$\frac{\delta E_{xc}}{\delta \phi_i} = \frac{\delta E_{xc}}{\delta(\rho + \rho_c)} \frac{\delta(\rho + \rho_c)}{\delta \phi_i} = V_{xc}(\rho + \rho_c) \; 2q_i \; \phi_i \tag{3.42}$$

The technical details of the partial core charges analytic form and of the implementation of NLCC are discussed in the next chapter. While good corrections for spin polarization effects can be achieved with practically no increase in the computational effort, the modifications of the DFT code needed for the inclusion of NLCC are relatively simply as well.

Of course, the presence of NLCC requires the use of a pseudopotential that was generated in order to achieve optimal accuracy and transferability for the partial core charge distribution given for its atom type. From another point of view, the exact shape of said charge distribution can be considered as a part of the pseudopotential, and is typically read from the same input files that contain the remaining pseudopotential data.

3.9 Pseudopotentials with relativistic corrections

Pseudopotentials are not only a powerful tool to decrease the computational effort of an electronic structure calculation greatly, but they also allow the straightforward inclusion of additional correction terms. This is due to the approach of modelling an effective core potential that reproduces some data from an atomic reference calculation. An example of particular interest are relativistic effects, which are relevant when heavier atoms are present. As mentioned in the previous chapter, the formally correct way to access these effects is to solve the Dirac equation rather than the Schrödinger equation. In essence, using atomic reference data from a relativistic all electron calculation should allow to generate a pseudopotential that reflects the relativistic effects in an efficient and formally very simple way.

To understand how it is possible to construct such a pseudopotential, some results of the previous chapter need to be readdressed. For the central potential, the Dirac equation reduces to a pair of coupled radial equations (2.59), (2.60), which allow to generalize the Kohn Sham equations for an atom to the relativistic

case. In summary, the solutions of these equations are two radial functions per orbital, the major P and the minor Q, which are each associated with a two component spin-angle function Y_{ℓ,j,m_j} that implies the angular and spin degrees of freedom. The spin-angle functions can be expressed with spherical harmonics (2.63),(2.64) and are related to the total angular momentum quantum numbers $j = \ell + s$ and $m_j = m + s$. The question arises how the spinorial form of the relativistic orbitals can be mapped to a pseudovalence that fulfills a Schrödinger equation with an effective core potential. Bachelet and Schlüter [19] have shown that such a construction scheme for a norm conserving pseudopotential is possible and indeed allows the inclusion of relativistic effects. Noting that in the limit of weak interactions, the Dirac equation reduces to a Schrödinger equation for the major component(2.68) and that the contribution of the minor to charge integral becomes negligible (3.43), they suggested to exclude the minor from the matching criteria and to construct the pseudovalence from properties of the major component only.

$$\int_0^\infty P^2(r)dr = 1 - \int_0^\infty Q^2(r)dr \approx 1 - c^{-2} \tag{3.43}$$

It can be noted that the minor component of the relativistic orbitals still plays a role when discussing the pseudopotentials quality in the sense of logarithmic derivatives. Bachelet and Schlüter derived the relativistic equivalent of the identity that relates the properties of norm conservation and the logarithmic energy derivatives. For eigenstates of the atomic Dirac equation, the corresponding identity (3.44) contains the ratio of the minor and major component, and the term $(2cQ)/P$ plays the same role as the logarithmic derivative in the non-relativistic case(3.10).

$$-2\pi \left(P \frac{\partial}{\partial E} \frac{2cQ}{P} \right)_R = 4\pi \int_0^R \left(P^2 + Q^2 \right) r^2 dr \tag{3.44}$$

The problem remains how to map the spin properties of the major to the pseudovalence in order to construct a semilocal pseudopotential. Since the valence orbitals are characterized by the quantum numbers ℓ and j, projectors on spin-angle functions Y_{ℓ,j,m_j} rather than the spherical harmonics $Y_{\ell,m}$ are necessary. However, considering the two components of the spin-angle functions separately allows to switch back to spherical harmonics.

$$\hat{P}_{\ell,s} = \sum_{m_j=-\ell+s}^{\ell+s} |Y_{\ell,\ell+s,m_j}\rangle\langle Y_{\ell,\ell+s,m_j}| \tag{3.45}$$

Using a short hand notation(3.45) for this type of total angular momentum projection operator, the ionic potential can be split into angular momentum channels(3.46), such that it takes a nonlocal form (3.25).

$$V_{ion} = \sum_\ell \left(V_{\ell,\ell+\frac{1}{2}}(r)\hat{P}_{\ell,\frac{1}{2}} \right) + \left(V_{\ell,\ell-\frac{1}{2}}(r)\hat{P}_{\ell,-\frac{1}{2}} \right) \tag{3.46}$$

Taking into account the j-degeneracy of the $\ell \pm \frac{1}{2}$ states, each ℓ component of the ionic potential can be rearranged into a (spin) average potential $\bar{V}_\ell$ and a difference potential V_ℓ^{SO}.

$$V_{ion} = \sum_\ell \hat{P}_\ell \left(\bar{V}_\ell + V_\ell^{SO} \boldsymbol{L} \cdot \boldsymbol{S} \right) \tag{3.47}$$

Using only the average potential(3.48) allows to match the pseudovalence to the spin averaged properties of the major part of the valence, such that scalar relativistic effects can be approximated reliably.

$$\bar{V}_\ell(\boldsymbol{r}, \boldsymbol{r}') = \frac{1}{2\ell+1} \left(\ell V_{\ell-1/2}(\boldsymbol{r}, \boldsymbol{r}') + (\ell+1) V_{\ell+1/2}(\boldsymbol{r}, \boldsymbol{r}') \right) \tag{3.48}$$

Taking into account also the difference potential(3.49) introduces an explicit spin dependence of the pseudopotential, such that both spin components of the major are matched and the spin degeneracy of

the pseudovalence is lifted. Therefore, the difference potential can be understood as a correction term to model the effect of spin-orbit-coupling.

$$\Delta V_\ell^{SO}(\boldsymbol{r}, \boldsymbol{r'}) = \frac{2}{2\ell + 1} \left(V_{\ell-1/2}(\boldsymbol{r}, \boldsymbol{r'}) - V_{\ell+1/2}(\boldsymbol{r}, \boldsymbol{r'}) \right) \tag{3.49}$$

Just as the norm conserving potentials discussed in the previous sections, a relativistic pseudopotential of this type can be expressed in a semilocal form, and the nonlocal part can be rearranged into separable terms. The only formal difference to the non-relativistic pseudopotentials is that the number of terms related to a nonzero angular momentum are doubled. For the local part and projectors to s-orbitals, no additional terms are needed, as there is no spin orbit splitting involved. It should also be noted that a relativistic pseudopotential that was generated to include a difference potential can be employed in two ways, either making use of the spin-orbit correction or neglecting it, for instance in a closed shell calculation. The latter yields results that often differ only slightly from the use of a non-relativistic pseudopotential, especially for lighter elements. But even then there are subtle differences between pseudopotentials fitted to all electron data from a non-relativistic, scalar relativistic or fully relativistic atomic reference calculation.

3.10 Some notes about ultrasoft pseudopotentials

The theory about the pseudopotential method discussed so far has a clear focus on norm-conserving pseudopotentials (NC PSP), which will be the subject of the work presented in the following chapters. Opposed to this family of pseudopotentials, ultrasoft pseudopotentials (US PSP) [24] release the condition of norm conservation in favor of very smooth pseudovalence orbitals. Even though ultrasoft pseudopotentials are not of further interest for the remaining parts of this work, it is well justified to explain briefly some of the key concepts, as these potentials have gained some popularity and because they expose some significant differences to norm conserving pseudopotentials.

Inside a core radius r_c around each atom, the pseudovalence is allowed to be as soft as possible, while an augmentation charge compensates for the resulting charge deficit in the core region(3.50).

$$\rho(r) = \sum_{occ} \left(\phi_i^*(r)\phi_i(r) + \sum_{m,n} Q_{m,n}(\boldsymbol{r})\langle \phi_i \mid \beta_m \rangle \langle \beta_n \mid \phi_i \rangle \right) \tag{3.50}$$

For consistency the functions β_m that form the projectors for the augmentation charge also serve for constructing the separable form of the pseudopotentials nonlocal part(3.51).

$$V_{NL} = \sum_{m,n} D_{m,n} \mid \beta_m \rangle \langle \beta_n \mid \tag{3.51}$$

It can be noted that the index m (or n) typically runs over one or two β projectors per angular momentum number ℓ, which are products of spherical harmonics and radial functions.

Without going into the technical details one can summarize that the price for the reduction of the basis set size is an increase in the complexity of a DFT programs core routines. This is mainly due to the resulting general eigenvalue formalism (3.52), where the Hamiltonian (3.53) and overlap matrix (3.54) again use β projector functions.

$$H \mid \phi_i \rangle = \varepsilon_i S \mid \phi_i \rangle \tag{3.52}$$

$$H = T + V_{xc} + V_H + V_{loc} + (D_{m,n} + U_{m,n}) \mid \beta_n \rangle \langle \beta_m \mid \tag{3.53}$$

$$S - \mathbf{1} = \sum_{m,n} \int_{r=0}^{r_c} Q_{m,n}(\boldsymbol{r}) d^3\boldsymbol{r} \mid \beta_n \rangle \langle \beta_m \mid = \sum_{m,n} q_{n,m} \mid \beta_n \rangle \langle \beta_m \mid \tag{3.54}$$

The nonlocal part of the Hamiltonian contains a screening term $U_{m,n}$ (3.55), which in return depends on the local potential $V = V_{loc} + V_{HA} + V_{xc}$, i.e. the sum of the pseudopotentials local part, the Hartree potential and the exchange correlation potential.

$$U_{m,n} = \int_{r=0}^{r_c} V(\boldsymbol{r}) Q_{m,n}(\boldsymbol{r}) d^3\boldsymbol{r} \tag{3.55}$$

In this sense, the properties of norm conservation are generalized to a more complicated augmentation formalism, and the nonlocal part of the Hamiltonian resulting from the augmentation charge can be understood as a part of the pseudopotential that evolves during the calculation.

The description and employment of ultrasoft potentials can be related to projector augmentation schemes, a family of methods that traditionally compete with pseudopotentials and follow a very different approach. Those schemes are compared in the following section.

3.11 Comparison with augmentation schemes

The common motivation for pseudopotential and augmentation methods is the observation that planewaves are suitable for the description of valence bands, but ill suited to capture the sharp oscillations close to the atomic nuclei. While the pseudization schemes discussed so far aim to replace the Hamiltonian with a smooth pseudo-Hamiltonian in the core region, augmentation schemes instead modify the description of the orbitals near the atomic sites. This concept of augmentation serves as the basic ingredient for the projector augmented wave method (PAW)[25], which can be seen as a generalization of the method of linearized augmented planewaves (LAPW) [26, 27] or its precursor, the augmented planewaves (APW) method [28, 29].

For all of these augmentation methods, the computational volume is formally split into spherical augmentation regions of radius r_c around each atomic site and an interstitial region covering the remaining space between the atoms. While this terminology is typical for the PAW method, the non-overlapping spheres around each atom are named muffin-tin spheres in the context of the APW method and sometimes also for the LAPW method. The muffin-tin (MT) approximation, which plays an important role for the early development of these schemes, implies that within the augmentation region, only the spherically symmetric component of the potential is taken into account. This is in contrast to the full potential linearized augmented waves (FLAPW) method [30], a variation of the LAPW method where spherical approximations of the potential are avoided.

The basic idea of the APW method proposed by John C. Slater is to use two different basis sets to represent the orbitals in each region, spherically symmetric functions centered on the atomic sites within the MT spheres (3.56) and planewaves in the interstitial region.

$$\varphi_{\boldsymbol{r}} = \begin{cases} \sum_{\ell,m} A_{\ell,m} u_\ell(r) Y_{\ell,m} & r = \mid \boldsymbol{r} - \boldsymbol{R_i} \mid < r_c \\ \Omega^{-1/2} \sum_G c_G \, e^{\imath(\boldsymbol{G}+\boldsymbol{k})\cdot\boldsymbol{r}} & \text{else} \end{cases} \tag{3.56}$$

This allows to describe the core region with atomic like orbitals, as the radial basis functions u_ℓ are defined inside each MT sphere as the eigenstates (3.57) of the Hamiltonians spherical component.

$$\left(-\frac{\partial^2}{\partial r^2} + \frac{l(l+1)}{2r^2} + V(r) - E_\ell \right) r u_\ell = 0 \tag{3.57}$$

Although equation (3.57) is equivalent to the radial Kohn Sham equations of an atom, the context is different here. The eigenvalue E_ℓ is a parameter that should match the band energy of φ and $V(r)$ is given as the spherical component of the potential inside the MT sphere. The augmentation functions u_ℓ are thus not obtained from an eigenvalue problem, but by solving for the roots of the secular equation with a given values of E_ℓ. Expanding the valence in u_ℓ functions for the MT region (3.56) means to match the planewave representation in the interstitial with a spherical expansion, such that orthogonality is ensured to all radial eigenstates that are strictly localized in the MT sphere, i.e. to the core orbitals. Thus E_ℓ act as variational parameters for representing the orbitals and define the basis functions u_ℓ in the MT spheres in dependence of the potential. Since the orbitals need to be continuous at the MT sphere boundaries, the expansion coefficients $A_{\ell,m}$ in the MT spheres are determined by the planewave coefficients c_g via their spherical harmonic expansion. Thus the planewave expansion in the interstitial region and the energy parameters E_ℓ are the variational degrees of freedom in the APW method. The term augmented planewave (APW) usually stands for the representation of an orbital with respect to these parameters.

The LAPW method adds more variational freedom for the expansion of the orbitals near the atomic sites (3.58) using the energy derivative $\dot{u}_\ell$ of the augmentation functions u_ℓ.

$$\varphi_{\boldsymbol{r}} = \begin{cases} \sum_{\ell,m} \left(A_{\ell,m} u_\ell(r) + B_{\ell,m} \dot{u}_\ell(r) \right) Y_{\ell,m} & r = \mid \boldsymbol{r} - \boldsymbol{R_i} \mid < r_c \\ \Omega^{-1/2} \sum_G c_G \, e^{\imath(\boldsymbol{G}+\boldsymbol{k})\cdot\boldsymbol{r}} & \text{else} \end{cases} \tag{3.58}$$

The energy derivatives $\dot{u}_\ell$ are obtained from the potential within the MT sphere and the linearization parameters E_ℓ via another set of radial equations (3.59), just as u_ℓ is determined by equation (3.57). The coefficients $B_{\ell,m}$ are determined in analogy to $A_{\ell,m}$ by matching the derivative of the planewave expansion at the MT sphere boundary.

$$\left(-\frac{\partial^2}{\partial r^2} + \frac{l(l+1)}{2r^2} + V(r) - E_\ell \right) r \dot{u}_\ell = r u_\ell \tag{3.59}$$

The motivation for this choice is to avoid problems with the energy dependence of the radial functions u_ℓ. In the sense of a Taylor expansion, the accuracy is of second order with respect to the deviation of the linearization parameters E_ℓ to the band energy. As the spherical expansion is feasible for a broader energy range, one common set of E_ℓ can be used for all bands, which simplifies the method greatly compared to the APW.

The PAW method is closely related to the LAPW method, although the starting point appears different. It introduces the concept of a smooth pseudovalence Ψ_n^{PS} which can be mapped to the true or all electron orbitals Ψ_n with a linear transformation τ (3.60).

$$\mid \Psi_n \rangle = \tau \mid \Psi_n^{PS} \rangle = \mid \Psi_n^{PS} \rangle + \sum_i \left(\varphi_i - \varphi_i^{PS} \right) \langle p_i \mid \Psi_n^{PS} \rangle \tag{3.60}$$

While the pseudovalence Ψ_n^{PS} is expanded in planewaves, properties of the true valence are then accessible in operator form (3.61).

$$\langle \Psi_n \mid A \mid \Psi_n \rangle = \left\langle \Psi_n^{PS} \middle| \tau^\dagger A \tau \middle| \Psi_n^{PS} \right\rangle \tag{3.61}$$

The index i runs over all partial waves φ_i centered on the atomic sites, which are solutions of the radial Schrödinger equation and thus expressed with radial functions and spherical harmonics. p_i are projector functions dual to the smoothened pseudo partial waves φ_i^{PS} (3.62).

$$\langle p_i \mid \varphi_j^{PS} \rangle = \delta_{i,j} \tag{3.62}$$

Only inside the augmentation region the partial waves φ_i differ from the smoother pseudo partial waves φ_i^{PS}, and so do the orbitals Ψ_n compared to the pseudo orbitals Ψ_n^{PS}. Accordingly, the atomic centered projectors vanish in the interstitial region.

This projector formalism is evidently related to the concepts of the LAPW method and resembles the augmentation scheme of ultrasoft pseudopotentials (US PSP). The PAW and LAPW methods essentially differ in the way the projectors are constructed and the partial waves are matched with the pseudovalence at the boundaries between the interstitial and the augmentation regions. For this the PAW method uses a more general projector formalism which adds more variational freedom and thus more flexibility. Similarly, US PSP use a more complicated projector formalism to gain more flexibility for the construction of a soft pseudovalence. In return, augmentation schemes can be transformed in such a way that they formally appear like a pseudopotential method, which has for instance been demonstrated in detail by Goedecker and Maschke for the LAPW method [31, 32]. The comparison of and interconnections between these methods may give some insights to understand why and under which circumstances pseudopotentials work well. For example, the inert core region mentioned in the section about limitations of the pseudopotentials method is related to the augmentation region in the PAW or the MT spheres of the LAPW. However, the augmentation spheres are typically much wider than the core radius r_c of norm conserving PSP. The latter is more localized and rigid, as there is less flexibility in the projector approach of NC PSP. From a simple point of view, US PSP establish some compromise in this sense.

This short comparison marks the end of the introductory chapter about the pseudopotential method. In the following chapter, one particular type of norm conserving pseudopotential is introduced. The process of generating these potentials is explained in detail and various modifications to that procedure are presented, which lead to the results presented in a successive chapter.

Chapter 4

Determination of the pseudopotentials parameters

In the following sections, GTH-HGH type pseudopotentials are introduced, going from the closed form and analytic properties of these norm conserving pseudopotentials to the concepts and strategy in use to construct them. Thereafter, some modifications and enhancements to the procedure of generating GTH-HGH type pseudopotentials are presented. Besides minor changes, the new functionality allows access to a broader variety of XC-functionals, fitting to spin polarized atoms, the simultaneous treatment of multiple atomic configurations, the inclusion of better constraints for enhanced softness and, last but not least, the inclusion of nonlinear core corrections, which play an important role for the results discussed in the following chapter.

4.1   Gaussian type separable pseudopotentials

The norm conserving pseudopotentials proposed by Goedecker, Teter and Hutter [33] have some unique properties that make them highly efficient and reliable. A key feature of the GTH pseudopotentials is their purely analytic form with a small number of free parameters. In contrast to most other semilocal pseudopotentials, there is no need to tabulate a radial grid for the local part or any of the projector elements that constitute the separable part. The analytic form is designed in such a way that it implies some desired optimality criteria. These can be understood as a well localized, smooth shape in both real space and Fourier space. Gaussians serve as a natural choice for the radial functions in the separable part to achieve optimal dual space decay properties. This is why the GTH-HGH pseudopotentials are referred as dual-space Gaussian pseudopotentials. As a direct consequence, efficient real space integration of the separable part is possible, which results in only a quadratic scaling with respect to the system size, in contrast to the cubic scaling of a Fourier space integration scheme.

In the following section, the actual choice of the pseudopotentials analytic form is discussed briefly. The local part uses an error function term (4.1) to cut away the singularity from the central potential within the local radius r_{loc}, much in the spirit of the cutting function discussed in a previous section about the BHS construction. Furthermore, a short range potential is added in form of a spherical Gaussian times an even polynomial with up to four coefficients(4.2).
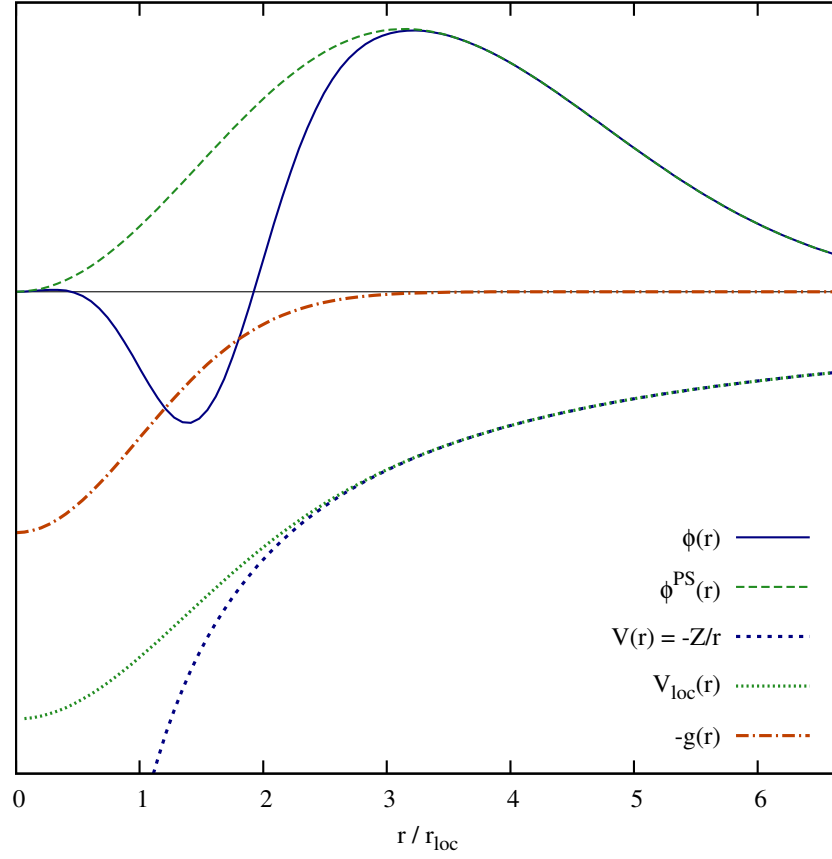
Figure 4.1: The local radius r_{loc} controls the smoothness of the GTH-pseudopotentials local part V_{loc} and can be understood as the width of a Gaussian charge distribution $g(r)$.

$$V_{loc}(r) = -\frac{Z_{ion}}{r} erf\left(\frac{r}{\sqrt{2}r_{loc}}\right) \tag{4.1}$$

$$+exp\left(-\frac{1}{2}\left(\frac{r}{r_{loc}}\right)^2\right)\left(\sum_{k=1}^{n\leq 4}C_k\left(\frac{r}{r_{loc}}\right)^{2k-2}\right) \tag{4.2}$$

It should be noted that figure 3.1 of the previous chapter, which illustrates the concept of pseudization, shows a pseudopotential $V^{PS}(r)$ equal to the local part V_{loc} given by equation (4.1), while the polynomial coefficients C_k (4.2) are set to zero. This choice of V_{loc} is equivalent to the electrostatic potential arising from an ionic charge smeared out in the shape of a Gaussian with the width r_{loc}.

For clarity, the same curves are shown in figure 4.1, where the radial coordinate is scaled with respect to the local radius r_{loc}, and the corresponding Gaussian charge distribution is indicated. The local radius r_{loc} in figure 4.1 corresponds to 0.3 times the core radius r_c indicated in figure 3.1. However, it must be emphasized that a core radius r_c does not exist in the strict sense of a matching boundary for the GTH

pseudopotential: The central potential and valence orbitals are matched in a smooth manner by the local potential and pseudovalence, respectively, yet there are asymptotically small deviations. A typical choice for r_{loc} is between a quarter and a sixth of the covalent bond radius.

The nonlocal part takes a separable form (5.3), where each ℓ component may contain several projectors. For a GTH pseudopotential, the weights h_i^ℓ for summing up the projectors as well as a radial length scale r_ℓ are the free parameters of each ℓ- channel in the separable part.

$$V_\ell(\mathbf{r},\mathbf{r'}) = \sum_{i=1}^{n \leq 2} \sum_{m=-\ell}^{\ell} \mid Y_{\ell,m} \rangle p_i^\ell(r) \ h_i^\ell \ p_i^\ell(r') \langle Y_{\ell,m} \mid \tag{4.3}$$

The radial function $p_i^\ell(r)$ of the projector is an atomic centered Gaussian times a polynomial(5.4).

$$p_i^\ell(r) = C_i^\ell \ r^{2\ell+i} e^{\left(-\frac{1}{2} \left(\frac{r}{r_\ell} \right)^2 \right)} \tag{4.4}$$

Here C_i^ℓ is just a derived constant as given by equation (4.5), such that the radial projectors suffice the normalization condition of equation (4.6).

$$C_i^\ell = \frac{\sqrt{2}}{r_\ell^{\ell+(4i-1)/2} \sqrt{\Gamma \left(\ell + \frac{4i-1}{2} \right)}} \tag{4.5}$$

$$\int_0^\infty p_i^\ell(r)^2 r^2 dr = 1 \tag{4.6}$$

In a following study by Hartwigsen, Goedecker and Hutter[34], the GTH pseudopotentials were generalized to include relativistic effects and a set of parameters was presented for all elements in the periodic table up to Radon (Rn). As discussed in the previous section, the separable part then consists of an average potential $\bar{V}$ and a difference potential V^{SO}, where the latter introduces spin-orbit effects that are optional when employing the pseudopotential. Since transition metals and other elements with semicore orbitals are considered, a more general form for the separable part is introduced. Its form is extended in such a way that the projection operators can contain two unequal radial functions. The weights $h_{i,j}^\ell$ for the average potential(4.7) and $k_{i,j}^\ell$ for the difference potential(4.8) are arranged accordingly in two symmetric matrices.

$$\bar{V}_\ell(\mathbf{r},\mathbf{r'}) = \sum_{i,j=1}^{n \leq 3} \sum_{m=-\ell}^{\ell} \mid Y_{\ell,m} \rangle p_i^\ell(r) \ h_{i,j}^\ell \ p_j^\ell(r') \langle Y_{\ell,m} \mid \tag{4.7}$$

$$V_\ell^{SO}(\mathbf{r},\mathbf{r'}) = \sum_{i,j=1}^{n \leq 3} \sum_{m=-\ell}^{\ell} \mid Y_{\ell,m} \rangle p_i^\ell(r) \ k_{i,j}^\ell \ p_j^\ell(r') \langle Y_{\ell,m} \mid \tag{4.8}$$

From a simple point of view, multiplying a bell shaped curve with a power of r introduces a node at the origin, and higher powers of r will push the peak of the product distribution further away, as illustrated by figure 4.2.

As the use of off-diagonal matrix elements $h_{i,j}^\ell$ in the separable part allows to couple radial projector functions with different powers of r, this form may help to model the interactions between orbitals of different spatial extensions. This can be of interest when semicore states are present.

The difference potential V_ℓ^{SO} introduces a splitting between the spin up and spin down states. Following the definition of the average potential (3.48) and difference potential(3.49) in the previous section, the coefficients $h_{i,j}^\ell$ and $k_{i,j}^\ell$ are easily related to the corresponding coefficients for spin up(4.9) and spin down electrons(4.10).
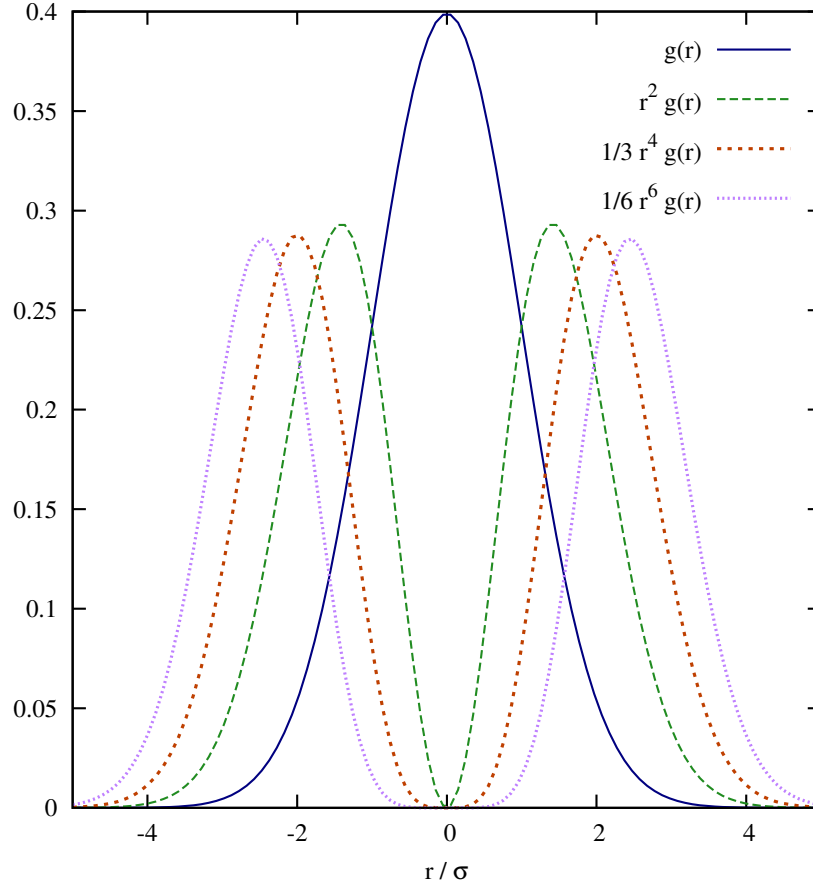
Figure 4.2: The GTH-HGH-pseudopotentials are based on Gaussians $g(r)$ times an even power of the radial coordinate r. The shown curves are normalized for the one dimensional case.

$$h_{i,j}^{\ell+\frac{1}{2}} = h_{i,j}^{\ell} + \frac{\ell}{2}k_{i,j}^{\ell} \tag{4.9}$$

$$h_{i,j}^{\ell-\frac{1}{2}} = h_{i,j}^{\ell} - \frac{\ell+1}{2}k_{i,j}^{\ell} \tag{4.10}$$

These and the above conventions are sufficient to define the analytic form of the GTH-HGH pseudopotentials. In summary, the free parameters that determine a potential of this form are

- the local radius r_{loc} and up to four coefficients C_k for the local part,
- up to four angular momentum channels $\ell \leq 3$ for the separable part, each of them containing
  - a length scale r_ℓ for the Gaussian projectors and
  - up to three by three coefficients $h_{i,j}^{\ell}$ for the non-relativistic or average potential,
  - and in the relativistic case for $\ell > 0$, the corresponding coefficients $k_{i,j}^{\ell}$ for the difference potential.

46

When a pseudopotential for a particular chemical element is generated, a minimal set of nonzero coefficients must be chosen, while the remaining possible terms are dropped. The actual procedure to optimize the free parameters of the pseudopotential will be described in the following sections.

As mentioned before, the closed form of the pseudopotentials in real space is chosen in such a way that its Fourier transform remains simple and well localized. To close the section about the analytic properties of the GTH-HGH pseudopotentials, this dual space property is shown briefly. The closed form of the local part in Fourier space (4.11) can be derived analytically and consists of a Gaussian times a polynomial.

$$V_{loc}(k) = -\frac{4\pi Z_{ion}}{\Omega k^2} e^{\left(\frac{(kr_{loc})^2}{2}\right)} + \sqrt{8\pi^3} \frac{r_{loc}^3}{\Omega} e^{\left(\frac{(kr_{loc})^2}{2}\right)} P_{loc}(k\, r_{loc}) \tag{4.11}$$

Here Ω is the volume of the unit cell and P_{loc} is the polynomial given in equation (4.12).

$$P_{loc}(k) = C_1 + C_2(3 - k^2) + C_3(15 - 10k^2 + k^4) + C_4(105 - 105k^2 + 21k^4 - k^6) \tag{4.12}$$

The analytic form of the separable part in real space (5.4) and Fourier space (4.13) is very similar as well.

$$V_\ell(\,\mathbf{k},\mathbf{k'}) = (-1)^\ell \sum_{i,j=1}^{n \leq 3} \sum_{m=-\ell}^{\ell} |\, Y_{\ell,m}\rangle p_i^\ell(k) h_{i,j}^\ell p_j^\ell(k') \langle Y_{\ell,m}\,| \tag{4.13}$$

Again it can be shown analytically that the Fourier transform of each radial projector conserves the analytic form of a Gaussian times a polynomial. For the relevant cases (4.14)-(4.22), the explicit forms of the radial projectors are given below.

$$p_{i=1}^{\ell=0}(k) = \frac{4\sqrt{2r_\ell^3}\pi^{5/4}}{\sqrt{\Omega} exp(kr_\ell/2)} \tag{4.14}$$

$$p_{i=2}^{\ell=0}(k) = \frac{\sqrt{8\frac{2r_\ell^3}{15}}\pi^{5/4}(3 - k^2 r_\ell^2)}{\sqrt{\Omega} exp(kr_\ell/2)} \tag{4.15}$$

$$p_{i=3}^{\ell=0}(k) = \frac{16\sqrt{\frac{2r_\ell^3}{105}}\pi^{5/4}(15 - 10k^2 r_\ell^2 + k^4 r_\ell^4)}{3\sqrt{\Omega} exp(kr_\ell/2)} \tag{4.16}$$

$$p_{i=1}^{\ell=1}(k) = \frac{8\sqrt{\frac{r_\ell^5}{3}}\pi^{5/4}k}{\sqrt{\Omega} exp(kr_\ell/2)} \tag{4.17}$$

$$p_{i=2}^{\ell=1}(k) = \frac{16\sqrt{\frac{r_\ell^5}{105}}\pi^{5/4}k}{\sqrt{\Omega} exp(kr_\ell/2)} \tag{4.18}$$

$$p_{i=3}^{\ell=1}(k) = \frac{32\sqrt{\frac{r_\ell^5}{1155}}\pi^{5/4}k(35 - 14k^2 r_\ell^2 + g^4)r_\ell^4}{3\sqrt{\Omega} exp(kr_\ell/2)} \tag{4.19}$$

$$p_{i=1}^{\ell=2}(k) = \frac{8\sqrt{\frac{2r_\ell^7}{15}}\pi^{5/4}k^2}{\sqrt{\Omega} exp(kr_\ell/2)} \tag{4.20}$$

$$p_{i=2}^{\ell=2}(k) = \frac{16\sqrt{\frac{2r_\ell^7}{105}}\pi^{5/4}k^2(7 - k^2 r_\ell^2)}{3\sqrt{\Omega} exp(kr_\ell/2)} \tag{4.21}$$

$$p_{i=1}^{\ell=3}(k) = \frac{16\sqrt{\frac{r_\ell^7}{105}}\pi^{5/4}k^3}{\sqrt{\Omega}exp(kr_\ell/2)} \tag{4.22}$$

4.2 The pseudopotential fitting cycle

The GTH-HGH pseudopotentials have a well defined, purely analytic form with a relatively small number of free parameters. When a pseudopotential is constructed for a given chemical element, these parameters are not determined by some matching criteria or rigid constraints, but rather optimized carefully in order to obtain a good compromise for a manifold of desired properties. In contrast to most implementations of norm conserving pseudopotentials, there are no core radii for the explicit matching of the pseudovalence and valence, and the former rapidly converges to the latter in a smooth and continuous manner. For this purpose, a subset of the pseudopotentials parameters is picked and fitted to minimize a penalty function, as will be described in the following section. This leaves much freedom for the consideration and weighting of particular features, such as the required precision for the eigenvalues and norm conservation of the valence, semicores or unoccupied orbitals, as well as other terms related to the pseudopotentials accuracy, transferability and softness.

The heart of the construction scheme for GTH-HGH pseudopotential is the fitting cycle, where the free parameters of the pseudopotentials analytic form are optimized. For this purpose, a user defined penalty function is minimized using a very simple, yet robust optimization scheme, the downhill simplex method. The actual dependence of the penalty value on the free variables can be very complicated, such that more sophisticated minimization schemes might fail to converge. In order to evaluate the penalty function for a given set of pseudopotential parameters, the radial Schroedinger equation of the pseudo-atom must be solved at each step of the fitting cycle. Said penalty function consists of a weighted sum of square deviations to the reference data, where the weights are chosen carefully to reflect the desired accuracy of each contribution to the penalty function. For instance, a set of eigenvalues $\varepsilon_{n,\ell}^{PS}$ is considered, each with a corresponding all electron eigenvalue denoted by $\varepsilon_{n,\ell}^{AE}$ and a weight $w_{\varepsilon,n,\ell}$ for fitting. The pseudopotential parameters are then optimized to obtain a low value of the resulting penalty function (4.23).

$$P = \sum_{n,\ell} w_{\varepsilon,n,\ell}^2 \left(\varepsilon_{n,\ell}^{AE} - \varepsilon_{n,\ell}^{PS}\right)^2 \tag{4.23}$$

The above penalty function of square deviations may contain contributions not only from valence eigenvalues, but also from other states with lower accuracy requirements, such as semicores or unoccupied orbitals. For example, valence eigenvalues are assigned a weight of 10^6, while other orbitals have a weight of 10^3. In that case, a penalty value in the order of one will roughly correspond to errors of less than 10^{-6} Ha for the valence and less than 10^{-3} Ha for the other eigenvalues considered. The trade-off between the accurate description of the various orbitals is simply the result of least square fitting. This is in contrast to the construction of a pseudopotential by inversion of the Schroedinger equation, where the valence eigenvalues are matched very strictly, while unoccupied orbitals are not considered at all.

4.3 The role of the confining potential

The possibility to take into account not only the occupied atomic states provides a powerful method to enhance the pseudopotentials transferability. Typically one unoccupied orbital for each angular momentum channel ℓ is considered, going from s-type orbitals up to the first ℓ channel that does not hold any electrons. However, matching orbitals of high energy eigenvalues is problematic for an isolated atom, as the wavefunctions resemble that of free particles and have no asymptotic decay behavior. For this

reason, it is necessary to apply a confinement that ensures all orbitals of interest have a well defined shape. This means that both, the pseudo-atomic and the all electron reference calculation are carried out with a certain type of external potential well. This will qualitatively lead to a contraction of the orbitals and a positive shift of the eigenvalues, as well as to faster convergence for the self consistency cycle when solving the radial Kohn Sham equations. Nevertheless, it turns out that the confinement does not impose a serious problem for the pseudopotentials accuracy. As previously discussed, the pseudopotential approximation relies on the assumption that an effective core potential can be employed in various chemical environments even though it was generated from an atomic calculation. In other words, the pseudopotential should be transferable. In that context, the isolated atom is not necessarily the better choice than an atom that is embedded into some confining potential. If the confinement can lead to some improvements in the pseudopotentials transferability, this choice is certainly desirable.

The actual form of the confinement is a simple parabolic potential with one adjustable parameter.(4.24)

$$V_{prb}(r) = \frac{1}{2} \frac{r^2}{r_{prb}^4} = \frac{m_e \omega^2}{2} r^2 \tag{4.24}$$

Here the free parameter is r_{prb}, the natural length scale (4.25) of a harmonic oscillator in atomic units.

$$r_{prb} = \sqrt{\frac{\hbar}{m_e \omega}} \tag{4.25}$$

Wider r_{prb} lead to a weaker and broader confining potential. Therefore r_{prb} is chosen in accordance with the size of the studied atom, typically taking a value of about twice the covalent radius. Other choices for r_{prb} are usually possible in a broad range of values, but care must be taken that good convergence is ensured for all virtual orbitals under consideration. In practice, some different values for r_{prb} are examined and plots of the resulting orbitals are surveyed carefully.

4.4 Amoeba - the simplex downhill method

As already mentioned, the pseudopotential parameters are optimized with a minimization scheme. The idea is that finding a minimum of some penalty function is equivalent to the least square fitting of the pseudopotential to various atomic properties, which contribute to said penalty and are discussed later in detail. A reliable and robust minimisation algorithm is necessary because the summands of the penalty function, such as square deviations of atomic eigenvalues, are affected in a very nontrivial way by moves in the space of the pseudopotentials parameters. In other words, the object function is not necessarily smooth and predictable. All fitting is therefore performed using the simplex downhill method [35], which is also known as the amoeba or Nelson Mead method. This heuristic search algorithm is based on simple geometric manipulation of a simplex, i.e. a set of $N+1$ vertices in the space of N free fitting parameters. The search for low penalty values basically consists of expansion and contraction movements of the simplex and resembles the pseudopodia motion of an amoeba.

Each vertex of the simplex corresponds to a set of pseudopotential parameters that was tried at some stage of the optimization process. While moves of the coefficients C_k and $h_{i,j}^{\ell}$ of the pseudopotential are mapped directly to coordinates of the vertex v, the mapping of the localisation radii r_{loc} and r_ℓ is based on a sigmoid function. This is done such that changes of the radii with respect to the input guess pseudopotential are limited to at most ten percent (4.26).

$$r_{new} = r_{init} \left(1 + 0.1 \, \frac{arctan(v)}{2\pi} \right) \tag{4.26}$$

For the initial simplex, the mapping of the input guess pseudopotential is taken for one vertex, and one coordinate each is randomly shifted for the remaining vertices. Then fitting cycles are performed until

the simplex converges or no progression is made for a given number of steps. To illustrate the simplicity of the amoeba method, one step of the fitting cycle is summarized below.

- Get the center of the simplex (average of all vertices).

- Reflect the vertex with the highest penalty value at the center.

- Accept the reflected vertex if it no longer has the highest penalty.

- If the reflected vertex has the lowest penalty value, then

    – try to move it further away along the reflection axis.

    – Accept the moved vertex if it has the lowest penalty.

    – Keep the reflected vertex if it still has the lowest penalty.

- If the reflected vertex still has the highest penalty, then

    – Reject the reflection.

    – Contract the vertex towards the other vertices.

    – If the contracted vertex still has the highest penalty, then contract the entire simplex towards the vertex with the lowest penalty.

Each step involves the evaluation of at least one new vertex of the simplex, which requires to solve the radial Schrödinger equation for a new set of pseudopotential parameters. In the majority of the moves only that vertex with the highest penalty value is manipulated. Accepting a move of this vertex means to replace it with a new set of parameters that correspond to a better guess for the pseudopotential. If the simplex expands over a region that does not allow a systematic improvement with such simple steps, all vertices are contracted, which corresponds to averaging all pseudopotential samples with the best set of parameters found so far.

Depending on the number of terms in the pseudopotential, many thousand cycles may be needed to obtain desirable results. However, this strongly depends on the input guess pseudopotential, as will be discussed later. Since there typically exists a manifold of local minima for a given penalty function, finding a suitable set of pseudopotential parameters can be a very delicate task. Before these aspects are addressed, it should be clarified how a penalty function can be assembled in the first place.

4.5 The penalty function of conventional HGH pseudopotentials

As already stated, pseudopotentials of the GTH-HGH form are generated by least square fitting of a penalty function, which reflects various properties of the confined pseudo-atom. As a result, there is no unique solution for finding an optimal pseudopotential and a good compromise between many requirements must be found. First, there are plenty of ways to choose a set of contributions to the penalty function and to assign different weights for summing them up. Second, a number of free parameters of the pseudopotential has to be chosen for fitting, while other parameters are kept constant or are excluded from the pseudopotential. Third, there typically exists a vast variety of local minima with respect to the nonzero parameters of the pseudopotential for any useful choice of the penalty function. In order to obtain a norm conserving pseudopotential of high quality, many more contributions to the penalty function are taken into account than in the example of the previous section, where just a set of eigenvalues was considered. These ingredients for a good penalty function are briefly discussed in the following section.

To ensure good norm conservation properties, a penalty term is included to match the charge integral of each orbital within a chosen sphere, that is usually up to the atoms covalent radius. The upper limit of the radial charge integrals is hence denoted by r_{cov}, but other choices than the covalent radius may be considered. Typically a radius r_{cov} is picked near the first peak of all relevant orbitals. Again, each orbital may have its individual weight, such that semicores or unoccupied orbitals can be fitted at lower precision. This weighting is necessary to improve the pseudopotentials transferability without degrading the accuracy of the valence.

$$P = \sum_{nl} w_{c,nl}^2 \left(\int_0^{r_{cov}} r^2 \phi_{nl}^{PS} dr - \int_0^{r_{cov}} r^2 \phi_{nl}^{AE} dr \right)^2 \tag{4.27}$$

It is furthermore possible to use the second(4.28) or fourth moment of the orbitals radial charge distribution, which might be helpful for fitting widely extending orbitals, but usually does not improve the fit. These integrals are evaluated not only up to r_{cov}, but for the entire computational volume.

$$P = \sum_{nl} w_{c2,nl}^2 \left(\int_0^\infty r^4 \phi_{nl}^{PS} dr - \int_0^\infty r^4 \phi_{nl}^{AE} dr \right)^2 \tag{4.28}$$

A further type of orbital properties that may be included in the penalty function are the charge integrals between undesired nodes. This is a valuable tool to eliminate wiggles, as the smoothness of the pseudovalence is an essential key property of soft and efficient pseudopotentials. Of course, these integrals have no meaningful all electron counterpart and are directly suppressed by including them in the penalty function with a suitable weight.

A similar set of weights can be used to penalize the norm of the residue vector for each orbital. If the residues are small, the orbital is well represented in the chosen basis set. Such a penalty term for the residues is useful to keep them sufficiently small compared to the errors of the eigenvalues when very strict accuracy requirements are desired. Furthermore, one may attempt to switch to a coarser basis set and do some additional fitting cycles in order to improve the pseudopotentials softness. Care must be taken that the pseudopotential remains accurate when switching back to a suitable basis set, which is not necessarily the case.

Finally, there is one more weight for a penalty term related to the amplitude to the lowest s-type valence orbital evaluated at the origin $r = 0$. While this quantity is often quite small, no clear evidence was found that penalizing the value of the lowest $\varphi_s(0)$ leads to a quantitative improvement of the pseudopotential. In summary, the penalty function to be minimized by means of least square fitting is defined by a set of weights as follows, which can be assigned individually for each atomic orbital.

- matching of atomic eigenvalues $\epsilon_{n,\ell}$
- norm conservation within a sphere of radius r_{cov}
- no charge integral between undesired nodes
- small norm of the orbitals residue vector
- matching of higher order radial moments
- low amplitude at the origin (lowest s-state only)

In the present work, this set of ingredients for the penalty function is expanded in various ways. These enhancements of the fitting procedure are described in the following sections.

4.6 Fitting to multiple configurations in parallel

Apart from the penalty terms listed in the previous section and used in earlier work, some features were added to access further contributions for building up a penalty function. One major advance is to parallelize the method over several atomic reference configurations. This does not only allow to further enhance the transferability by fitting orbital properties of excited or ionized atoms, but is mainly useful to assess the total energy differences of said configurations. This way it is possible to optimize the pseudopotential to accurately reproduce excitation energies, electron affinities or ionization energies. To avoid convergence issues for the isolated atoms, changes in the occupancy of only half an electron per orbital are typically considered. In order to minimize a global penalty function that takes into account the information of multiple configurations, some new weights for the fitting procedure need to be defined. Most of all, this includes a weight w_{excit} for matching all of the excitation energies, i.e. the total energy differences between all pairs of configurations considered. If we denote the Kohn Sham energy difference of configurations i and j by $\Delta E_{i,j}$, the corresponding penalty term takes the form of equation (4.29).

$$P = w_{excit}^2 \sum_{i<j} \left(\Delta E_{i,j}^{PS} - \Delta E_{i,j}^{AE}\right)^2 \tag{4.29}$$

Furthermore, each configuration is associated with one multiplier for the penalty weights of all orbital related quantities, such as the valence eigenvalues and norm conservation properties of the excited atoms. This allows to fit each configuration at a certain relative level of accuracy while keeping the number of distinct weights well-arranged.

The implementation of the fitting procedure for several configurations requires very little communication, which takes place only once for each evaluation of the penalty functional and when updating the pseudopotential parameters. The Kohn Sham equations for each atom, however, are solved independently. For this reason, the number of compute processes is restricted to the number of atomic configurations of interest, which can be raised ideally without increasing the overall runtime per fitting cycle.

The parallel treatment of several atomic systems is not only useful to consider multiple electronic configurations, but the very same approach may serve to take into account the effect of different external potentials. As discussed earlier, the confining external potential is important to have well defined unoccupied orbitals. This confinement leads to a change in the atomic eigenvalues, which is dominated by but not limited to a shift towards more positive energies. Even though the impact on the eigenvalue spectrum is much the same for the all electron reference and the pseudo-atom, the accuracy of the eigenvalues matched by the pseudopotential does indeed depend on the confinement used. A very high accuracy in the micro Hartree regime cannot be conserved when switching to another value of r_{prb}, but when generating the pseudopotentials, such subtle changes in the accuracy are the ingredients for the penalty function. Indeed, the loss of the accuracy of the valence eigenvalues when turning off the confinement entirely can typically be two orders of magnitude larger. Yet, high accuracy for matching orbital properties is a useful tool to construct high quality pseudopotentials and a needed indicator to compare results on the fly while fitting.

For these reasons, it can be beneficial to solve the ground state configuration of the atom for two or more different values of r_{prb} and to construct the penalty function as a weighted sum or average. One configuration will usually have more weight than the others, unless the strength of the confinements is very similar. This allows to monitor high accuracy for one system, while using the atoms with different confinements as extra terms like the excited states. The resulting pseudopotential is expected to match over a wider range of r_{prb} for the confinement, which in return can be understood as a tool to improve the pseudopotentials transferability.
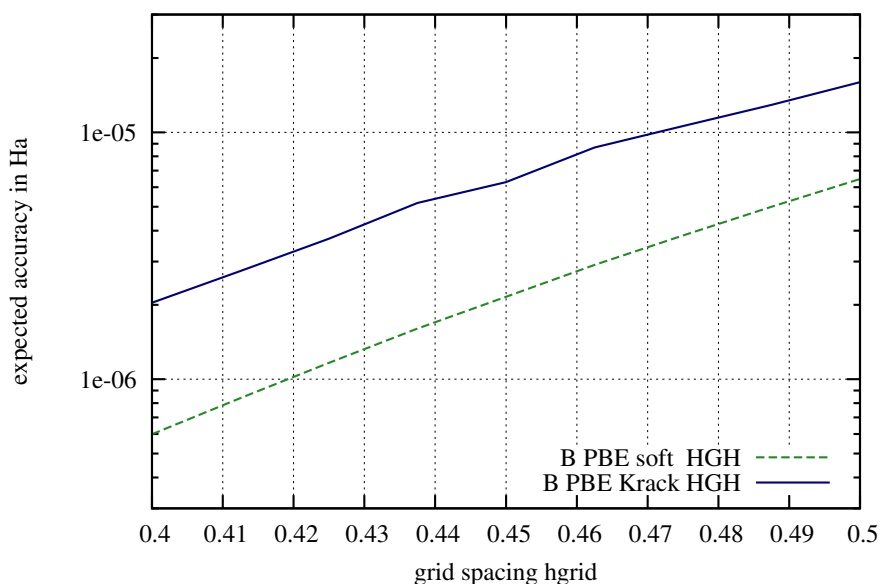
Figure 4.3: Expected accuracy as a function of the wavelet grid spacing parameter *hgrid* (4.31) for a conventional HGH pseudopotential [36] and an improved fit for enhanced softness. Both pseudopotentials are optimized for Boron (B) and the PBE XC functional.

4.7 Wavelet transformations for improved softness

Another major enhancement for the pseudopotential generation scheme is the inclusion of a sophisticated penalty term for considerations of softness. The idea is to capture this property much in the sense softness is experienced in a DFT calculation with the *BigDFT* package. There the grid spacing for the wavelet basis set is a key parameter for tuning the computational costs and the relative accuracy of a calculation. The softer the pseudopotential is, the coarser is the grid spacing that will be needed to meet a desired accuracy requirement. In return, the expected accuracy for a wavelet basis set in dependence of the grid spacing gives a systematic measure to compare the softness of various pseudopotentials.

Figure 4.3 illustrates the softness in terms of expected accuracy versus grid spacing for the example of two Boron PBE pseudopotentials. One of the two pseudopotential was optimized using a penalty term for improved softness. It gives about the same overall accuracy and transferability as the conventional HGH PBE pseudopotential by Krack [36], but the convergence of the discretization errors is much faster. Compared to the conventional pseudopotential, the grid spacing can be increased by about ten percent in this case, which corresponds to a reduction of the memory requirements by roughly 25 percent and a speedup that may be even larger, but actually depends on multiple factors.

A simple and fast procedure to estimate the expected accuracy is to apply the convolution for the kinetic energy operator to the wavelet representation of an atomic orbital and then to compare the result with the analytic value in a given Gaussian basis set. So to assess the softness during the optimization of the pseudopotential, the radial valence orbitals are transformed from a Gaussian basis to Daubechie wavelets on a Cartesian grid. This procedure is repeated for several values of the grid spacing and the deviations are summed up giving more weight to the deviations on the denser grids. The reason for the use of multiple grid spacings is to avoid a situation where the smoothness of the pseudovalence is adapted to

the sensitivity of a certain grid. The actual range of the grid spacing h is user defined, typically taking values of about 0.7 to 1.5 times the local radius r_{loc}. Since the theoretical convergence rate with respect to the grid spacing h of the wavelet basis is known to be of the order h^{14}, the same power law is used for the summation of the deviations per grid spacing. These enter the penalty function of the fitting scheme with a user defined overall weight w_{soft}. The resulting weights (4.30) for summing up the penalty term (4.31) are shown below.

$$w_h = \left(\frac{h_{min}}{h}\right)^{14} \; ; \; q_{soft} = \sum_h w_h \tag{4.30}$$

$$P = \left(\frac{w_{soft}}{q_{soft}}\right)^2 \sum_h w_h^2 \left(E_{kin}(g) - E_{kin}(h)\right)^2 \tag{4.31}$$

In this short notation $E_{kin}(h)$ denotes the kinetic energy obtained in a wavelet representation with an underlying grid spacing of h atomic units, while h_{min} stands for the densest grid spacing. $E_{kin}(g)$ is the reference value of the kinetic energy in a basis set of up to thirty atomic centered Gaussians. This procedure allows to minimize the deviations in the kinetic energy directly over a certain range of grid spacings, effectively improving the pseudopotentials softness for usage with the BigDFT code.

4.8 Empirical penalty terms

Another enhancement of the penalty function is composed of simple terms that directly act on the free parameters of the pseudopotential. These empirical terms are straightforward to include and were added for two reasons: First, it was experienced that long chains of fitting cycles may result in pseudopotential parameters that lead to numerical instabilities and have to be adjusted by hand. Keeping the parameters in a predefined range in the first place may help to improve the process of fitting. Second, it may be desirable to enforce a different value for some parameters in order to explore different local optima of the pseudopotential problem. Doing so with a smooth transition driven by the penalty function can be much more efficient than an abrupt change of the input parameters of the pseudopotential. The latter typically results in poor convergence for the self consistency cycle of the pseudo-atomic code, such that further fitting may be difficult.

The empirical penalty summands to keep the free parameters in a desired range penalize large coefficients of the separable part (4.32) and for the spin orbit splitting (4.33) which helps to avoid unstable regions in the free parameter space.

$$P_h = w_{sep} \sum_{\ell,i,j} \left(\frac{h_{i,j}^\ell}{10}\right)^{12} \tag{4.32}$$

$$P_k = w_{sep} \sum_{\ell,i,j} \left(\frac{k_{i,j}^\ell}{0.5}\right)^{12} \tag{4.33}$$

The terms (4.32) and (4.33) are obviously equivalent, while the weights are defined such that the input parameter w_{sep} controls the penalty contribution of $h_{i,j}^\ell$ in the order of ± 10 or $k_{i,j}^\ell$ of about $\pm\frac{1}{2}$, while coefficients of smaller magnitude lead to much lighter penalty terms. In the same spirit, an empirical penalty term can be enabled to avoid narrow radii (4.34), which can be useful for considerations of softness.

$$P_r = \left(\frac{h_{max}}{r_{loc}}\right)^{12} + \sum \left(\frac{h_{max}}{r_\ell}\right)^{12} \tag{4.34}$$

Here the tolerance length scale h_{max} is actually the same input parameter that is used for the systematic evaluation of the pseudopotentials softness via wavelet transformations, where it stands for the coarsest grid spacing of the wavelet basis set.

Penalizing the localization radii can be a simple trick to keep the pseudopotential soft, because localization radii of the projectors or the local part that get very short lead to problems for resolving the pseudopotential on a real space grid. On the other hand, if the length scales get too wide, there might result problems with the pseudopotentials locality. Another empirical penalty term (4.35) can therefore be used to avoid long range terms in the difference function between the local part and the central potential given by an ionic point charge.

$$P_{loc} = w_{loc} \int_{r_{cov}}^{\infty} V_{loc} + \frac{Z_{ion}}{r} \ dr \tag{4.35}$$

This can be helpful as a constrain when fitting the pseudopotential for optimal softness. Each of the above penalty terms related to the pseudopotential is controlled with an individual weight. The set of new weights introduced to enhance the penalty function are summarized below, taking into account the summands described earlier as well.

- matching of energy differences for all configurations
- weight multipliers per configuration for orbital properties
- softness assessed via wavelet transformation
- empirical terms to prevent hard projectors
- empirical terms to prevent narrow radii
- empirical weight for a compact local part

4.9   Inclusion of Nonlinear Core Corrections

A major improvement of the fitting scheme for HGH pseudopotentials is the inclusion of nonlinear core corrections (NLCC). In essence, the charge distribution of the core orbtials is approximated by some model function, which is added to the pseudovalence charge whenever the exchange correlation (XC) terms are evaluated. As described earlier, this provides a simple and effective method to reduce errors resulting from linearization effects, especially when spin polarized atoms are considered. Unlike most implementations of NLCC, our scheme uses a very simple analytic form for the entire model core charge and no cutoff radius is utilized beyond which the reference core charge is matched precisely. There are two reasons for these considerations. First of all, the pseudopotentials shall remain as soft as possible, and according to our observations, a smooth and simple shape for the core charge distribution is highly beneficial in this regard. Second, a minimalistic analytic form of the core charge with few adjustable parameters allows to fit the core charge in tandem with all other pseudopotential parameters. This means that the core charge for the nonlinear corrections can adapt to the features of the pseudopotential and vice versa. As the shape of the pseudovalence differs from its all electron counterpart, the true core charge is not necessarily the best ingredient for a nonlinear correction to accurately match reference properties such as atomic polarization energies. Treating the coefficients and width of the core charge as free fitting parameters, such properties can be optimized efficiently and with great flexibility.

The actual parameters of the model core charge are defined as the localisation radius r_{core} and the fraction C_{core} of the total core electron charge $Z_{nuc} - Z_{ion}$ (4.36).

$$\rho_{core}(r) = C_{core} \frac{Z_{nuc} - Z_{ion}}{\left(r_{core}\sqrt{2\pi}\right)^3} \ exp\left(-\frac{1}{2}\left(\frac{r}{r_{core}}\right)^2\right) \tag{4.36}$$

The idea is to ease the comparison of core charges for various elements, using a parameter in the range from zero to one, rather than the amplitude or total charge of the Gaussian.

During the course of implementing and testing nonlinear core corrections for HGH pseudopotentials, more complicated forms of the core charge (4.37) have been tried and rejected, as the best results were indeed obtained with a single atomic centered Gaussian for the charge(4.36).

$$\rho_{core}(r) = \sum_g exp\left(-\frac{1}{2}\left(\frac{r}{\sigma_g}\right)^2\right)\left(\sum_{k=1}^{n\leq 4} C_{g,k}\ r^{2k-2}\right) \tag{4.37}$$

The more general form of the core charge was found to be less reliable, especially for calculations carried out in the generalized gradient approximation (GGA), as the XC functionals tend to be very sensitive to steep changes of the density gradient. In this regard, the use of a single Gaussian for the core charge is preferred not only for considerations of the pseudopotentials softness, but it is also an essential part of our strategy to obtain the highest possible accuracy and robustness for our NLCC scheme.

4.10 Treatment of collinear spin polarization

One particular objective for improvements to the fitting procedure for HGH type pseudopotentials is the treatment of spin polarized atoms. As mentioned earlier, the presence of nonlinear core corrections is mainly beneficial for systems with net magnetic moments, so in order to fit the NLCC dynamically, it is absolutely necessary to consider spin polarized configurations during the process of optimizing the pseudopotential parameters. For this purpose, a spin polarized implementation of the exchange correlation functionals is necessary, with the corresponding interfaces and treatment of spin densities in both, the all electron code that generates the reference data for the fit as well as the routines that solve the pseudo-atomic problem dynamically during the fit. For this reason, the closed shell LDA and PBE exchange correlation libraries found in previous versions of the two codes were replaced with interfaces to the *libXC* package, a large and portable library of exchange correlation functionals which is also supported by the *BigDFT* code. This allows the direct comparison of the results and enables the largest possible variety of functionals in a form easily accessible for a spin polarized DFT calculation. Some of the technical details of the corresponding modifications to the atomic programs are described in a previous chapter about practical considerations for atomic DFT codes. While said chapter describes atomic all electron calculations in particular, the very same concepts apply to the atomic pseudopotential code as well.

4.11 Energy terms with Nonlinear Core Corrections

When nonlinear core corrections are included, the expression that relates the Kohn Sham energy to the band structure energy (1.44) depends on the charge density of the valence ρ and the core electrons ρ_c. While only the former is related to the Kohn Sham orbitals, the latter is represented with some model density and only used for evaluating the exchange correlation terms, $E_{xc}(\rho + \rho_c)$ and $V_{xc}(\rho + \rho_c)$. This needs to be taken into account when relating the Kohn Sham eigenvalues to the total energy term and results in a modified expression for the Kohn Sham energy (4.38).

$$E(\rho) = E_{BS} + E_{xc}(\rho + \rho_c) + E_{n-n} - \int \rho\left(V_{xc}(\rho + \rho_c) + \frac{1}{2}V_H\right)d^3\boldsymbol{r} \tag{4.38}$$

When computing the Kohn Sham energy, care must be taken that for the integral term that is subtracted from the band structure energy, the valence charge density ρ and not the total charge density $\rho + \rho_c$ is multiplied with the exchange correlation potential $V_{xc}(\rho + \rho_c)$.

A typical implementation of the exchange correlation terms will access some library of XC functions for a given charge density on some grid and then return both, the exchange correlation energy and the integral of the density times the exchange correlation potential on the grid. In this case, the volume integral (4.39) of said potential times the core charge ρ_c has to be subtracted out after executing the exchange correlation routines.

$$\int V_{xc}(\rho + \rho_c) \, \rho_c d^3 \boldsymbol{r} \tag{4.39}$$

Another question to keep in mind when working with NLCC and GGA functionals is how the White-Bird terms should be incorporated, i.e. the contributions to the XC-Potential from partial derivatives with respect to the density gradient, as discussed in a previous chapter. The relevant formula (2.48) is readdressed for the presence of a core charge ρ_c for NLCC (4.40), using the variation of the energy in the sense of equation (3.42).

$$V_{GGA} = \frac{\partial \epsilon_{xc}(\rho + \rho_c, \nabla(\rho + \rho_c))}{\partial(\rho + \rho_c)} - \left\langle \nabla \left| \frac{\partial \epsilon_{xc}(\rho + \rho_c, \nabla(\rho + \rho_c))}{\partial \nabla(\rho + \rho_c)} \right. \right\rangle \tag{4.40}$$

Here only the total charge density $(\rho + \rho_c)$ enters the equation, yet there can be differences in how the two contributions to the density gradient $\nabla \rho_v + \nabla \rho_c$ are computed. The model core charge ρ_c and therefore its gradient is expressed analytically, while the partial derivatives of the exchange correlation energy density ϵ_{xc} are only accessible per real space grid point. For this reason, it is not possible to evaluate the gradient of the second summand in equation (4.40) in precisely the same manner as the density gradient is obtained from the two density terms. This finding may be a reason why it is important to pick a very smooth and simple curve for the model core charge ρ_c, such that strong variations of the density gradient are avoided.

As a final side note, it can be useful to subtract out the exchange correlation term resulting from the core charge interacting with itself(4.41), since the resulting shift in the total energy expression gives an arbitrary offset.

$$E_{xc}(\rho_c) + \int V_{xc}(\rho_c)\rho_c d^3 \boldsymbol{r} \tag{4.41}$$

Of course, the absolute value of the total energy in a pseudopotential based calculation is not physically relevant, in contrast to energy differences, yet it is convenient to avoid a potentially large offset when comparing different pseudopotentials.

4.12 Guidelines for generating HGH pseudopotentials

As mentioned earlier, the construction of a GTH-HGH pseudopotential can be a delicate task. A unique solution for a set of optimal pseudopotential parameters does not exist, and the number of pseudopotentials of comparable quality may increase abruptly as one moves to more complex pseudo-atoms. The complexity of the pseudo-atomic system stands for the number and character of valence orbitals to be pseudized, the features of the underlying frozen core and most notably, the presence of semicore orbitals. As discussed in the previous sections, there is much freedom to pick a set of properties to be fitted and to assign weights for constructing a penalty function. Furthermore, it can be challenging to assess a minimal set of pseudopotential parameters, and even if all weights of the penalty function and all free parameters are given, many local minima are possibly found.

On the other hand, if no a-priori information is available, it is extremely difficult to guess for a set of pseudopotential parameters that are suitable to describe a third row element or a heavier atom. The procedure to solve the pseudo-atoms Kohn Sham equations may fail to converge properly, which makes

the assessment of the simplex penalty value problematic or even impossible, so no improvements to the pseudopotential can be made by means of fitting. If the search for a pseudopotential gets stuck in such a way, it is necessary to start over again or to adjust the parameters by hand, which involves much trial and error.

For these reasons, it is very important and useful to start the optimization of the pseudopotential parameters from a reasonable input guess. A typical task is to construct a new pseudopotential for a particular exchange correlation functional. In this case, it is highly beneficial to start from a HGH pseudopotential that was already generated for a similar XC functional, for example a PBE fit [36] can be used as the starting point for use with another GGA functional. Alternately, LDA pseudopotentials that are also available for most elements of the periodic table [34] may provide a more robust input guess, and they tend to lead to softer pseudopotentials.

A remarkable property of HGH pseudopotentials that may help for the construction of input guess parameters are trends across the periodic table. If pseudopotentials are available for neighboring chemical elements, a guess for some parameters can be obtained by simple interpolation. It must be emphasized that highly accurate pseudopotentials require further optimization and are not directly accessible by interpolation. On the other hand, trends of the pseudopotential parameters for a set of chemical elements can be a very useful constrain. If multiple solutions are available for a certain element or set of elements, checking for trends across the periodic table may give a valuable clue which pseudopotentials should be picked and further optimized. In return, if only one solution is available, it may be difficult to search for other, possibly better minima of the penalty function. In that case, it can be a useful strategy to manipulate a single parameter of the pseudopotential such that a trend across a set of elements is established. As mentioned in the section about empirical penalty terms, such adjustments can be rather difficult to achieve and require careful optimization of the remaining parameters.

One particular pseudopotential parameter that needs to be tuned with special care is the local radius r_{loc}. As previously noted and visualized in figure 4.1, this length scale is a key parameter for the softness of the pseudopotentials local part. In general, it is advised to keep this quantity fixed during the fit, and to make adjustments to r_{loc} only by gradually changing the input pseudopotential in a sequence of fitting cycles, such that the remaining parameters can be adapted accordingly. One reason not to use r_{loc} as a free fitting parameter is that the Gaussian basis set is scaled with respect to r_{loc}, so when several fitting cycles are performed with an evolving value of r_{loc}, the basis set parameters should be checked and adjusted accordingly. A more serious problem with dynamic fitting of r_{loc} is that this parameter may take quite a large value and still produce low penalty terms for some atomic configurations, even though the local part of the pseudopotential gets too smooth to ensure good transferability properties. This can be related to the concept of core radii in other pseudopotential methods, which must be sufficiently small to obtain a transferable pseudopotential. However, clear rules or guidelines for a save range of r_{loc} are difficult to establish, so in practice, it may be necessary to generate several pseudopotentials with different values of r_{loc} and to test them for their transferability.

Another noteworthy point is the assessment of the confining potential, as already explained in the corresponding section of this chapter. If higher unoccupied orbitals are of interest, the confinement should be rather strong, i.e. relatively small values of r_{prb} are necessary. On the other hand, when excitation energies and polarization energies are included in the penalty function, it turns out that weaker confinements allow a more accurate description of these terms. In any case, it is important that both the all electron reference data as well as the pseudo-atoms orbital properties are well converged, i.e. sufficiently dense grids and basis sets are used. Furthermore, the corresponding plots of the radial density distributions should always be checked carefully: All orbitals should appear as smooth and continuous curves, the pseudovalence should have no wiggles in the core region and the difference to the valence orbitals should decay rapidly. If one of these points is not fulfilled, it is likely that something went wrong, for example with the choice of the Gaussian basis set.

4.13 Fitting of HGH pseudopotentials with NLCC

In the following section, the strategy for the construction of those pseudopotentials is discussed in detail for which benchmark results are presented in the next chapter.

The input guess for the pseudopotentials was taken as the set of GTH pseudopotentials [33], a collection of parameters fitted to non-relativistic LDA data for chemical elements up to the third period. This input guess was preferred to a set of PBE pseudopotentials [36], as the GTH potentials typically have a simpler form and since a significant change of the pseudopotential parameters is to be expected with the inclusion of nonlinear core corrections (NLCC). Furthermore, the GTH pseudopotentials expose clear trends across the periodic table. Since the local radius r_{loc} was held constant during the optimization of the pseudopotential, at least this parameter will share such trends with the GTH pseudopotentials. Finally, relativistic effects were not included for the NLCC HGH pseudopotentials, so it is also reasonable to take the non-relativistic GTH potentials as input guess.

As stated in the section about NLCC, the model core charge takes the very simple form of a single Gaussian, which is initially fitted to the density of the all electron core orbitals and held constant during the first stage of the pseudopotential generation. For all elements, the GTH pseudopotential in conjunction with NLCC based on this core charge was found to give rather large initial errors, yet the fitting procedure quickly converges to an accurate set of parameters for most systems when executed in serial and taking only the closed shell atom as reference configuration. Once a decent NLCC-pseudopotential is obtained, further configurations are added to the fit, including the lowest energy configuration according to Hund's rule, as well as occupancies where half an electron is removed, added or excited. The trade-off between the accuracy of the various configurations makes it much more difficult to find a well defined optimal set of pseudopotential parameters compared to the serial stage of the optimization. A highest accuracy of about 10^{-6} Ha is thus enforced for the closed shell atom only, while moderate accuracy of about 10^{-4} Ha is achieved for the valence orbitals of the remaining configurations. It is found that accurate corrections for spin effects are obtained when the atomic polarization energies are well reproduced, while a highly accurate description of the polarized atoms orbitals is much less important. In order to obtain the highest possible accuracy for the energy differences between the closed shell atom and the spin polarized ground state, it is beneficial to free the parameters of the model core charge for the NLCC. During a last stage of optimization, the width r_c and charge fraction q_c of the core density can vary quite a bit, and so do the pseudopotential parameters as they are adapted to the dynamically evolving NLCC and vice versa. As already mentioned, this strategy differs from conventional NLCC schemes, as the core charge in the valence region is not restricted to that of the all electron orbitals. Instead, the Gaussian is allowed to relax such that the NLCC gives the best possible correction to accurately reproduce the all electron polarization energies.

All pseudopotentials were carefully tested for their accuracy and transferability by computing the atomization energies of the molecules in the G2-1 test set. In some cases, the pseudopotential parameters had to be reinvestigated to obtain desirable results, and indeed chemical accuracy has been achieved as will be presented in the next chapter. One notable problem with the fits derived from the GTH pseudopotentials was related to the fixed local radii r_{loc} of the third row elements. In particular for silicon, phosphorous and sulphur it was found that more narrow r_{loc} are necessary when NLCC are added to the GTH potentials, and careful adjustment of these parameters for the third row elements has lead to a systematic improvement of all results.

Even though it is to be expected that a conventional hydrogen pseudopotential for the PBE functional will give highly accurate results, it was found that replacing said pseudopotential with a new fit that was optimized for several configurations of the non-relativistic hydrogen atom lead to a systematic improvement of the results especially for the organic compounds of the G2-1 test set.

Some trends across the periodic table with the novel pseudopotentials for third row elements are shown in figure 4.4. For convenience, localization radii are shown, which also include the width r_c of the model
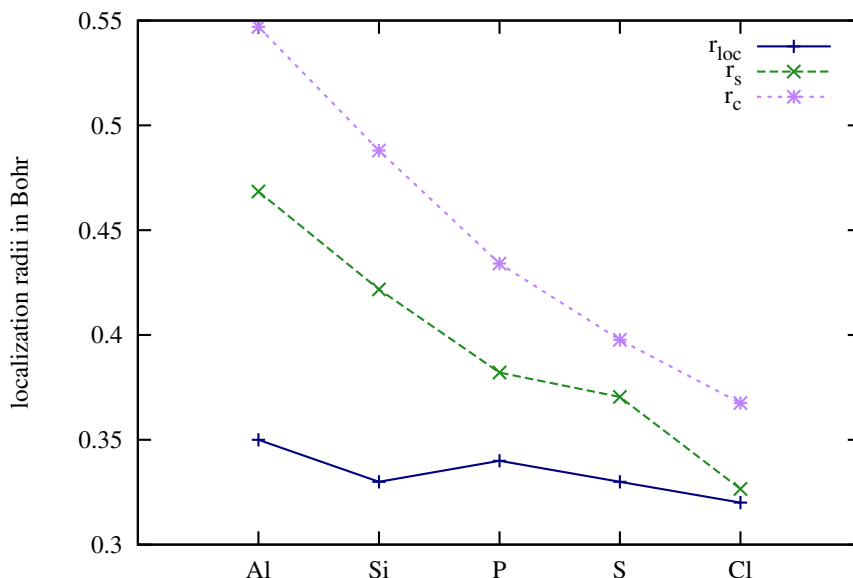
Figure 4.4: Trends across the periodic table for localization radii of NLCC pseudopotentials for third row elements. Shown are the local radii r_{loc}, the localization of the s-projectors r_s and the width r_c of the Gaussian core charge for the NLCC.

core charge. The full set of pseudopotential parameters and all systematic tests to verify their accuracy and transferability are presented in the next chapter.

4.14 Strategies for generating soft HGH potentials

In the closing section of this chapter, the aspect of the pseudopotentials softness is readdressed. In fact, the search for a systematic procedure to enhance the softness of the HGH pseudopotentials while conserving their remarkable accuracy and transferability was a key aspect for the revisions presented in this chapter. Indeed for some systems the inclusion of a systematic penalty term for the pseudopotentials softness allowed to achieve this goal with no serious trade-off. One such system is the Boron atom, for which a fit for the PBE XC functional was mentioned in the small section about wavelet based softness estimates. In that section the corresponding gain of softness as shown in figure 4.3 was used to illustrate the concept. Also for several other elements of the second period, including carbon, nitrogen and oxygen, surprisingly soft and reliable pseudopotentials could be generated. It should be noted that some applications of soft pseudopotentials are given in the last chapter. However, it turns out that for other systems the search for softer, yet equally transferable pseudopotentials can be very demanding or exceedingly difficult.

The reason for this is closely related to the problems mentioned in the section about fitting guidelines. While for some pseudopotentials, the mere addition of a penalty term for softness may be enough to find a new pseudopotential with desirable properties, the situation is different in most cases. Usually some substantially different local minima of the penalty surface (or rather, the portion of the penalty related to the accuracy) must be explored to find a significantly softer pseudopotential of comparable quality. In return, small deviations from a well tested pseudopotential often lead to a steep trade-off between softness

and accuracy, and the transferability may suffer even more than the accuracy during a local search for softer potentials. Especially for pseudopotentials with semicore electrons it can be tedious to overcome the barriers on the penalty surface that separate different regions of numerically stable pseudopotential parameters. When solving the KS equations of a pseudo-atom with poor pseudopotential parameters, numerical instabilities make it effectively impossible to explore the penalty surface, especially when the entire simplex is stuck with such parameters. Therefore the search for new pseudopotentials, for example with wider localization radii, can involve a lot of trial and error: The pseudopotential parameters need adjustment by hand, while a smaller and coarser Gaussian basis set, low weights for the penalty terms related to accuracy and stronger empirical penalty terms may help to search for distinct input guess pseudopotentials. This type of coarse grained search is done without taking into account the penalty term for softness to speed up the procedure. Once new parameters are found that give no instabilities and decent accuracy in the coarse basis set, the penalty weights are switched back for a focus on accuracy terms, and the basis set is enlarged accordingly. After some further fitting cycles the pseudopotential may restore most of the accuracy paid during the brute force search. However, the entire procedure may need to be repeated if the resulting accurate pseudopotential is not any softer than comparable pseudopotentials, or if sufficient accuracy cannot be achieved at all.

The trial and error in the search for softer pseudopotentials is even worse when checking the transferability, as a softer pseudopotential that looks reasonably accurate for some atomic configurations may perform rather poorly when employed in various chemical environments. Again, this can be a reason to discard a pseudopotential and start another search from scratch. It is thus not only difficult to make a larger move on the penalty surface without ruining the pseudopotential, but conserving good transferability properties is even more so. Yet, even if an extended search for softer and reliable pseudopotentials was not successful, it is not certain that the best compromise between softness, accuracy and transferability has already been found.

These problems, together with the fact that the evaluation of the penalty term for softness (4.31) is computationally much more demanding than solving the radial KS equations, make the search for soft pseudopotentials a protracted process. The availability of hardware accelerated subroutines for the wavelet transformations and the corresponding kinetic energy convolutions has improved the situation, but the process is still cumbersome.

For example, dozens of different pseudopotentials were generated and rejected in the attempt to improve the softness of tungsten (W) semicore ($Z_{ion} = 14$) pseudopotentials. Here the valence pseudopotential ($Z_{ion} = 6$) for both LDA and PBE functionals are much softer than the semicores, but they are usually not suitable and give rather large errors, for example for the structure prediction of tungsten clusters. A reasonable compromise between the accuracy of the semicore- and the softness of the valence-pseudopotential could not be found, and the overall gain of softness without losing the accuracy of the conventional semicore pseudopotentials is modest. However, for some lighter chemical elements, like the previously mentioned Boron, the construction of softer pseudopotentials was successful.

As already stated in the previous section, a novel set of HGH pseudopotentials with nonlinear core corrections (NLCC) is presented and thoroughly benchmarked in the next chapter. It can be noted that for this work, the focus is on the construction of pseudopotentials with the highest possible level of accuracy and transferability, in particular to reach chemical accuracy for several well established chemical test sets. Therefore no penalty terms or fitting strategies related to softness were taken into consideration. Nevertheless, the resulting set of pseudopotentials conserves the softness properties of the conventional HGH-PBE pseudopotentials [36], so improvements resulting from the inclusion of NLCC have not lead to any trade-off in this regard.

Chapter 5

Norm-conserving pseudopotentials with chemical accuracy compared to all-electron calculations

By adding a non-linear core correction to the well established Dual Space Gaussian type pseudopotentials for the chemical elements up to the third period, we construct improved pseudopotentials for the Perdew Burke Ernzerhof (PBE) [37] functional and demonstrate that they exhibit excellent accuracy. Our benchmarks for the G2-1 test set show average atomization energy errors of only half a kcal/mol. The pseudopotentials also remain highly reliable for high pressure phases of crystalline solids. When supplemented by empirical dispersion corrections [12, 13] the average error in the interaction energy between molecules is also about half a kcal/mol. The accuracy that can be obtained by these pseudopotentials in combination with a systematic basis set is well superior to the accuracy that can be obtained by commonly used medium size Gaussian basis sets in all-electron calculations.

5.1   Introduction

During the last decades, density functional theory (DFT) has proven its pivotal role for computational studies in the fields of condensed matter physics and quantum chemistry. Particularly the Kohn-Sham (KS) formalism of DFT has gained enormous popularity as an *ab initio* method applicable to relatively large systems. An essential ingredient for many large scale implementations of KS-DFT are pseudopotentials which are also frequently denoted as effective core potentials. By eliminating the strongly bound core electrons pseudopotentials reduce the number of occupied electronic orbitals that have to be treated in an electronic structure calculation. In addition the valence wavefunctions arising from a pseudopotential are much smoother than the all-electron valence wavefunction in the core region, since the orthogonality constraints to the rapidly-varying wavefunctions carrying core electrons are missing. Since it is not necessary to describe rapidly varying wavefunctions the size of the basis set used for their representation can be reduced. These two factors lead to a significant reduction of the computational effort of a pseudopotential calculation compared to an all-electron calculation.
Even though it is well known that the valence electrons are responsible for the majority of chemical and physical properties of atoms, pseudopotentials have to be constructed very carefully in order to reproduce the properties of the all-electron atom accurately. If a pseudoatom, i.e an atom described by a pseudopotential, reproduces the all-electron behavior accurately for any chemical environment the pseudopotential is said to be transferable.

Pseudopotentials (PSP's) are an essential ingredient of most electronic structure codes and different solutions are implemented in present-day DFT codes. Traditional norm-conserving (NC) approaches, e.g. [38] are formally the simplest approach, since they give rise to pseudowavefunctions which lead to a valid charge density. By introducing atomic like orbitals as additional basis functions any atomic Hamiltonian arising either from an all-electron potential or from a norm conserving pseudopotential [39] can be transformed into an Linearized Augmented Plane Wave (LAPW) like Hamiltonian [40, 41, 42]. The widespread Projector-Augmented Wave (PAW) methods [43] and the ultrasoft pseudopotentials [44] are derived by such a transformation from an all-electron atom Hamiltonian. The number of required basis functions is reduced by this transformation, but the calculation of the charge density is more complicated and a generalized eigenvalue problem has to be solved even for the case of an orthogonal basis set. For applications in quantum chemistry, effective core potentials [45, 46, 47] are often optimized for a certain basis set and usually employed for heavier elements only.

In this paper, the Dual Space Gaussian pseudopotentials of Goedecker-Teter-Hutter (GTH) and Hartwigsen-Goedecker-Hutter (HGH) [34] PSP are generalized by the inclusion of a Non-Linear Core Correction (NLCC) term. These new pseudopotentials are able to provide an accuracy that is comparable to that of the very best all-electron calculations.

The starting point for understanding why pseudopotentials work is the subdivision of space into muffin-tin spheres centered on the atom in a molecule or solid and the remaining interstitial region [48]. A non-selfconsistent Schrödinger equation can be solved exactly in the interstitial region if one knows the scattering properties on the surface of the muffin-tin spheres [49]. The scattering properties are typically specified by the logarithmic derivative as a function of energy. This function is the quotient of the radial outward derivative and the functional value of the wavefunction on the surface of the muffin-tin sphere. In this way the boundary conditions are specified which are necessary to integrate the Schrödinger equation, a second order partial differential equation where the amplitude of the solution is fixed by a normalization constraint. A necessary but not sufficient condition for a pseudopotential to be transferable is therefore that the logarithmic derivatives of the all-electron and pseudo-atom agree over the relevant energy interval. The construction of pseudopotentials is typically done using as the reference state a neutral isolated atom which has been spherically symmetrized. This symmetrization can be achieved by using identical and generally fractional occupation numbers for all the orbitals with the same n and ℓ quantum numbers, e.g. for the set of $2p_x$, $2p_y$ and $2p_z$ orbitals. The norm conservation condition [50] ensures that the logarithmic derivative function describes well the scattering properties of a muffin-tin sphere containing the charge distribution of this reference configuration. In a selfconsistent calculation the charge distribution changes however when the free atom is inserted in a molecule or solid and the potential in the muffin-tin region will in general differ from the potential within a muffin-tin sphere of the same radius around the reference atom. Hence the scattering properties change and the pseudopotential constructed using the charge distribution in the muffin-tin sphere of the isolated atom might not well reproduce these modified scattering properties of a new chemical environment. Due to screening effects there exists however an invariant muffin-tin sphere within which the total electronic charge distribution is nearly independent of the chemical environment [51]. The radius of this invariant muffin-tin sphere is a fraction of the covalent bondlength and thus considerably smaller than the muffin-tin radii used in other methods such as the LAPW method. The scattering properties of this invariant muffin-tin sphere hardly vary as a function of the chemical environment of the atom. If the separable terms of a pseudopotential as well as the difference between the local part of the pseudopotentials and the pure coulombic potential remain localized within this invariant sphere the pseudopotential is expected to be highly transferable. This recipe was followed in the construction of the GTH [33] and HGH [34] pseudopotentials which are indeed well transferable for non-spinpolarized systems.

Despite the fact that the total charge in the invariant muffin-tin sphere is nearly identical in different chemical environments, the spin polarization is not, as illustrated in Fig. 5.1. Shown are the changes in the radial charge and spin densities if one adds half an electron to the unoccupied spin channel of
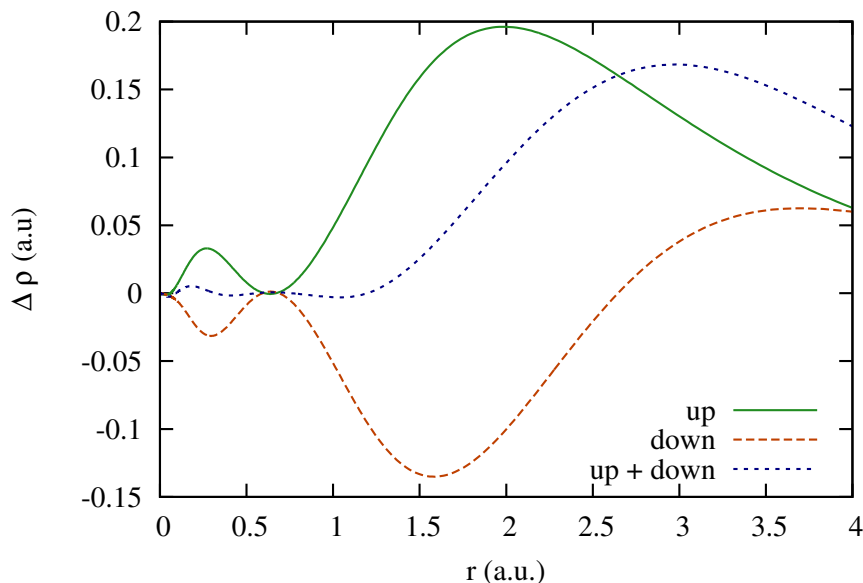
Figure 5.1: Difference in the radial spin densities and total charge density when adding half an electron to a phosphorus atom ($[Ne]3s^23p^{3.5}$). The inert core region of the total charge is not observed for the individual spin densities.

the $3p$-orbital. For spin polarized calculations the concept of an invariant muffin-tin sphere is therefore not applicable. One possibility to overcome this problem is to construct pseudopotentials which have an explicit spin dependence [22]. The other possibility is to include nonlinear core corrections (NLCC) [23] in the pseudopotential.

In the NLCC schemes the spin and charge densities in the muffin-tin sphere are not just the ones from the valence electrons treated explicitly by the pseudopotential but they are both the respective sums of the valence charge and the core charge given by the nonlinear core correction. Since the core electrons can be considered to be frozen, i.e to be invariant with respect to different chemical environments, this core charge is fixed once and for all. It is obvious that the spin polarization, i.e. the quantity $\theta(\boldsymbol{r}) = (\rho_{up}(\boldsymbol{r}) - \rho_{down}(\boldsymbol{r}))/(\rho_{up}(\boldsymbol{r}) + \rho_{down}(\boldsymbol{r}))$ is very poorly represented without a core charge. If for instance all valence orbitals are spin up then the spin down charge density $\rho_{down}(\boldsymbol{r})$ would be zero and the spin polarization θ would be equal to one. In the real atom θ is not equal to one in the core region since the core electrons are never spin polarized. Since the density of the core electrons is much larger than the density of the valence electrons in the core region the spin polarization actually has typically small values. These correct small values of θ are reestablished by the core charge of a NLCC pseudopotential and exchange correlation functionals can provide reliable total energies. Nonlinear core corrections have therefore the potential to substantially improve the description of spin polarized states.

Whereas previous implementations of NLCC pseudopotentials [52] tried to faithfully represent the core charge, we follow here another approach. In the spirit of the GTH pseudopotentials where all terms have simple parametrized analytical forms we also represent the core charge density just as one single Gaussian. The amplitude and width of this Gaussian core charge distribution are then optimized by a fitting procedure in the same way as the other parameters of the pseudopotential.

5.2 Methodology

The procedure for constructing the NLCC pseudopotentials is very similar to the one used for the construction of the GTH and HGH pseudopotential. In contrast to the original GTH and HGH pseudopotentials which were fitted to a single atomic configuration, the new NLCC pseudopotentials are fitted not only to the ground state but also to several excited and ionized electronic configurations where half an electron is added or removed possibly to or from different valence orbitals. The atoms are always considered to be spherically symmetric, but some of the configurations used for the fit have a spin polarization. The parameters of the dual space Gaussian ansatz [33] are fitted such that:

- The occupied and first few unoccupied valence eigenvalues of the all-electron and pseudo atom match for all configurations used in the fit.

- The charge inside the inert region of the pseudo atom matches the all-electron valence charge in the same region for all the orbitals for which the eigenvalues are matched for all configurations used in the fit. This means that the pseudopotential is norm conserving for all the configurations used in the fit.

- A high precision of 10^{-6} a.u. is achieved for valence eigenvalues and charge integrals of the non-polarized ground state, whereas only a moderate precision of 10^{-4} a.u. is enforced for all other orbitals and configurations considered.

- The total energy differences of the all-electron atom are reproduced for all configurations used in the fit.

- The spin polarization energies of the all-electron atom are reproduced for all spin polarized configurations used in the fit.

Since the considered quantities are fitted for several configurations atomic transferability is already built in to these new pseudopotentials by construction.

The core charge is represented by a single Gaussian which is optimal for numerical efficiency. It is initialized such that it approximates well the physical core charge density and it is held fixed during an initial stage of the fit. Then both the amplitude and the width of the Gaussian are released and considered as fitting parameters. As a consequence the total amount of core charge and the width can differ from the physical value.

The parameters of the core charge constitute thus a small set of only two additional degrees of freedom. Yet this allows to optimally reproduce atomic polarization energies without degrading the transferability and accuracy of other atomic properties. It was found that the inclusion of a more complicated core charge is not beneficial. Furthermore, it should be emphasized that the novel NLCC pseudopotentials are not harder than their HGH counterparts. The smoothness of the core charge seems to play an important role for the fact that the hardness is not affected, and roughly the same grid spacings or energy cutoffs can be employed as for conventional HGH pseudopotentials.

In particular, pseudopotentials with NLCC were generated for boron, carbon, nitrogen, oxygen, fluorine, aluminium, silicon, phosphorous, sulfur and chlorine. Very weak spin dependences are expected for the rare gasses, and for all remaining chemical elements up to the third row, NLCC are found to be unnecessary, as HGH pseudopotentials are available that either include semicores (sodium and magnesium) or leave no core states at all (hydrogen, lithium and beryllium). For the special case of hydrogen, it was found that the multi configuration fit gave slightly improved results even though obviously no core charge was added. Since the focus of this paper is on systems made out of light elements, no relativistic effects such as spin-orbit coupling were included in the pseudopotentials.

5.3 Computational Setup

To assess the accuracy of the new pseudopotentials extensive calculations were performed for different test sets. The accuracy of covalent bond formation energies was examined for the standard G2-1 test set [53, 54, 55, 56]. For the assessment of the accuracy of non-bonded interactions the S22 [57] test set was used. To check the performance for materials under high pressure we chose carbon, silicon, silicon carbide and boron nitride as test systems.

All pseudopotential calculations were done with the BigDFT package [58]. The BigDFT code uses a systematic wavelet basis set which allows to obtain the exact density functional solution with arbitrarily small error bounds. The parameter were set such that an accuracy of at least 10^{-6} Hartree was obtained. The LibXC library [17] is used within BigDFT for the evaluation of the exchange correlation functional. Semi-empirical van-der Waals corrections were added in BigDFT according to the DFT-D2[12] and DFT-D3[13] methods for the calculations of the S22 test set.

To obtain reliable all-electron reference values for the atomization energies of the G2-1 test set, we performed all-electron calculations with the NWChem software package [59] using one of the largest available Gaussian type basis sets, namely an augmented correlation consistent polarized valence quintuple zeta Gaussian type basis set (aug-cc-pV5Z). Care was taken to disable symmetry detection and to check for the lowest energy spin multiplicity. For the chemical elements Li, Be Na and Mg, the aug-cc-pV5Z set was not available, so the corresponding quadruple zeta set (aug-cc-pVQZ) was used to compute the atomization energies of Li_2, LiF, BeH, Na_2, $NaCl$, MgH and $Mg2$. To obtain the atomization energies of the relaxed molecules, geometry optimizations were carried out using the very same basis set.

Atomic all-electron calculations of the spin polarization energies were done with our non-spherical atomic code, which expresses the wavefunctions as a product of spherical harmonics and radial functions. The radial function are given numerically on a logarithmic grid. The settings were chosen such that a precision of at least 10^{-8} Hartree can be obtained for the total energy. This required angular integration grids of 232 points and multipole representations up to $\ell = 4$. The atomic LSDA reference energies from the National centre of science and technology (NIST)[60] where reproduced within the given precision for all elements considered.

We calculated the atomization energies also with the three different sets of PAW [43] potentials available in VASP [61]. Those PAW potentials are derived from the all-electron atomic Hamiltonian and aim at all-electron accuracy. In order to obtain the required high precision some parameters had to be set to tighter values than the default values. We had to use for the general accuracy (PREC = HIGH ACCURATE and LASPH = TRUE) to activate nonspherical gradient corrections inside the PAW spheres. It was carefully checked that the calculations were converged with respect to the size of the periodic simulation cell. Furthermore, care was taken that the correct spin multiplicity and non-fractional occupations were produced. Hard PAW potentials were available for all required elements except for Li, Be, Na and Mg, for which semicore potentials were used instead. For comparison, all energies were recomputed with a set of default potentials. The third set consists of soft potentials for the elements B, C, N, O and F and default potentials otherwise. For the periodic solids, all-electron calculations have been performed using the full-potential linearized augmented plane wave (FLAPW) and augmented plane wave plus local orbitals (APW + lo) methods as implemented in the WIEN2k[62] software package. We used a reduced muffin-tin radii for all atomic sorts in order to avoid their overlap up to the highest studied pressures. The sphere radii were kept fixed throughout the whole set of lattice parameters to obtain the best possible error cancellation. Semicore states were treated as valence, because high compressions can lead to an overlap of their wavefunctions, which will give a contribution to the energy. Inside the spheres, the partial waves were expanded up to LMAX = 10. The number of plane waves was limited by a cutoff parameter RMTKMAX = 9.0 for all the compounds under consideration. The charge density was Fourier expanded with GMAX = 14 a.u. For the majority of the systems we used a very dense k-points grid ($15 \times 15 \times 15$) to ensure total energy convergence.

H	Li	B	C	N	O	F	Na	Al	Si	P	S	Cl
25.4	6.8	10.4	31.7	72.0	43.7	16.0	5.1	7.1	19.7	43.1	23.8	7.6

Table 5.1: Atomic correction terms in kcal/mol as used for the two step procedure.

All the calculations were done at zero electronic temperature, i.e. no Fermi smearing was used. Zero point energies were not included in any of our results.

5.4 Atomization energies of the G2-1 test

Atomization energies are frequently used to assess the quality of various exchange correlation functionals as well as other approximations used in electronic structure calculations. The Gaussian G2-1 test set [53, 54, 55, 56] is a standard benchmark set of 55 molecules in this context. Since this test set does not contain molecules with the chemical elements B, Al and Mg we added the molecules BH, BH2, AlH, AlH2, Mg2 und MgH. We used this augmented test set to compare our pseudopotential results with all-electron calculations. Because of Hund's rule most isolated atoms are strongly spin polarized. When an atom is inserted into a molecule or solid, its spin polarization is typically strongly reduced. Since standard pseudopotentials are based on a non-spin polarized reference configuration they can typically better describe atoms in molecules or solids than isolated atoms themselves. Since the atomization energy is the difference between the total energy of the molecule and the sum of the total energies of its constituent isolated atoms, the largest contribution to the error in the atomization energy of a pseudopotential calculation comes actually from the atomic energies.

The atomization energies of the molecules in the G2-1 test set were first computed using conventional HGH pseudopotentials [36] for the PBE exchange correlation functional. A comparison with all-electron data is shown in figure 5.2. The spin multiplicity of systems with a net magnetic moment are indicated in brackets and omitted for closed shell systems. Deviations of ±1 kcal/mol are indicated with a (green) shading to relate the errors to the requirements for chemical accuracy.

It is found that the direct computation of the electronic atomization energies with the conventional pseudopotentials leads to significant disagreement with the results obtained in an all-electron calculation. An rather high mean absolute deviation (MAD) of 6.83 kcal/mol to the electron reference values for all 55 molecules in the G2-1 set is found. However, the main contribution to the error in the atomization energies comes from the estimation of the energy of the isolated atoms. Therefore, the atomization energies can be improved significantly by a two step procedure where the atomization energies are calculated as a sum of two terms. The first term is the energy difference between the molecule and the sum of the total energies of isolated, spherical and non-spinpolarized atoms. It thus can be considered as the atomization energy with respect to a set of non-physical atoms. This energy difference is calculated with the HGH pseudopotentials and is fairly accurate since no strong spin polarizations are involved. The second term is the difference in total energy between the real, i.e non-spherical and spin polarized, atom and the previously defined non-physical atom. This second term is calculated with our all-electron program for non-spherically symmetric atoms and is therefore exact. Since the atomic spin polarization energies and energy terms for breaking the spherical symmetry are only a property of the atoms they can be considered as a set of atomic correction terms for the accurate calculation of atomization energies. The atomic correction terms for the chemical elements considered in this study are listed in Table 5.1.

It has to be stressed that these atomic spin polarization energies drop out in most instances such as in the calculation of energy differences in a chemical reaction where only molecules are involved. Using this two step scheme, the errors in the atomization energies are decreased considerably to a MAD of 1.56 kcal/mol. Because of the cancellation effect, this is the accuracy that can be expected in the majority of
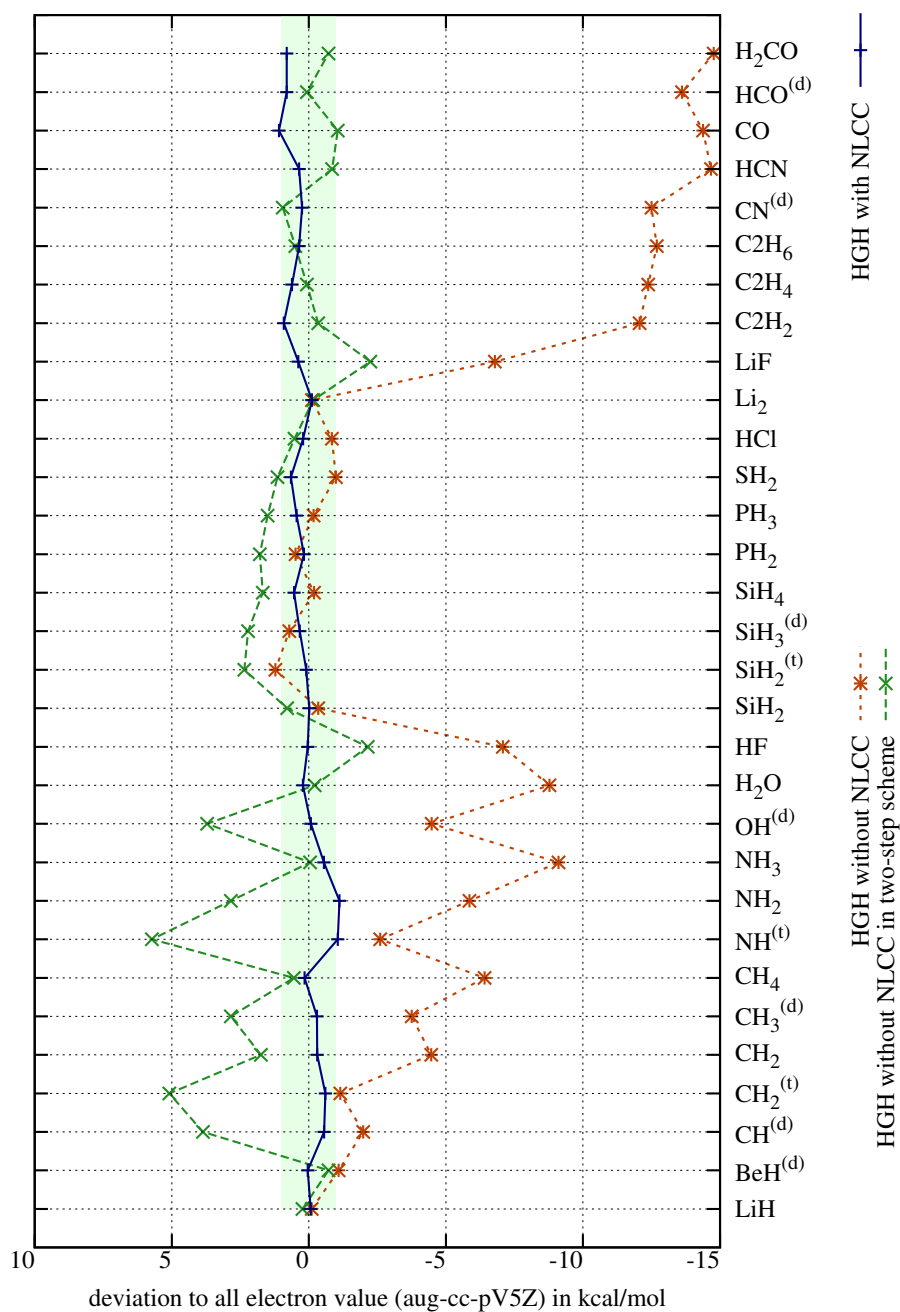
Figure 5.2: Accuracy of PBE atomization energies computed with HGH pseudopotentials. Explanations are in the text.
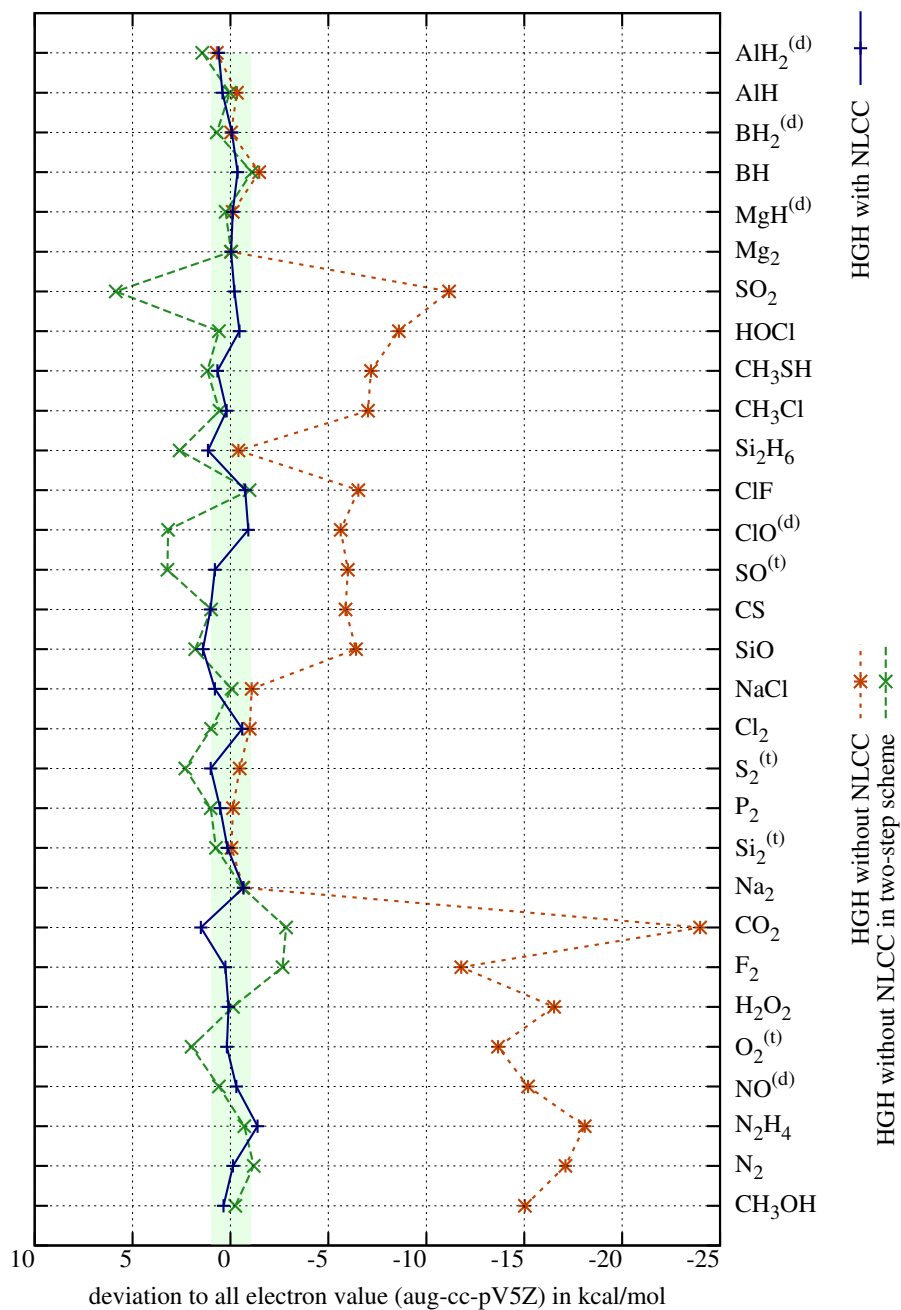
Figure 5.3: Continuation of figure 5.2. Explanations are in the text.

energy differences calculated with the standard HGH type pseudopotentials. The above MAD value was obtained with the bond lengths and angles fixed as given on the computational chemistry comparison and benchmark database[63]. Using instead the equilibrium geometries of each method, i.e. the HGH pseudopotential and the all-electron calculation, the MAD value is slightly decreased to 1.52 kcal/mol. This last value is actually more relevant in practice since atomization energies for an unknown system necessarily have be calculated with theoretically determined geometries.

The new Gaussian type pseudopotential with a NLCC can however still considerably improve the accuracy without the need of using a two step procedure. The error of a direct computation of the atomization energies decreases to a MAD of only 0.52 kcal/mol. Using the equilibrium geometries obtained with the new NLCC pseudopotential the error drops again slightly to 0.51 kcal/mol. More important than this small improvement of the MAD is the fact that the result could be improved for the few molecules where the error was well above the average.

Comparison with the atomization energies obtained by other methods

In figure 5.4 the accuracy of the HGH pseudopotentials with NLCC is shown for relaxed molecular geometries and compared with the results of PAW calculations published by Paier et. al.[64]. In this work hard PAW potentials were used and we were able to reproduce their results. In essence, the absolute errors of the new NLCC pseudopotentials are comparable with those using hard PAW potentials. As shown in Figure 5.6 the accuracy however goes down significantly when one uses the default or even the soft PAW potentials of the VASP package [61]. Furthermore, the same figures shows the discrepancies between all-electron results obtained in two large Gaussian basis sets while keeping the molecular geometries fixed. Even at this size the differences between the two basis sets are not negligible compared to the deviations to other methods and the accuracy of the pseudopotential method is indeed close to the discrepancies between different choices of all-electron reference values. This is quite surprising given the fact that these simple chemical compounds show only straightforward covalent type bonding properties which are certainly easier to describe with a Gaussian basis set than other more complex bonding patterns. It has also to be stressed that the computational cost rises very steeply when one goes from a medium size basis set to these very large basis sets. This is in contrast to the wavelet method where a modest decrease of about 15 percent in the grid spacing h results in an gain of a factor of ten in accuracy because of the high order convergence rate of h^{14}.

The accuracy problems of Gaussian basis sets become even more evident if one employs medium size or small standard basis sets in an all-electron calculation. The 6-31G, 6-31++G*, 6-31+G** and 6-311++G(3df,3pd) basis sets were employed to compare the relative accuracy of the pseudopotential method with the incompleteness of and disagreement between standard Gaussian basis of various sizes. Figure 5.6 clearly shows that the accuracy obtained with these basis set is considerably lower than the accuracy with the NLCC pseudopotentials or also with the standard HGH pseudopotential within the two step procedure described above.

A summary of the deviations in the atomization energies averaged over the molecules of the G2-1 test set is given for fixed and relaxed geometries in tables 5.2 and 5.3, respectively. Indicated are the MAD, RMSD, mean signed deviation (MSD), maximum absolute deviation (maxAD) and minimum absolute deviation (minAD).

The last row of table 5.3 describes the change in the all-electron reference values when going from the fixed, experimental (CCCBDB) to relaxed geometries in the aug-cc-pV5Z basis set. This gain in energy upon geometry relaxation is significant compared to the assessed accuracy of the pseudopotential based methods, which are found to be very reliable for geometry optimizations.

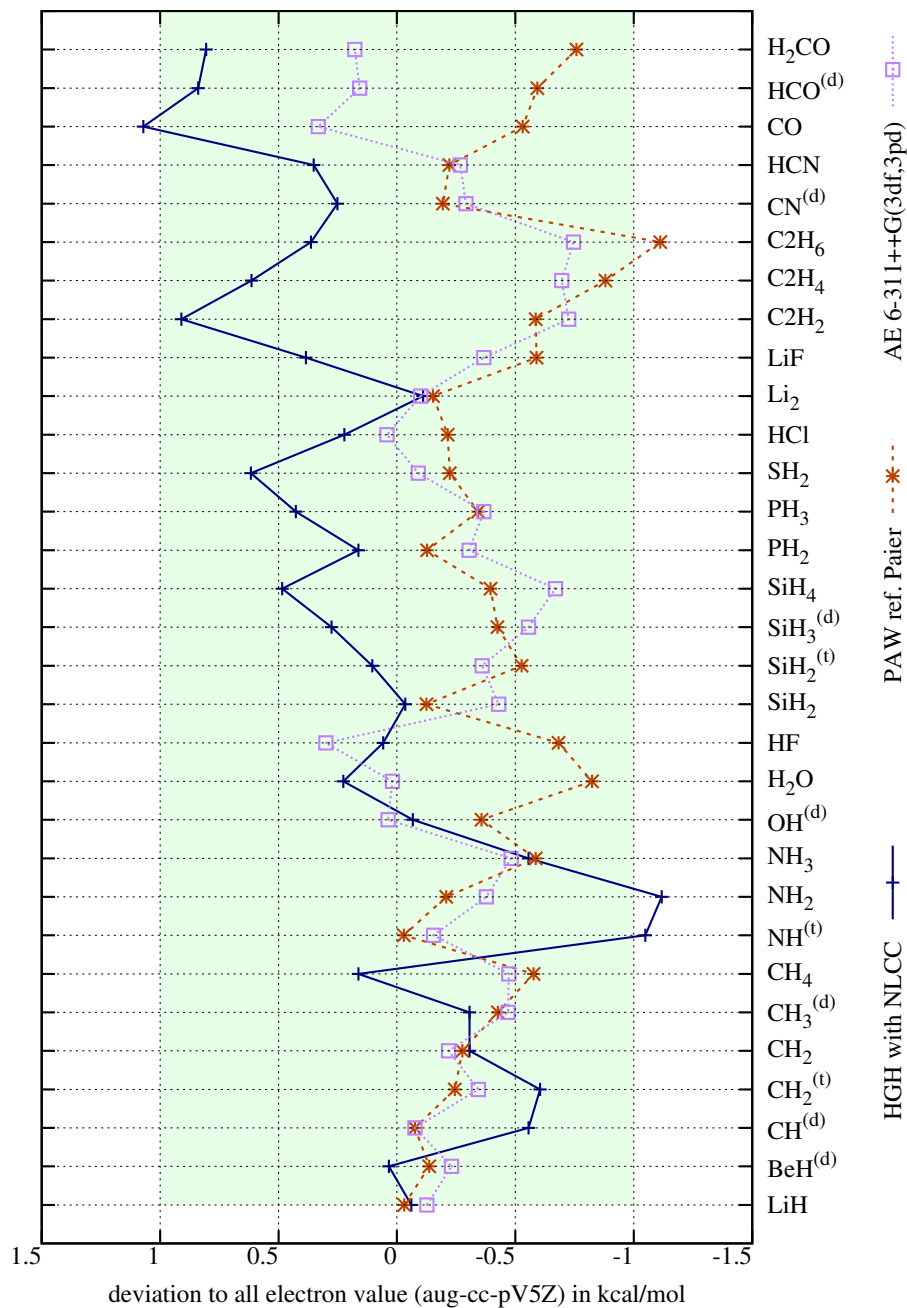Figure 5.4: Comparison of PBE atomization energies from NLCC-HGH pseudopotentials with other methods. Explanations are in the text.
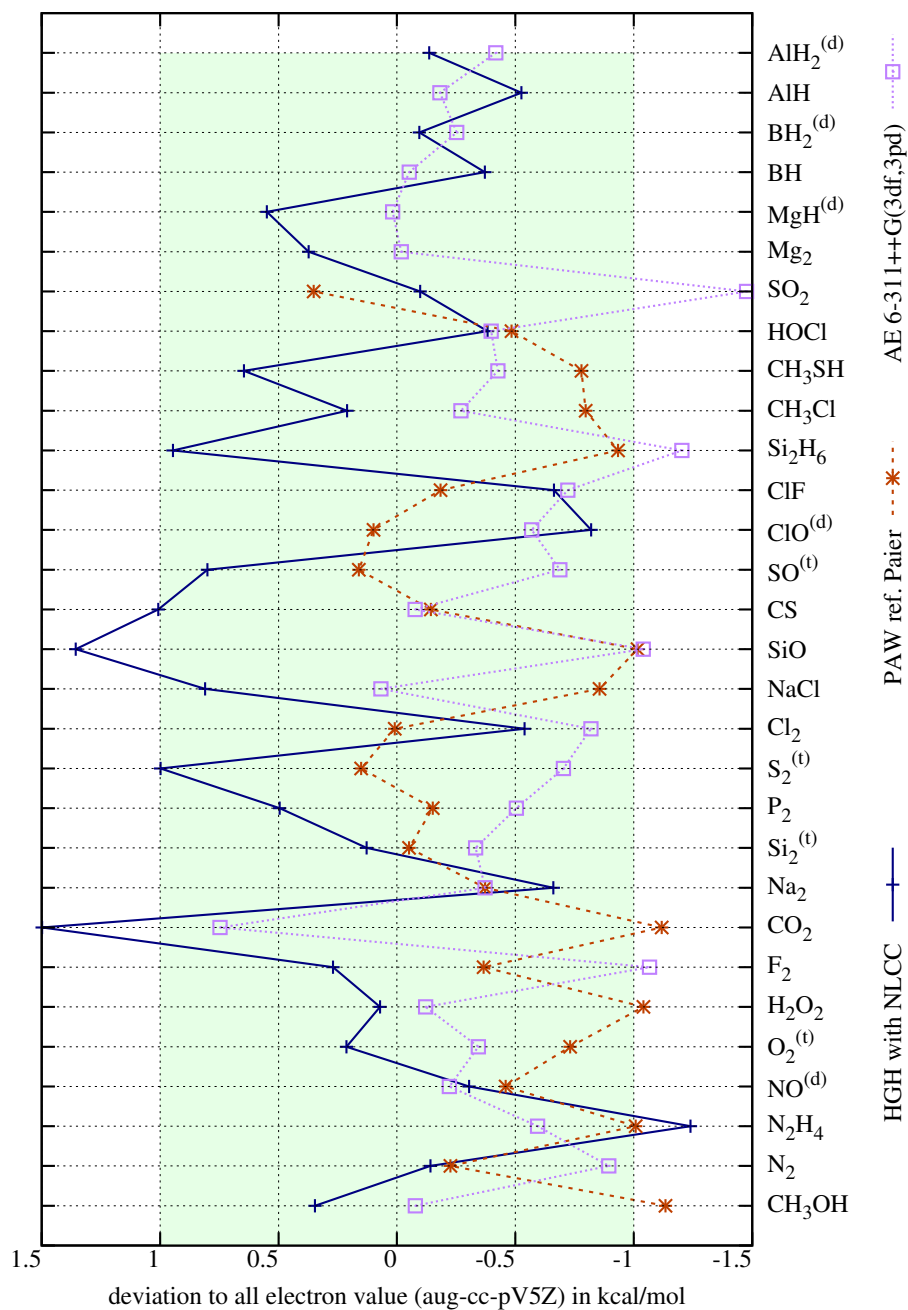
Figure 5.5: Continuation of figure 5.4. Explanations are in the text.
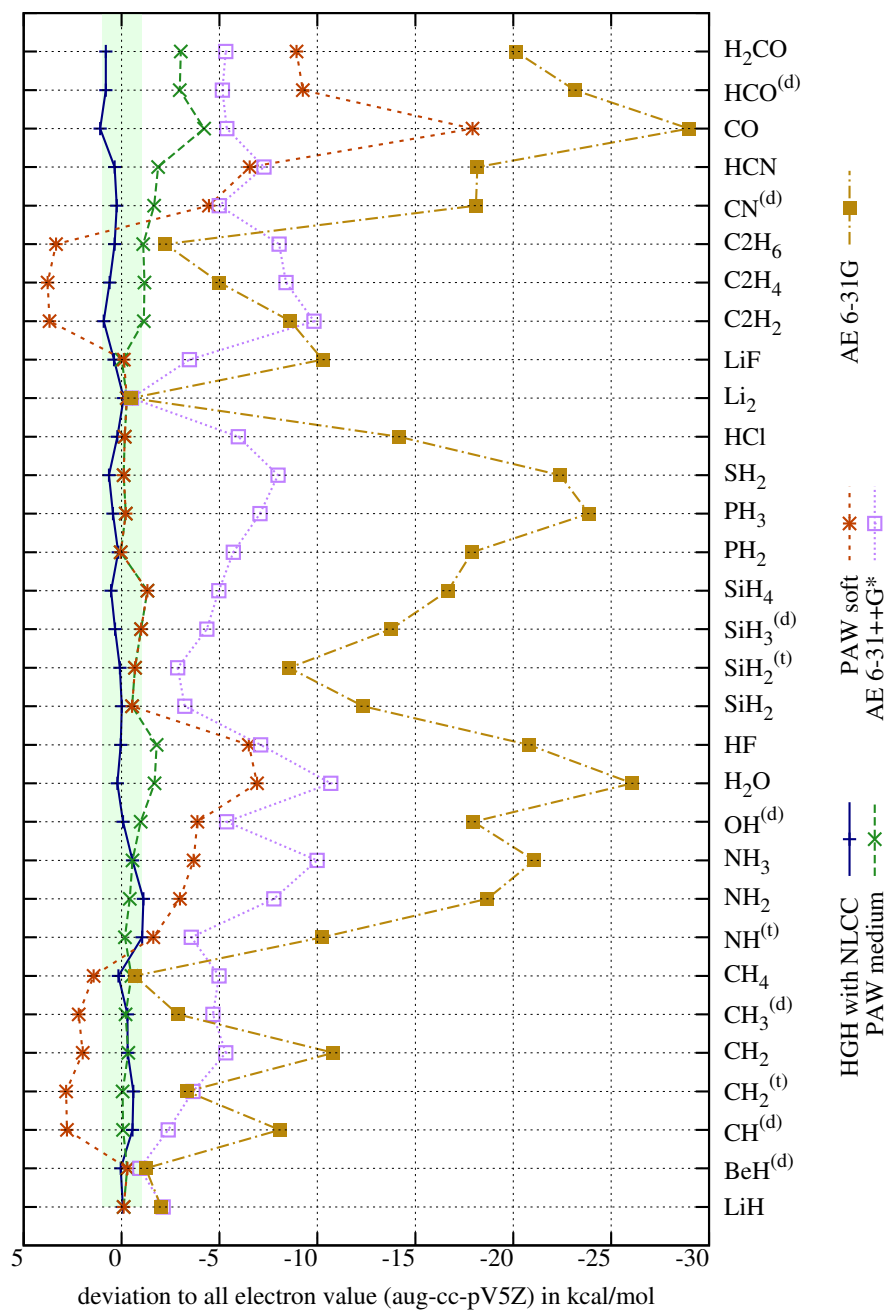
Figure 5.6: Comparison of PBE atomization energies from NLCC- HGH pseudopotentials with less accurate methods. Explanations are in the text.
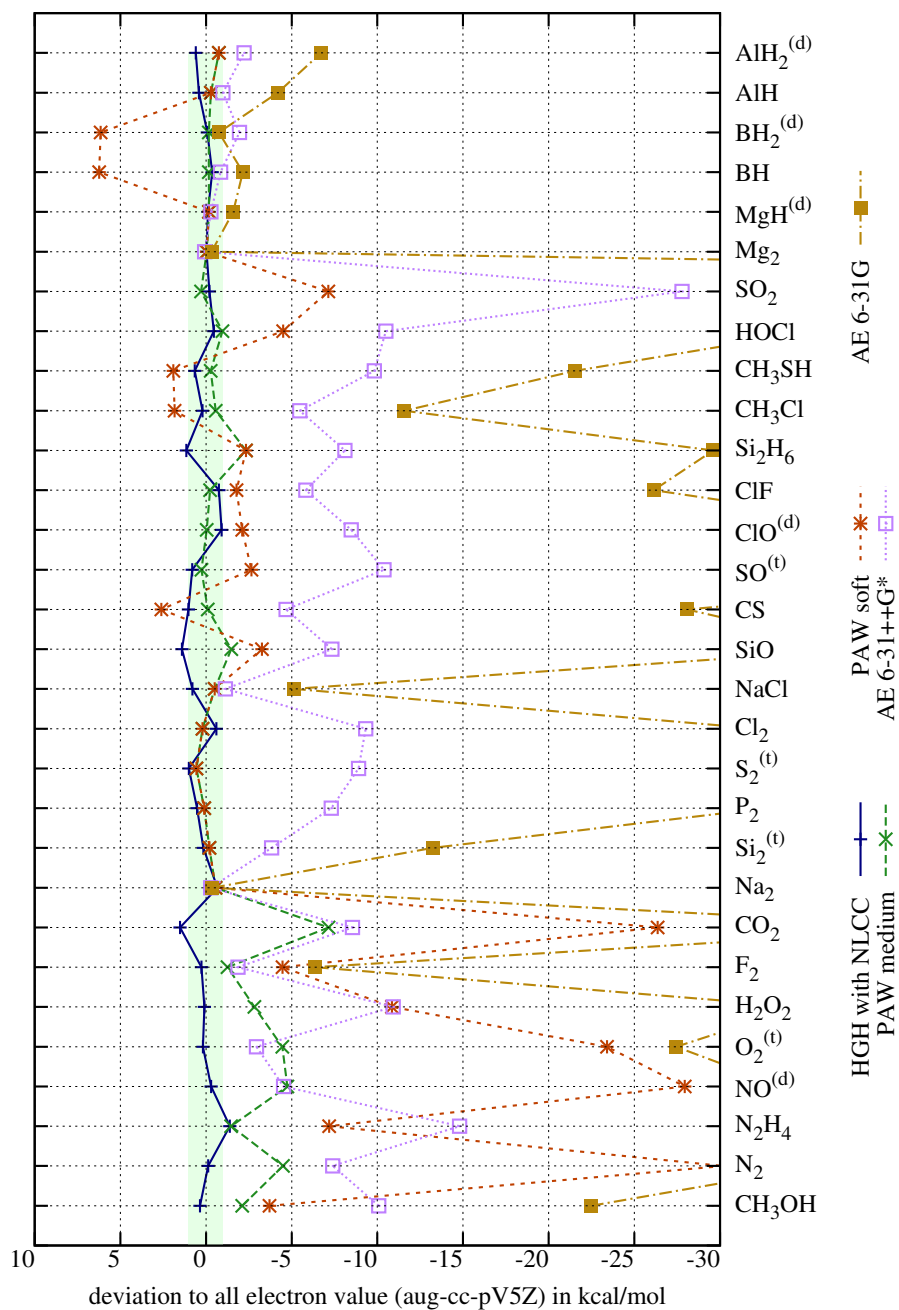
Figure 5.7: Continuation of figure 5.6. Explanations are in the text.

	MAD	RMSD	MSD	maxAD	minAD
NLCC-HGH	0.52	0.65	0.15	1.52	0.01
HGH Krack	6.82	9.13	-6.74	23.98	0.05
Two-step	1.56	2.09	0.91	5.86	0.04
PAW medium	1.20	1.89	-1.14	7.15	0.01
PAW soft	4.84	8.53	-3.77	30.23	0.05
6-311++G(3df,3pd)	0.43	0.53	-0.36	1.48	0.02
6-31++G*	6.53	7.76	-6.53	27.78	0.27
631-G	22.13	31.16	-22.13	151.88	0.37

Table 5.2: Deviation measures of the electronic atomization energies in kcal/mol for the 55 molecules of the G2-1 test set compared to the all-electron result obtained in the aug-cc-pV5Z basis set. All geometries are fixed.

	MAD	RMSD	MSD	maxAD	minAD
NLCC	0.51	0.63	0.16	1.50	0.03
HGH Krack	6.85	9.13	-6.76	23.94	0.10
Two-step	1.52	2.05	0.88	5.73	0.01
PAW Paier	0.46	0.56	-0.43	1.13	0.01
all-electron geopt	0.29	0.70	-0.29	4.21	0.00

Table 5.3: Deviation measures of the electronic atomization energies in kcal/mol for the 55 molecules of the G2-1 test set, where all molecular geometries are optimized for each method considered. For comparison, PAW data are extracted from work of Paier et. al[64]. The last row gives the change of the all-electron energy upon geometry relaxation.

5.5 Accuracy of the equilibrium geometries

In order to compare the accuracy of the equilibrium geometries of the pseudopotential and all-electron calculations, the optimized geometry of each molecule is aligned with its all-electron counterpart, such that the RMSD is minimized [65]. The resulting RMSD values are shown in figure 5.9. It is observed that conventional HGH pseudopotentials yield already very good agreement with the all-electron data. Nevertheless, the inclusion of NLCC leads to a systematic improvement of the equilibrium geometries.

It can be noted that in a previously mentioned work [64], a similar test was carried out for the bond lengths of some dimers in order to verify the accuracy of the PAW method. It is found that our pseudopotential approach yields geometry data of at least the same or even better accuracy, and that the high precision is maintained when moving to more complicated geometries.

5.6 Evaluation of pressure of extended systems

Next we benchmark pseudopotential (PSP) calculations for extended systems. A few crystalline systems made of light elements (diamond carbon, Silicon Carbide, Bulk Silicon and Boron Nitride) were selected and the pressure at a given lattice parameter was then compared between different approaches.
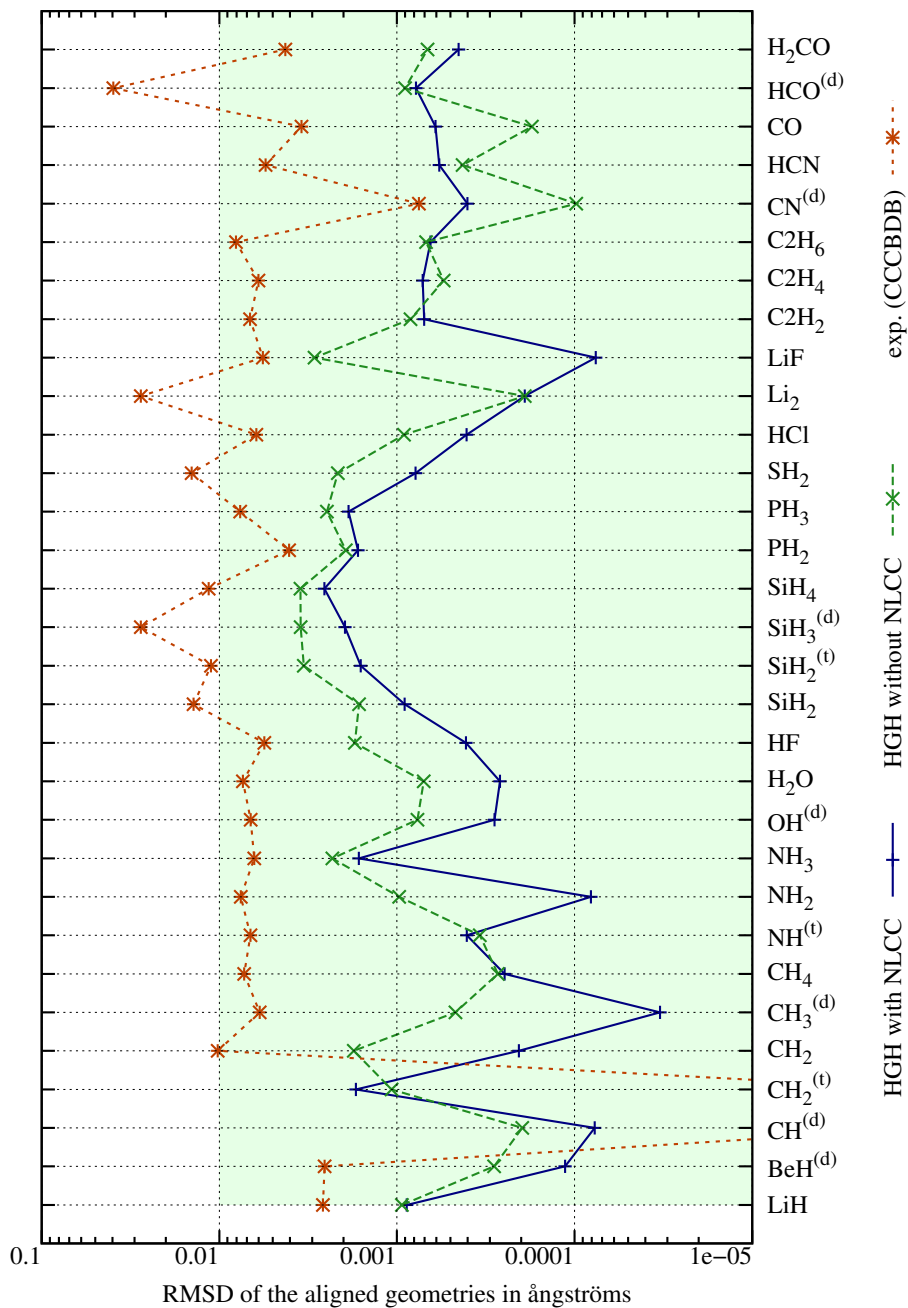
Figure 5.8: RMSD values of the experimental and relaxed geometries with respect to those relaxed with all-electron calculations in the aug-cc-PV5Z set.
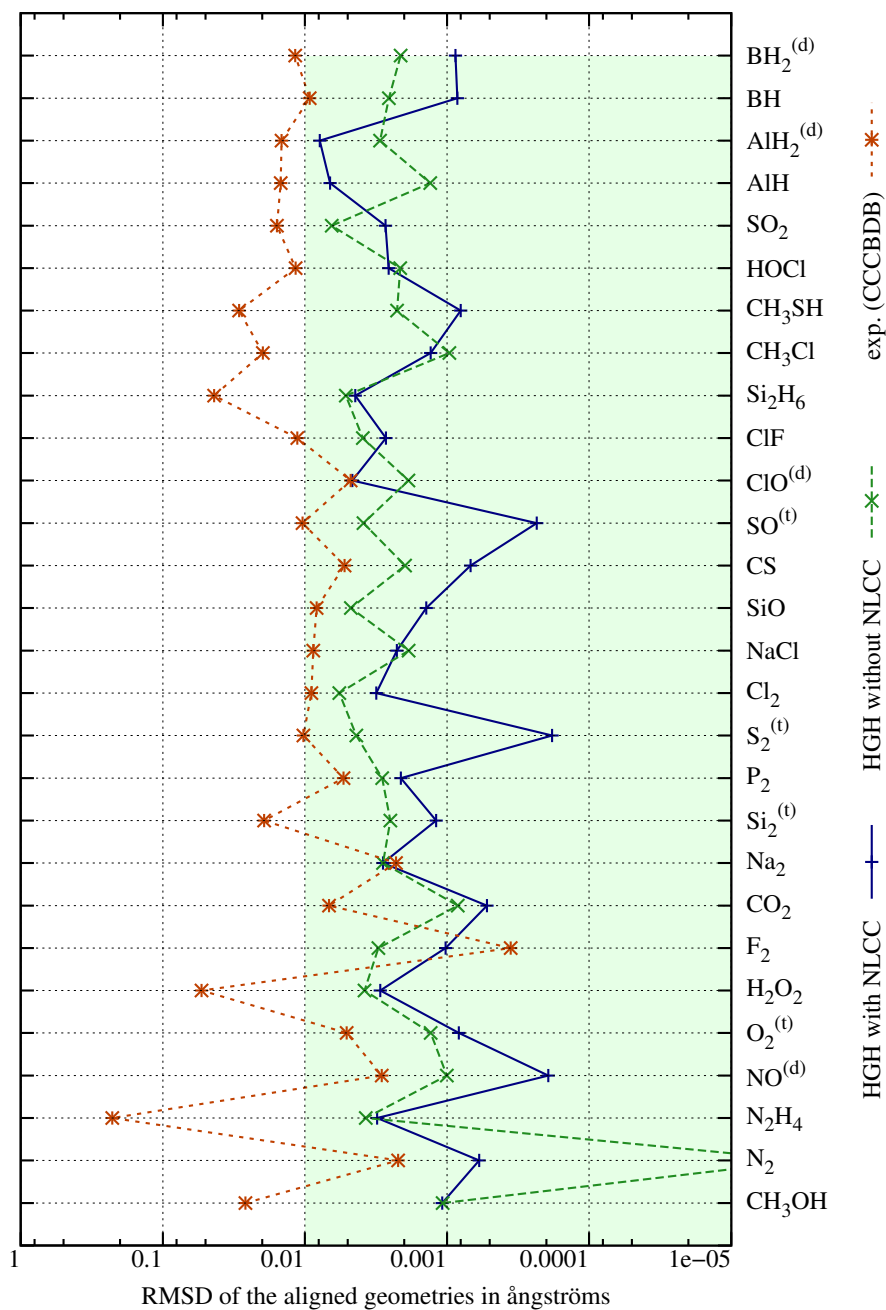
Figure 5.9: Continuation of figure 5.9.

The details on how the stress energy tensor can be calculated in GGA for NLCC terms are given in the appendix. Figures 5.10 and 5.11 show the difference between the LAPW results and the PSP results at the same lattice parameter. In addition we also show the results for the hard PAW potentials. In order to show the relative accuracy of the pressure we specify the lattice constant along the x axis of the figure in terms of the pressure. At the highest pressures the lattice constant is reduced by about 10 percent compared to the lattice constant with zero pressure. With NLCC PSP, an excellent relative accuracy of about 10^{-3} is found. In this case, it can be noticed that the inclusion of a NLCC term improves further the results even though the systems under pressure are not spin-polarized. Results of similar quality can be obtained within the hard PAW scheme described above.

5.7 Dispersion-corrected functionals

Long range van der Waals interactions are missing in all standard LDA and GGA density functionals. Adding semiempirical classical van der Waals interactions has however recently been demonstrated to give a rather accurate description of weakly bonded systems and is now frequently used. We will therefore examine the accuracy of the semiempirical models in the context of our pseudopotential calculations with a systematic wavelet basis set.

In BigDFT, we implemented two semiempirical models to correct dispersion energies and energy gradients DFT-D2[12] and DFT-D3[13]. The parameters of these models were separately fitted for each exchange correlation functional based on thermochemical data for weakly interacting systems. Since BigDFT uses a wavelet basis and pseudopotentials Figures 5.12 and 5.13 and Table 5.4 show the comparison of interaction energies of the benchmark database S22[57], with a reference calculation using Coupled Cluster CCSD(T) in the complete basis limit (CBS)[66]. The inclusion of dispersion correction D2 into BigDFT clearly improves the description of weak interactions within PBE, even though the S22 data set was not used as the fitting data set. The root-mean-square-deviation (RMSD) between the CCSD(T) reference values and the NLCC-DFT interaction energies is 0.58 kcal/mol. The absolute maximum difference corresponds to acetic acid dimer $(COOH)_2$, where the overestimation is 1.57 kcal/mol, that means an 8% of the total interaction energy. The largest relative error of 35 % is found for the methane dimer whose interaction energy is only 0.2 kcal/mol. The errors for these systems are comparable to those that are obtained when PBE-D2 and PBE-D3 are used with a large basis set (aug-cc-pVDZ and aug-cc-pVTZ). On average the PBE-D2 scheme performs better with BigDFT than with any Gaussian basis set, while the PBE-D3/BigDFT results are comparable to the results obtained with PBE-D3/aug-cc-pVTZ electron calculations.
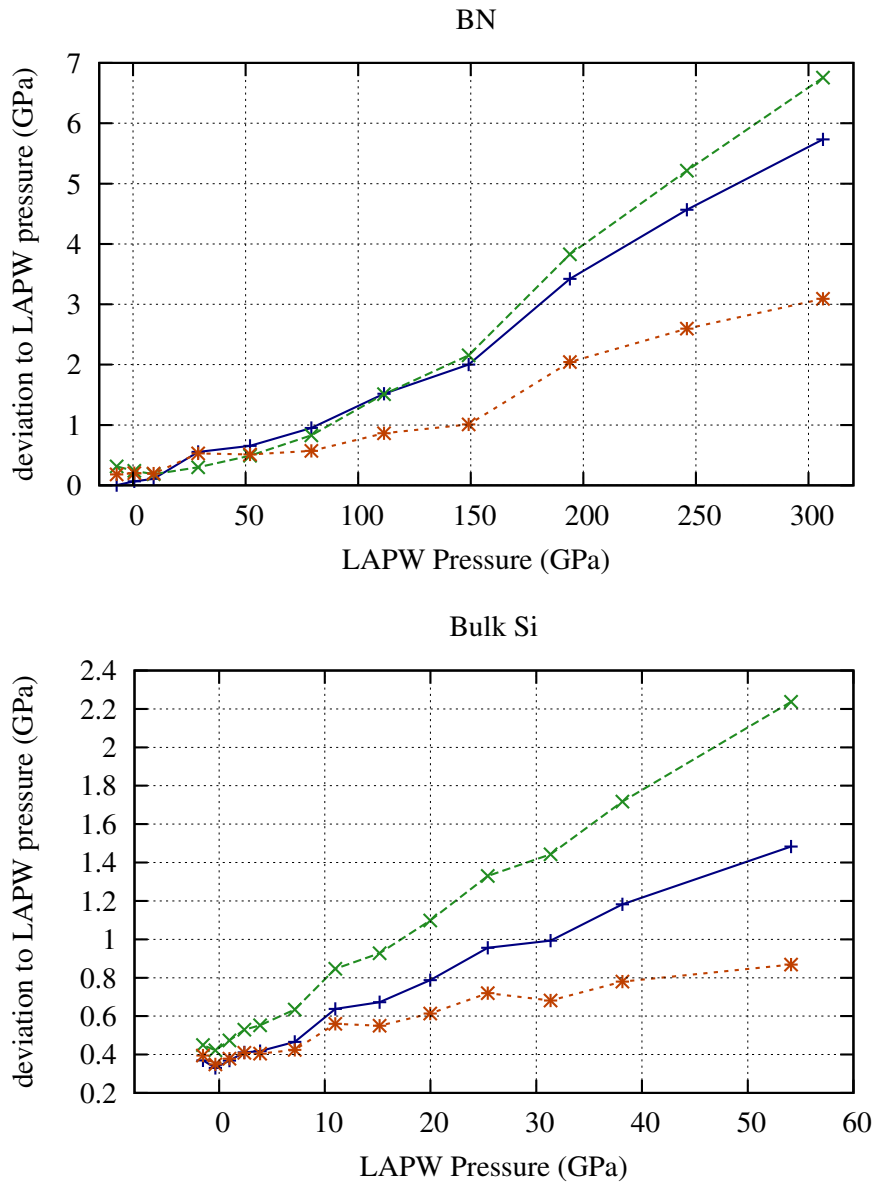
Figure 5.10: Comparison of pressures for Boron Nitride and bulk silicon.
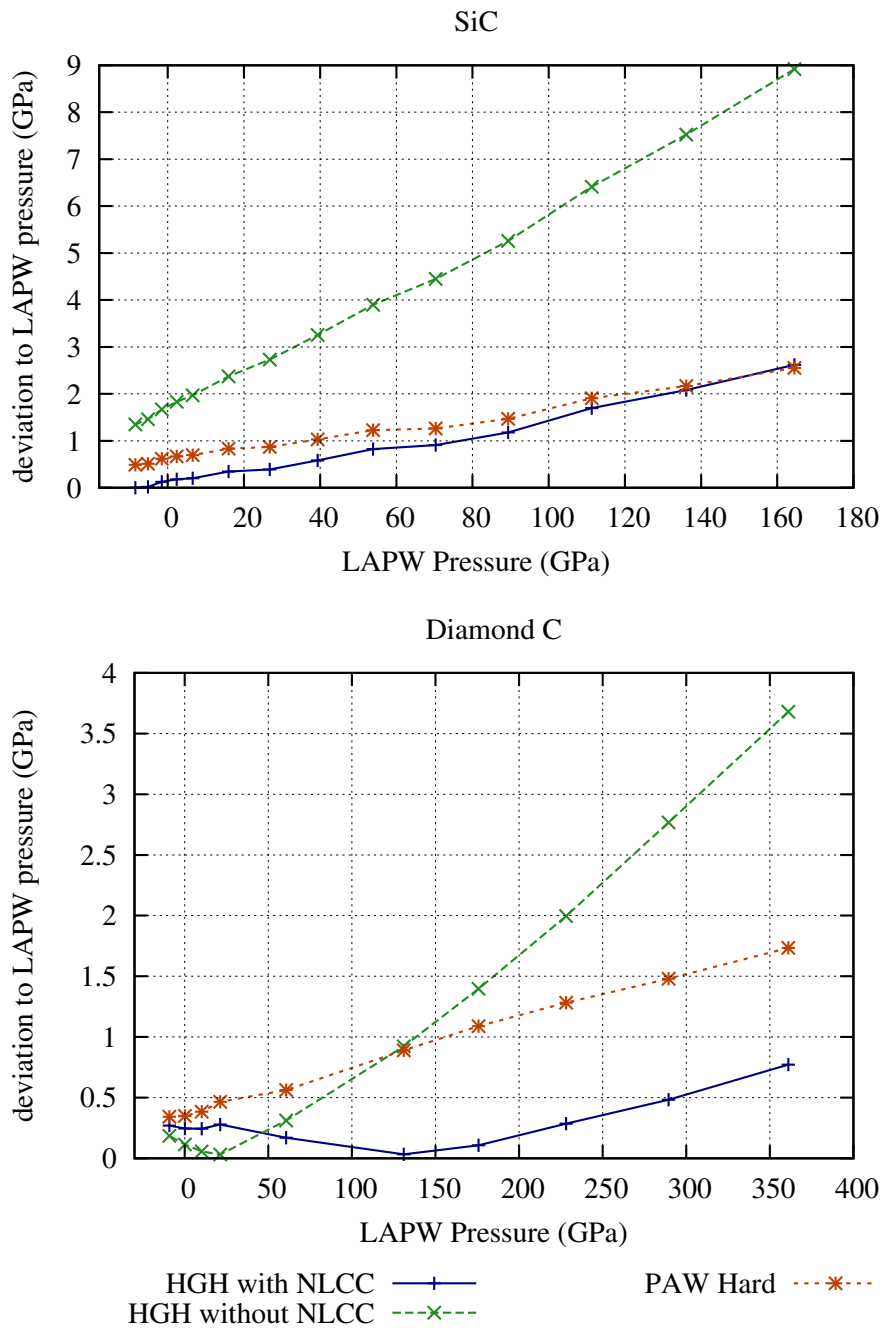
Figure 5.11: Comparison of pressures for Silicon Carbide and diamond carbon.
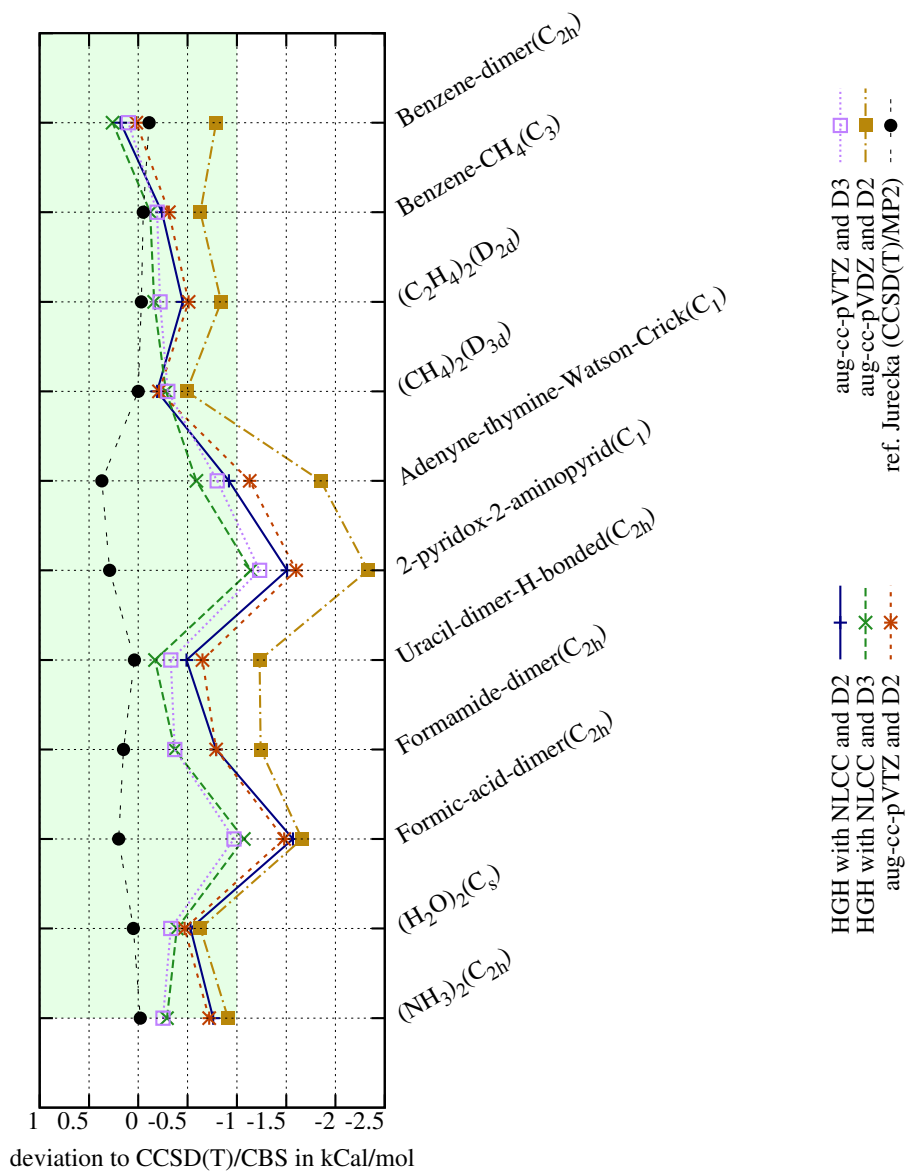
Figure 5.12: First half of the S22 test set: Comparison between PSP and all-electron calculations within PBE XC functional.
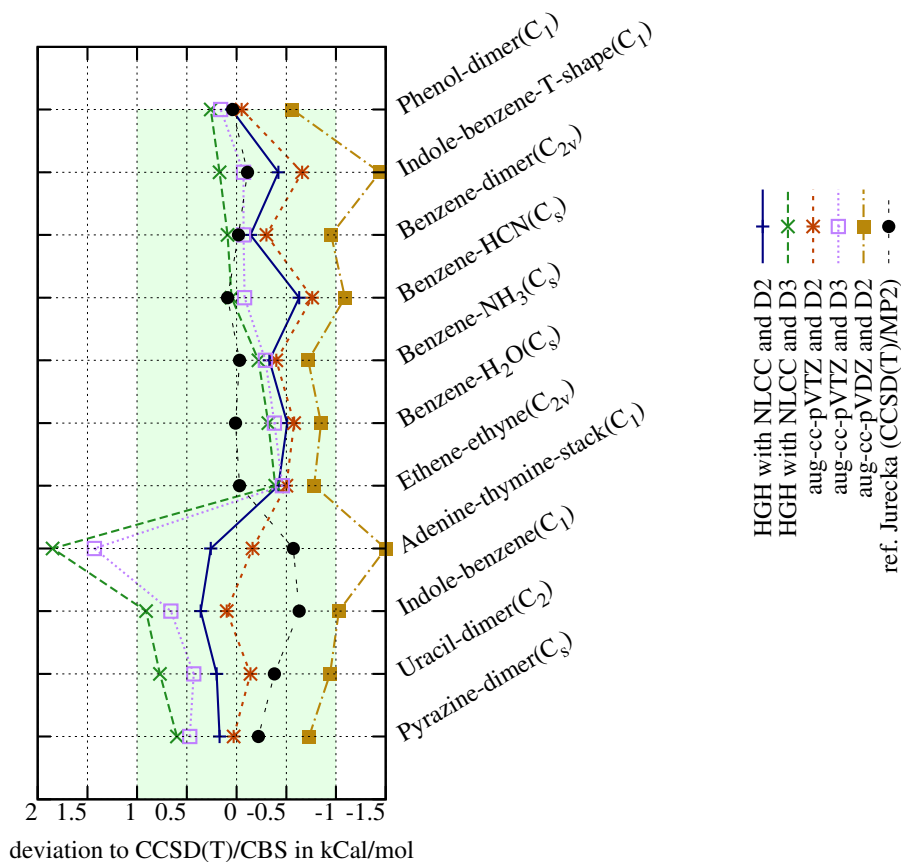
Figure 5.13: Second half of the S22 test set: Comparison between PSP and all-electron calculations within PBE XC functional.

5.8 Discussion and conclusions

We have shown that our new NLCC PSP's give very high accuracy for a wide range of applications. In particular they give atomization energies with chemical accuracy compared to all-electron calculations for the G2-1 test set. This accuracy can easily be obtained with a systematic basis set such as wavelets where one has to change only a single parameter to obtain arbitrarily high accuracy. Obtaining such a high accuracy with Gaussian basis sets requires using the largest available basis sets and is therefore frequently not feasible in practice. Contrary to a widespread belief, PAW calculations do not necessarily give all-electron accuracy. Soft PAW potentials can actually lead to appreciable errors. Well constructed hard PAW potentials on the other hand give very high accuracy and are together with our new norm-conserving pseudopotentials in practice the only feasible way to highest quality results for large systems.

	MAD	RMSD	MSD	maxAD	minAD
NLCC-no corr.	2.59	3.61	2.59	10.08	0.05
HGH Krack-no corr.	2.64	3.66	2.64	10.18	0.01
NLCC-D2	0.51	0.64	-0.39	1.57	0.05
HGH Krack-D2	0.50	0.58	-0.34	1.25	0.13
NLCC-D3	0.48	0.64	-0.03	1.14	0.05
HGH Krack-D3	0.47	0.64	0.02	1.95	0.03
aug-cc-pVDZ-D2	1.05	1.15	-1.05	2.33	0.49
aug-cc-pVTZ-D2	0.53	0.68	-0.51	1.60	0.02
aug-cc-pVTZ-D3	0.44	0.57	-0.14	1.43	0.07

Table 5.4: Deviation measures in kcal/mol for the S22 test set with respect to CCSD(T) calculations. For the PBE XC functional, PSP and all-electron calculations are compared including semiempirical dispersion corrections (D2 and D3).

5.9   Appendix

NLCC HGH pseudopotentials in Kohn-sham DFT formalism

The PSP format is based on HGH-Krack form [36]:

$$\hat{V}_{PSP} = \hat{V}_{loc} + \hat{V}_{nl}\,, \tag{5.1}$$

where the first part is a local potential

$$V_{loc}(r) = -\frac{Z_{ion}}{r}\text{erf}\left(\frac{r}{\sqrt{2}r_{loc}}\right) + \exp\left(-\frac{r^2}{2\,r_{loc}^2}\right)\left(\sum_{k=1}^{n\leq 4} c_k \left(\frac{r}{r_{loc}}\right)^{2k-2}\right) \tag{5.2}$$

and the second part the non-local term which is separated into different channels $\hat{V}_{nl} = \sum_{\ell} V_{\ell}(\boldsymbol{r}, \boldsymbol{r'})$, each one defined in terms of separable projectors

$$V_{\ell}(\boldsymbol{r}, \boldsymbol{r'}) = \sum_{i,j=1}^{n\leq 2} \sum_{m=-\ell}^{\ell} p_i^{\ell m}(\boldsymbol{r})\, h_{ij}^{\ell}\, p_j^{\ell m}(\boldsymbol{r'}) \tag{5.3}$$

$$p_i^{\ell m}(\boldsymbol{r}) = \frac{\sqrt{2}\, r^{2\ell+i} e^{\left(-\frac{1}{2}\left(\frac{r}{r_{\ell}}\right)^2\right)}}{r_{\ell}^{\ell+(4i-1)/2}\sqrt{\Gamma\left(\ell + \frac{4i-1}{2}\right)}} Y_{\ell m}(\theta, \phi)\,. \tag{5.4}$$

The core charge ρ_c of the new PSP's is given by

$$\rho_c(r) = c_{\text{core}} \frac{Z - Z_{ion}}{\left(\sqrt{2\pi}r_{\text{core}}\right)^3} e^{-\frac{r^2}{2r_{\text{core}}^2}}\,. \tag{5.5}$$

The pseudopotentials parameters according to equations (5.2) to (5.5) are given in tables 5.5 and 5.6.

H	1	1		Z	Z_{ion}	
	0.20000	-4.07312	0.68070	r_{loc}	c_1	c_2
B	5	3		Z	Z_{ion}	
	0.43250	-4.26853	0.59951	r_{loc}	c_1	c_2
	0.37147	6.30164		r_s	h_{11}^s	
	0.33352	0.43364		r_{core}	c_{core}	
C	6	4		Z	Z_{ion}	
	0.31479	-6.92377	0.96360	r_{loc}	c_1	c_2
	0.30228	9.57595		r_s	h_{11}^s	
	0.36878	-0.00996		r_p	h_{11}^p	
	0.27440	0.76008		r_{core}	c_{core}	
N	7	5		Z	Z_{ion}	
	0.24180	-10.04328	1.39719	r_{loc}	c_1	c_2
	0.25697	12.96802		r_s	h_{11}^s	
	0.15686	-0.73453		r_p	h_{11}^p	
	0.24612	0.66037		r_{core}	c_{core}	
O	8	6		Z	Z_{ion}	
	0.26100	-14.15181	1.97830	r_{loc}	c_1	c_2
	0.22308	18.37181		r_s	h_{11}^s	
	0.26844	0.10004		r_p	h_{11}^p	
	0.25234	0.44314		r_{core}	c_{core}	
F	9	7		Z	Z_{ion}	
	0.20610	-19.86716	2.79309	r_{loc}	c_1	c_2
	0.19518	23.47047		r_s	h_{11}^s	
	0.17154	0.61254		r_{core}	c_{core}	

Table 5.5: Pseudopotential parameters of HGH potentials with NLCC. The ionic charge Z_{ion}, local radius r_{loc} and coefficients C_k define the local part (5.2), while the separable part (5.3) is determined by the localization radii r_ℓ and coefficients h_{ij}^ℓ. The parameters for the core charge (5.5) are c_{core} and r_{core}.

The core density is then used in the Kohn-Sham total energy expression as follows:

$$E_{\text{KS}} = \sum_i \langle \psi_i | \{ -\frac{1}{2}\nabla^2 + V_H[\rho] + V_{xc}[\rho + \rho_c] + V_{PSP} \} | \psi_i \rangle$$

$$- E_H[\rho] + E_{xc}[\rho + \rho_c] - \int d\mathbf{r}\rho(\mathbf{r})V_{xc}[\rho + \rho_c](\mathbf{r}) , \quad (5.6)$$

where E_{xc} and $V_{xc}[n] = \frac{\delta E_{xc}[n]}{\delta n}$ are the XC energy and potential respectively, V_H is the Hartree potential and the ψ_i's are KS wavefunctions, whose summed squares give the valence density $\rho = \sum_i |\psi_i|^2$. Eq.5.6 ensures Hellmann-Feynman condition at self-consistency, $\frac{\delta E_{\text{KS}}}{\delta \rho} = 0$.

Al	13	3		Z	Z_{ion}	
	0.35000	-1.20404	-2.14849	r_{loc}	c_1	c_2
	0.46846	2.69262	0.00000	r_s	h_{11}^s	h_{21}^s
			2.15425			h_{22}^s
	0.54697	2.13804		r_p	h_{11}^p	
	0.48775	0.38780		r_{core}	c_{core}	
Si	14	4		Z	Z_{ion}	
	0.33000	-0.07846	-0.79378	r_{loc}	c_1	c_2
	0.42179	2.87392	0.02559	r_s	h_{11}^s	h_{21}^s
		0.00000	2.59458			h_{22}^s
	0.48800	2.47963		r_p	h_{11}^p	
	0.44279	0.41540		r_{core}	c_{core}	
P	15	5		Z	Z_{ion}	
	0.34000	-1.62258	-0.72412	r_{loc}	c_1	c_2
	0.38209	3.47754	-0.01267	r_s	h_{11}^s	h_{21}^s
			3.47461			h_{22}^s
	0.43411	3.37859		r_p	h_{11}^p	
	0.39868	0.45667		r_{core}	c_{core}	
S	16	6		Z	Z_{ion}	
	0.33000	1.49043	-0.73314	r_{loc}	c_1	c_2
	0.37046	6.18605	0.00000	r_s	h_{11}^s	h_{21}^s
			2.57761			h_{22}^s
	0.39772	3.89113		r_p	h_{11}^p	
	0.38622	0.57500		r_{core}	c_{core}	
Cl	17	7		Z	Z_{ion}	
	0.32000	-0.27448		r_{loc}	c_1	
	0.32659	4.20336	0.00000	r_s	h_{11}^s	h_{21}^s
			4.55652			h_{22}^s
	0.36757	4.22908		r_p	h_{11}^p	
	0.42148	0.29324		r_{core}	c_{core}	

Table 5.6: Continuation of table 5.6 for the third period elements.

Calculation of stress

The contribution to the stress tensor $T_{\alpha\beta}^{xc}$ coming from the XC term with NLCC can be shown to be given by

$$
\Omega\, T_{\alpha\beta}^{xc} = \delta_{\alpha\beta} E_{xc}[\rho + \rho_c] - \delta_{\alpha\beta} \int \mathrm{d}\mathbf{r} V_{xc}[\rho + \rho_c](\mathbf{r})\rho(\mathbf{r})
$$
$$
+ \int \mathrm{d}\mathbf{r} V_{xc}[\rho + \rho_c](\mathbf{r}) r_{(\alpha}\partial_{\beta)}\rho_c(\mathbf{r})
$$
$$
- \int \mathrm{d}\mathbf{r} \left(n(\mathbf{r})\varepsilon[n]^{(2)}(\mathbf{r})\frac{\partial_{(\alpha}n(\mathbf{r})}{|\nabla n(\mathbf{r})|} \right) \partial_{\beta)}n(\mathbf{r}) \Bigg|_{n=\rho+\rho_c} , \quad (5.7)
$$

where Ω is the supercell volume and $\varepsilon[n]^{(2)} = \partial\varepsilon[n]/\partial(|\nabla n|)$. The formula shows that the gradient of ρ_c is needed to evaluate $T_{\alpha\beta}^{xc}$, even for a LDA computation. A detailed derivation of DFT of stress (without NLCC) was shown by Dal Corso and Cresta [67].

Chapter 6

Outlook and applications

The results presented in this work clearly show that the methodology for constructing GTH-HGH pseudopotentials was systematically improved and that an outstanding level of accuracy can be reached with these highly efficient pseudopotentials. While these results are very encouraging, there remain several points that make future work in this area highly interesting. As explained in the earlier chapters, the treatment of nonlinear core corrections (NLCC) is just one aspect of the improved procedure to generate HGH pseudopotentials. It is therefore justified to give a brief outlook of further activities of pseudopotential research in this context.

Furthermore, it has to be emphasized that HGH pseudopotentials, albeit without NLCC, have been applied in numerous studies. Some of these publications make use of specifically optimized pseudopotentials generated with the methodology discussed in this work. In this last chapter, these articles are addressed briefly, following the authors list of publications. In the last section of this chapter, one of the studies based on HGH pseudopotentials is presented in detail. For that particular publication, no new pseudopotentials were specifically generated, yet it contains some earlier work of the author of this text and shares some common aspects with the other studies mentioned.

6.1   Future developments for HGH pseudopotentials

The purpose of the following section is to give a short overview of those topics that will be of interest in the scope of future work on HGH pseudopotentials. First of all, as the article presented in the previous chapter was limited to elements up to the third period, it will be interesting to try the inclusion of NLCC for the heavier elements of the periodic table. It remains to be shown if this will lead as well to systematic improvements, especially when semicore electrons are already treated en par with the valence. In that case, adding some NLCC for the nonlinear interactions between core and semicore electrons may have little effect on the pseudopotentials overall accuracy, as the inclusion of semicores typically already yields highly accurate pseudopotentials. On the other hand, when both semicore- and valence-only-pseudopotentials are available, the addition of NLCC to a valence pseudopotential may provide a very useful compromise between accuracy and softness. This approach has been tried for the example of Tungsten without notable success, but it might work just well for other chemical elements.

However, the inclusion of NLCC for heavier elements will require a careful evaluation of the combined treatment of spin-orbit corrections and spin polarization effects, which will need further modifications to the process of generating the pseudopotentials and their atomic reference data. In particular the all electron atomic code will need some adjustments to support relativistic LSDA and GGA calculations. This aspect has not been addressed so far and may play an important role for the heavier magnetic atoms. Furthermore, the aspects of optimizing the pseudopotentials softness without degrading the accuracy

and transferability will be of considerable practical interest for future work. Even though this is likely to require some major effort for some chemical elements, the possibility to succeed in this regard and to enhance the efficiency of the pseudopotentials is very encouraging. Indeed, as the *BigDFT* package has evolved into a highly optimized and efficient code for large scale calculations, the pseudopotentials can play the role of a bottleneck for certain applications, and slight improvements in terms of the pseudopotential softness can result in considerable improvements to the overall performance. A crucial aspect of this work is to get a better understanding of the pseudopotential features related to a trade-off between softness and transferability. If a better search strategy for softer and equally transferable pseudopotentials was found that involves a more systematic approach and less of trial and error, this could lead to a breakthrough for the optimization of all HGH pseudopotentials across the periodic table.

A third goal for future work on Gaussian-type pseudopotentials is to support hybrid functionals. As mentioned in the section about Jacob's ladder in the first chapter, this family of exchange correlation functionals implies a mixture of conventional XC parametrizations with a portion of the exact exchange term (1.13). The *libXC* package available for the construction of the pseudopotentials already includes a large collection of hybrid functionals in the sense of the recipes for mixing these terms. However, the exact exchange term (1.14) must first be computed from the orbitals and is not available yet in the atomic code used while fitting the pseudopotential. Once this problem is resolved, novel pseudopotentials can be benchmarked immediately with the *BigDFT* package, which provides full support of hybrid functionals. This will be of practical interest for many applications, as the reliability of hybrid functional based calculations with *BigDFT* is still limited by the lack of pseudopotentials specifically optimized for those functionals.

Finally, despite some attempts to make the construction of new pseudopotentials more intuitive and user friendly, the procedure remains rather complicated and intricate. Especially for the case where a given pseudopotential must be adopted from one XC functional to a another, yet similar one, the task should be simplified or automatized in some way. Generating new pseudopotentials still involves some quirks and tricks that make it tedious for a new user to get used to the procedure. In that sense, there is certainly room for improvements.

6.2 Applications of HGH pseudopotentials

There can be various reasons for the construction of new HGH pseudopotentials for a particular application, but in most cases, it is typically one of the following three points that leads to the optimization of new pseudopotential parameters.

- The employment of exchange correlation functionals for which no reliable HGH pseudopotentials are available yet.

- The need for soft pseudopotentials for better efficiency in large scale calculations involving many force evaluations of systems with hundreds of atoms.

- The use of highly transferable pseudopotentials optimized for high pressure phases.

While the first point does not pose a major challenge if pseudopotentials for similar XC functionals are already available as an input guess, improvements to the pseudopotentials softness can be an elaborate task, as already discussed in some detail. The last point, however, needs some further explanations. As mentioned earlier, the pseudopotentials are fitted to atomic reference data using a confining potential in order to have well defined unoccupied orbitals. In the corresponding section it was noted that multiple values for the strength of the confinement can be used in a parallel calculation to enhance the pseudopotentials transferability. While there is no direct consideration of pressure effects during the construction of the pseudopotential, the inclusion of strong confinements during the fitting tends to improve the reliability of the pseudopotential in high pressure calculations.

Pseudopotentials where specifically optimized for various studies, which are listed below in reverse chronological order.

1. *A comparison of the energy landscape roughness of biomolecules as described by force fields and quantum mechanical methods*,
   to be submitted to J. of Chem. Phys.

2. *Low-energy structures of zinc borohydride $Zn(BH_4)_2$*,
   Phys. Rev. B **86**, 224110 (2012).

3. *Crystal Structure of Cold Compressed Graphite*,
   Phys. Rev. lett. **108**, 065501 (2012).

4. *Energy Landscape of Fullerene Materials: A Comparison of Boron to Boron Nitride and Carbon*,
   Phys. Rev. lett. **106** 225502 (2011).

5. *The effect of ionization on the global minima of small and medium sized silicon and magnesium clusters*,
   J. Chem. Phys. **134** 124302 (2011).

All of these publications, as well as the article presented in the following section, contain results based on a common methodology: KS-DFT calculations with HGH pseudopotentials are carried out using the *BigDFT* software package [89] to explore the energy landscape of either some nanoscale systems or some solid state phases. In all of these studies except for the latest one (1.), the DFT calculations are coupled with a powerful search algorithm of global geometry optimization, the minima hopping method [87]. This methodology allows to study the structural stability of various systems directly in the framework of *ab initio* calculations, such that nano-structures or novel materials can be predicted from first principles.
While the minima hopping method is very efficient for exploring the energy landscape, a search that still involves hundreds of geometry optimizations on the DFT level is computationally demanding. Therefore soft and reliable pseudopotentials are very useful in this context. For the latest publication in the above list, the energy landscape of an organic molecule was characterized by systematic comparison of different levels of theory, using only local geometry optimizations on the DFT level. Even though the molecular system is not very large, soft and accurate pseudopotentials were an important ingredient here. Soft modes along torsional degrees of freedom require highly accurate evaluations of the forces to clearly identify a local minimum, which translates into extremely dense real space grids unless the pseudopotentials are rather soft.
The remaining study in this context, which is presented in the next section, investigates the structural stability of metal doped cages made of Silicon atoms. These hollow Silicon clusters that encapsulate some metal impurity are interesting nanoscale systems and potential building blocks for more complicated structures. As shown in the following article, however, $M@Si_{20}$ cages doped with various metals M are metastable, and the initial fullerene-like geometry of the Si_{20} cages is easily transferred into a lower energy structure of broken symmetry.

6.3 Structural Metastability of Endohedral Silicon Fullerenes

Endohedrally doped Si_{20} fullerenes appear as appealing building blocks for nanoscale materials. We investigate their structural stability with an unbiased and systematic global geometry optimization method within density-functional theory. For a wide range of metal doping atoms, it was sufficient to explore the Born Oppenheimer surface for only a moderate number of local minima to find structures that clearly differ from the initial endohedral cages, but are considerably more favorable in terms of energy. Previously proposed structures are thus all metastable.

Introduction

As miniaturization techniques are reaching their ultimate limits, the interest in novel silicon based nanoscale devices increases. Notwithstanding, most common materials in nano sciences to date are carbon based such as fullerenes and nanotubes. Si based clusters and nanoparticles have also been studied extensively and it was shown that their electronic structure as well as their mechanical, optical and magnetic properties can be manipulated by changing their shape, size and composition. There is widespread hope that such Si nanomaterials may be basic building blocks for more complicated structures, such as wires and layers [69, 70, 71, 72, 73]. Unfortunately, up to now no stable Si building blocks have been found that are as chemically unreactive and symmetric, and therewith attractive for cluster assembled materials, as the carbon fullerenes.

Endohedral doping with metal atoms is a primary avenue believed to stabilize cage-like Si geometries. In fact, clathrates are composed of corresponding polyhedral building blocks [74]. The exceptional elastic, thermoelectric, optoelectronic and super-conducting properties of these porous crystals [75, 76, 77, 78] already illustrate the unique potential offered if novel materials could be tailored out of such Si-based subunits. Considering that C_{20} forms the smallest known fullerene, Si_{20} clusters represent a particularly interesting size in this context that should in principle be large enough to encapsulate a metal atom [79]. In contrast to the intrinsically unstable hollow Si_{20} fullerene [80], endohedral doping with a range of metal atoms was indeed theoretically predicted to stabilize the cage structure [81, 82].

In these, as well as in numerous equivalent theoretical studies on other cluster sizes, the stability was inferred from computed embedding and binding energies of relaxed structures. By construction, corresponding geometry optimizations lead, however, only to the next *local* minimum on the Born-Oppenheimer potential energy surface (PES). While a harmonic frequency analysis may ensure that this local minimum has indeed been reached, this still does not tell anything about the *global* PES features. In particular such an approach does not tell us if there are other energetically even more favorable minima, or if the present structure indeed corresponds to the global minimum. Starting the geometry optimization from several initial configurations [83, 84] or using several stages of symmetry constraints [85, 86] may provide some information in this direction. Still, the corresponding exploration of the PES is by no means systematic, and the reliability of the deduced structural stability uncertain.

Structural metastability

In this work, we therefore reexamine the structure of metal-doped Si_{20} clusters using a global and unbiased geometry optimization technique within density-functional theory (DFT). For essentially the entire range of previously proposed metal dopants this readily identifies significantly more stable structures that no longer correspond to endohedral fullerene cages. The latter configuration thus only corresponds to a *local* PES minimum, and the partial information we obtain on the surrounding barriers even suggests that this minimum is in most cases quite shallow. With a corresponding at best feeble metastability restricted to low temperatures, doped Si_{20} fullerenes are unlikely useful building blocks for future nanoscale materials – unless additional stabilization mechanisms are identified.

The minima hopping method

The minima hopping method (MHM) [87] is designed to find the global minimum of complex polyatomic systems in an efficient way. The general idea is to limit repeated visits of the same local minima without penalizing crossings through important transition regions, such as hubs connecting superbasins of the potential landscape. The method is composed of an inner part, that attempts to escape from the current minimum by following short trajectories from molecular dynamics (MD), and an outer part that either accepts or rejects the new configuration by simple energy thresholding. A feedback mechanism on both parts allows to take advantage of the history of minima visited, as well as of the Bell-Evans-Polanyi principle, which correlates lower energy barriers with deeper basins [88].

Computational approach

In order to reach predictive quality, the PES explored by the MHM must be computed from first-principles. Here we use DFT as implemented in the BigDFT package [89] with valence-type pseudopotentials [90] for this purpose. In the spirit of the dual MHM [91] two levels of accuracy are considered to reduce the computational cost. During the MD escapes and in the initial stages of local geometry relaxations a coarser grid with smaller simulation boxes was chosen to define the employed adaptive wavelet basis. For the final geometry optimization and the evaluation of the total energy of the relaxed structure highly accurate parameter sets were used.

Results

In these calculations we rely on the widespread local-density approximation (LDA) [92] as an efficient general-purpose approach to treat electronic exchange and correlation (xc). In order to check the accuracy of the LDA xc functional we recomputed the energetic order of the identified minima with gradient-corrected (PBE [7]) and hybrid (PBE0 [93], B3LYP [94]) functionals. The latter computations were done with the accurate all-electron full-potential code FHI-aims [95] using the "tier2" basis-set composed of atomic-centered numeric orbitals. For the LDA and PBE functionals contained in both codes the obtained energetic differences agreed to within $150\,\mathrm{meV}$, thereby confirming the accuracy of the pseudopotentials employed in the initial BigDFT calculations and the near-completeness of the basis set used in the FHI-aims calculations.

A natural starting point for our investigation of the structural stability of metal-doped Si_{20} fullerenes are the perfect cages of I_h symmetry as illustrated in Fig. 6.1. As impurity atoms we consider a wide range of simple and transition metals (Ba, Ca, Cr, Cu, K, Na, Pb, Rb, Sr, Ti, V and Zr), which comprises in particular those elements contained in clathrate materials and those previously proposed to stabilize the Si_{20} cage structure [81, 82]. Surprisingly, only relatively short MHM searches over a few hundred PES minima were necessary *for all of these dopants* to reveal significantly more stable structures that deviate in either of two ways qualitatively from an endohedral fullerene configuration: As summarized in Fig. 6.1 and Table 6.1, for most impurity atoms exohedral structures were readily identified. In all other cases, the dopant was not expulsed, but encapsulated in a smaller cage with the remaining Si atoms forming an apical bud. For Ti, V, Cr and Cu dopants, this endohedral structure of the lowest-energy configuration is fully consistent with the interpretation of Ar physisorption experiments [79]. The specific size of the identified smaller cages is furthermore in line with a preferred stability of the corresponding $CuSi_{10}$, $CrSi_{15}$, and MSi_{16} ($M = $ Ti, V, Zr) clusters as deduced from their abundance in mass spectra or simple electron counting rules [79, 96, 97]. $TiSi_{16}$ and $ZrSi_{16}$ cages have also already been identified as local minima in DFT calculations [98].

The MHM searches were stopped as soon as configurations of significantly lower energy than the initial symmetric I_h cage were identified. During the runs typically also a number of more favorable configurations were visited, in which the cage was (partly heavily) distorted, but could still be considered intact,
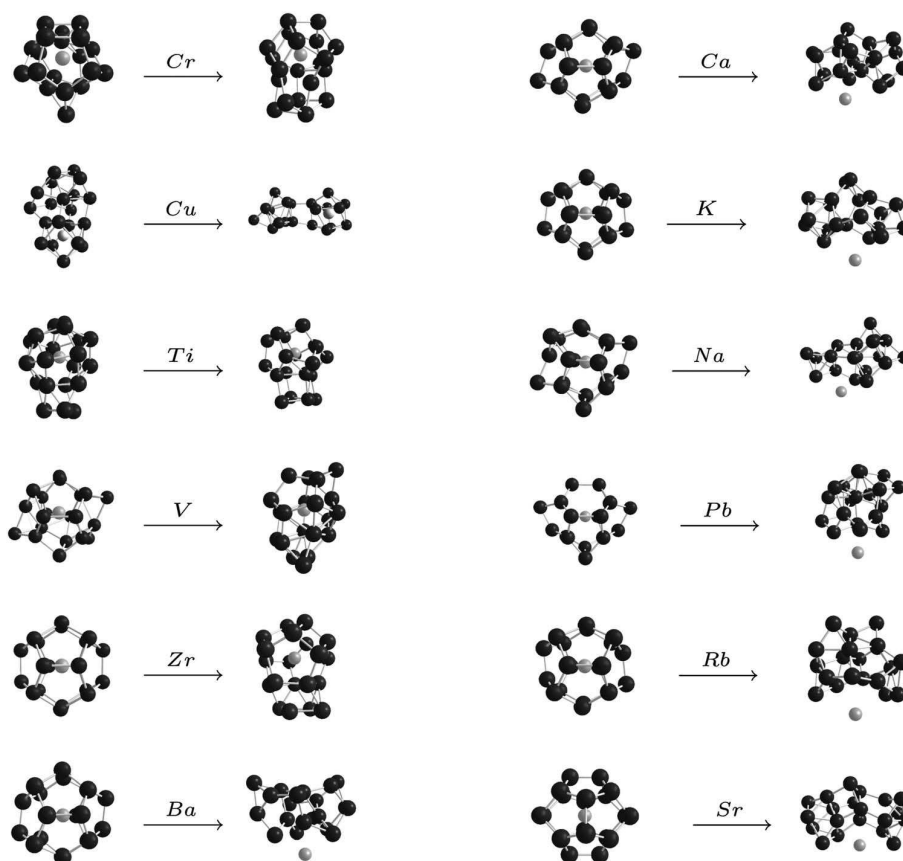
Figure 6.1: The energetically lowest-lying configurations found for all M@Si$_{20}$ systems as shown in the second and fourth columns have either lost their cage structure and dopant (bright) or undergone a transition to a smaller distorted cage with some peripheral silicon atoms. The corresponding most stable (distorted) cage-like structures are given in columns one and three. From top to bottom: M = Cr, Cu, Ti, V, Zr (transition metals) and Ba on the left, and M = Ca, K, Na, Pb, Rb and Sr on the right half.

	preferred	energy gap to cage			
	structure	LDA	PBE	PBE0	B3LYP
Cr@Si$_{20}$	Si$_{15}$	0.87	1.07	1.01	0.39
Cu@Si$_{20}$	Si$_{10}$	1.44	1.83	2.24	2.12
Ti@Si$_{20}$	Si$_{16}$	0.68	0.79	1.15	2.01
V@Si$_{20}$	Si$_{16}$	1.52	0.85	1.42	0.58
Zr@Si$_{20}$	Si$_{16}$	1.43	1.42	3.02	2.00
Ba@Si$_{20}$	broken	1.47	1.75	3.19	0.70
Ca@Si$_{20}$	broken	0.99	0.98	1.98	0.72
K@Si$_{20}$	broken	3.32	3.72	4.74	2.77
Na@Si$_{20}$	broken	1.36	1.45	1.57	0.59
Pb@Si$_{20}$	broken	2.63	2.67	2.98	2.02
Rb@Si$_{20}$	broken	2.13	2.72	3.52	2.57
Sr@Si$_{20}$	broken	1.39	1.72	2.31	1.09

Table 6.1: Results of the MHM search for the lowest-energy structure of doped Si$_{20}$ clusters, which either correspond to smaller Si$_n$ cages with peripheral bud (for all transition metals) or orexohedral configurations with broken cages (for all other dopants). Additionally shown is the energy difference (in eV) between this most stable structure encountered and the lowest-energy intact cage (see text). Summarized is the energetic data for a range of local, gradient-corrected and hybrid DFT xc functionals as obtained with FHI-aims [95]. The listed energies are always the energies that correspond to the lowest energy spin state.

cf. Fig. 6.1. For those dopant atoms ultimately leading to completely broken cages, a distinction of these structures from the lowest-energy exohedral ones is rather unambiguous. As shown in Table 6.1 the corresponding energy gap to the most stable of these identified intact cage structures is in all cases quite large. This holds for all of the employed xc functionals, even though quite some quantitative scatter can be discerned. With such a clear gap, it is unlikely that an intact cage structure would exist that is even lower in energy and that has been missed in the performed finite MHM searches. Instead, we rather expect that in analogy to pure Si clusters there exists a multitude of further disordered exohedral configurations, which are all extremely close in energy to the here identified most favorable structure [99]. With exohedral cages being also favorable in terms of entropy, we therefore conclude that the hitherto proposed endohedral Si$_{20}$ fullerenes for the corresponding dopant atoms are only metastable.

For those impurity atoms ultimately encapsulated by a smaller number of Si atoms, already a mere relaxation of the initial I_h cage resulted in rather heavy distortions as illustrated in Fig. 6.1. Subsequently sampled configurations exhibited more and more pronounced distortions, spanning a rather continuous range up to the smaller cage lowest-energy structure. In this situation the specification of an energy gap to the lowest-energy intact Si$_{20}$ cage is not well defined and we therefore quote in Table 6.1 the energy difference to the initial relaxed I_h cage. Again, this energy difference is sizable in all employed xc functionals. From this and the observed range of increasingly distorted cages we would therefore also rule out for these dopants that more stable fullerene configurations exist that were not identified in the present MHM searches.

The thus disclosed metastability of the endohedral Si$_{20}$ cages for a wide range of dopant atoms is in distinct contrast to the high-symmetry carbon fullerenes [100]. The latter correspond to the global PES minimum with a large energy gap to the next lowest-energy structures formed by point defects. Still,

if the barriers surrounding the local PES minima corresponding to the endohedral cages are sufficiently high, kinetic trapping might be sufficiently long. However, it is well known that clusters of low symmetry have a broad distribution of barrier heights [101] and that dynamic processes in such systems involve in general the crossing of several barriers. It is therfore unlikely that low symmetry cage minima are surrounded only by high barriers. Exploring a dozen saddle points of the $CaSi_{20}$ cage we found barriers that were in most cases higher than 1 eV. One barrier leading to an opening of the cage was even only 0.85 eV. According to kinetic rate theory such a barrier would correspond to a life time not longer than a few seconds at room temperature. Of course, this showcase does not allow to exclude kinetic trapping for all studied dopants in general. It neither provides a complete pathway from the cage to the exohedral structure. Even though more detailed studies of the dynamics of these clusters would be required to precisely predict their life time, our present results suggest that larger barriers than those identified here would be required to stabilize the metastable $CaSi_{20}$ cage over time spans relevant for materials applications.

In conclusion, we have used DFT based global geometry optimization to reexamine the proposed stabilization of Si_{20} fullerenes through endohedral metal doping. For a wide range of simple and transition metal dopants this readily reveals that the desirable symmetric cage structure is only metastable. Either exohedral compact configurations or endohedral smaller cages with excess Si atoms forming an apical bud are instead significantly more stable. Regardless of whether local, gradient-corrected or hybrid DFT xc functionals are employed, the resulting energy gap of these lowest-energy configurations to the metastable fullerene cage is in most cases in excess of 1 eV.

These findings put severe doubts on the dream of silicon based fullerenes as the building blocks for nano sciences. Beyond the specific Si_{20} cages examined here, our study furthermore underscores the importance of a systematic exploration of the configurational space when searching for novel nanoscale materials with predictive-quality theory.

List of publications

1. *Daubechies wavelets as a basis set for density functional pseudopotential calculations*,
   L. Genovese, A. Neelov, S. Goedecker, T. Deutsch, S. A. Ghasemi, **A. Willand**, D. Caliste, O. Zilberberg, M. Rayson, A. Bergman, and R. Schneider,
   J. Chem. Phys. **129**, 014109 (2008).

2. *Structural metastability of endohedral silicon fullerenes*,
   A. Willand, M. Gramzow, S. A. Ghasemi, L. Genovese, T. Deutsch, K. Reuter, and S. Goedecker,
   Phys. Rev. B **81**, 201405 (2010).

3. *The effect of ionization on the global minima of small and medium sized silicon and magnesium clusters*,
   S. De, S. A. Ghasemi, **A. Willand**, L. Genovese, D. Kanhere, and S. Goedecker,
   J. Chem. Phys. **134** 124302 (2011).

4. *Energy Landscape of Fullerene Materials: A Comparison of Boron to Boron Nitride and Carbon*,
   S. De, **A. Willand**, M. Amsler, M. Pochet, L. Genovese, and S. Goedecker,
   Phys. Rev. lett. **106** 225502 (2011).

5. *Crystal Structure of Cold Compressed Graphite*,
   M. Amsler, J. Flores-Livas, L. Lehtovaara, F. Balima, S. A. Ghasemi, D. Machon, S. Pailhès, **A. Willand**, D. Caliste, S. Botti, A. San Miguel, S. Goedecker, and M. A. L. Marques,
   Phys. Rev. lett. **108**, 065501 (2012).

6. *Low-energy structures of zinc borohydride $Zn(BH_4)_2$*,
   T. D. Huan; M. Amsler, V. N. Tuoc, **A. Willand**, and S. Goedecker,
   Phys. Rev. B **86**, 224110 (2012).

7. *Norm-conserving pseudopotentials with chemical accuracy compared to all-electron calculations*,
   A. Willand, A. O. Kvashnin, L. Genovese, A. Vázquez-Mayagoitia, A. K. Deb, A. Sadeghi, T. Deutsch, S. Goedecker,
   J. Chem. Phys. **138**, 104109 (2013)

8. *A comparison of the energy landscape roughness of biomolecules as described by force fields and quantum mechanical methods*,
   A. Sadeghi, S. Goedecker, M. Lill, **A. Willand**, S. A. Ghasemi, C.-K. Skylaris, and L. Genovese,
   to be submitted to J. of Chem. Phys.

Acknowledgements

I am deeply grateful to Stefan Goedecker who has offered me the unique opportunity to work on my PhD in an environment that was both very pleasant and inspiring. It is his constant encouragement, outstanding expert knowledge and invariable patience that made this work possible.

Also I would like to thank Jürg Hutter who kindly agreed to review my thesis and who was invited as an expert and examinator during my defense.

For their valuable teaching during my studies I would like to acknowledge the following lecturers: A. A'Campo, C. Bruder, H. Burkhart, M. Calame, H.-J. Güntherodt, K. Hencken, H.- J. Hug, W. Meier, E. Meyer, E. Van Nimwegen, S. Oberholzer, C. Schönenberger, M. Spiess, T. Schwede, H.-J. Wirz and D. Zumbühl.

Curriculum vitae

Personal information

Name	Alexander Willand
Date of birth	6 October 1983
Place of origin	Oberwil, Basel-Landschaft
Nationality	Switzerland

Education

From Mai 2008	to March 2013	PhD in theoretical physics, Universität Basel
From October 2006	to April 2008	Master of Science in Nanosciences, Universität Basel
From October 2003	to September 2006	Bachelor of Science, Major in Nanosciences Universität Basel
From August 1999	to Dezember 2002	Maturitätsprüfung Typus C, Gymnasium Oberwil BL

Bibliography

[1] A. Willand, A. O. Kvashnin, L. Genovese, A. Vázquez-Mayagoitia, A. K. Deb, A. Sadeghi, T. Deutsch, S. Goedecker, J. Chem. Phys. **138**, 104109 (2013)

[2] M. Born, J. R. Oppenheimer, Annalen der Physik **389**, 457 (1927)

[3] H.Hohenberg, W. Kohn, Phys. Rev. **136** B864 (1964)

[4] John P. Perdew, Karla Schmidt, AIP Conference Proceedings **577** (2001)

[5] J.C.Slater, Phys. Rev. **81** 385 (1951)

[6] V. I. Anisimov, O. Gunnarson, Phys. Rev. B **43**, 7570 (1991)

[7] J. Perdew, K. Burke, and M. Ernzerhof, Phys. Rev. Lett. **77**, 3865 (1996).

[8] W. Kohn, L.J. Sham, Phys. Rev. **140**, A1133 (1965).

[9] C. G. Broyden, Math. Comp. **19**,577 (1965)

[10] P.Pulay, Chem. Phys. Lett. **73**, 393 (1980)

[11] U. von Barth, L.Hedin, J. Phys. C **5** 1629 (1972)

[12] S. Grimme, J. Comput. Chem. **27**, 1787 (2006).

[13] S. Grimme, J. Antony, S. Ehrlich, and H. Krieg, J. Chem. Phys. **132**, 154104 (2010).

[14] S. Grimme, J. Comput. Chem. **25**, 1463 (2004)

[15] E. R. Davidson, J. Comput. Phys., **17**, 87 (1975).

[16] J.A.White, D.M.Bird, Phys. Rev. B **50**, 4954, (1994)

[17] Miguel A. L. Marques, Micael J. T. Oliveira, and Tobias Burnus, Comput. Phys. Commun. **183**, 2272 (2012).

[18] J.C. Phillips, L.Kleinman, Phys. Rev. **116**, 287 (1959)

[19] G. B. Bachelet, M. Schl uter, Phys. Rev. B **25**, 2103 (1982)

[20] L. Kleinmann and D. M. Bylander, Phys. Rev. Lett. 48, 1425 (1982)

[21] A. Zunger, Phys. Rev. B **22**, 649 (1980)

[22] S. C. Watson and E. A. Carter Phys. Rev. B **58**, R13309 (1998).

[23] S. G. Louie, S. Froyen, M. L. Cohen, Phys. Rev. B **26**, 1738 (1982).

[24] D. Vanderbildt, Phys. Rev. B **41**, 7892 (1990)

[25] P. E. Blöchl Phys. Rev. B **50**, 17953 (1994)

[26] O. K. Anderson Phys. Rev. B **12**, 3060 (1975)

[27] D. D. Koelling, G.O. Arbman J.Phys. F **5**, 2041 (1975)

[28] J. C. Slater Phys. Rev. **51**, 846 (1937)

[29] J. C. Slater Advances in Quantum chemistry **1**, 35 (1964)

[30] M. Weinert, J. Math. Phys. **22**, 2433 (1981)

[31] S. Goedecker, K. Maschke, Phys. Rev. B **42**, 8858 (1990)

[32] S. Goedecker, K. Maschke, Phys. Rev. B **45**, 1597 (1992)

[33] S. Goedecker, M. Teter, and J. Hutter, Phys. Rev. B **54**, 1703 (1996).

[34] C. Hartwigsen, S. Goedecker, and J. Hutter, Phys. Rev. B **58**, 3641 (1998).

[35] W. H. Press, S. A. Teukolsky, W. T. Vetterling and B. P Flannery, *Numerical Recipes*, Cambridge University Press, New York (1986)

[36] M. Krack, Theor. Chem. Acc. **114**, 145 (2005).

[37] J. Perdew, K. Burke, and M. Ernzerhof, Phys. Rev. Lett. **77**, 3865 (1996).

[38] D.R. Hamann, M. Schlüter, C. Chiang, Phys. Rev. Lett. **43**, 1494 (1979),

[39] G. Lippert, J.Hutter and M. Parrinello, Theor. Chem. Acc. 103, 124 (1999).

[40] David J. Singh und Lars Nordstrom, *P*lanewaves, Pseudopotentials, and the LAPW Method, Springer, New York, 2006.

[41] S. Goedecker and K. Maschke, Phys. Rev. B **45**, 1597 (1992).

[42] S. Goedecker and K. Maschke, Phys. Rev. B **42**, 8858 (1990).

[43] P. Blöchl, Phys. Rev. B **50** (1994) 17953, G. Kresse, D. Joubert, Phys. Rev. B **59** (1999) 1758, M. Torrent *et al.*, Comput. Mat. Sci. **42** (2008) 337-351.

[44] D. Vanderbilt, Phys. rev. B **41**, 7892 (1990).

[45] A. Bergner, M. Dolg, W. Kuechle, H. Stoll, H. Preuss, Mol. Phys. **80**, 1431 (1993).

[46] J.S. Binkley, J.A. Pople, W.J.Hehre, J. Am. Chem. Soc. **102**, 939 (1980) W.J. Stevens, H. Basch, M. Krauss, J. Chem. Phys. **81**, 6026 (1984)

[47] P. J. Hay and W. R. Wadt, J. Chem. Phys. **82**, 284 (1985).

[48] Richard P Martin (2004). Electronic Structure: Basic Theory and Applications. Cambridge University Press. ISBN 0-521-78285-6.

[49] B. J. Austin, V. Heine, and L. J. Sham Phys. Rev. **127**, 276 (1962).

[50] G. B. Bachelet, D. R. Hamann, and M. Schlüter, Phys. Rev B **26** (4199) (1982).

[51] S. Goedecker and K. Maschke, Phys. Rev. A **45**, 88 (1992).

[52] D. Porezag, M. R. Pederson, A. Y. Liu, Phys. Rev. B **60**, 14132 (1999)

[53] L. A. Curtiss, K. Raghavachari, P. C. Redfern, and J. A. Pople, J. Chem. Phys. **106**, 1063 (1997).

[54] J. A. Pople, M. Head-Gordon, D. J. Fox, K. Raghavachari, and L. A. Curtiss, J. Chem. Phys. **90**, 5622 (1989).

[55] L. A. Curtiss, C. Jones, G. W. Trucks, K. Raghavachari, and J. A. Pople, J. Chem. Phys. **93**, 2537 (1989).

[56] L. A. Curtiss, P. C. Redfern, K. Raghavachari, and J. A. Pople, J. Chem. Phys. **109**, 42 (1998).

[57] P. Jurecka, J. Sponer, J. Cerný, and P. Hobza, PCCP **8**, 1985 (2006).

[58] L. Genovese *et al.*, J. Chem. Phys. **129**, 014109 (2008).

[59] M. Valiev, E.J. Bylaska, N. Govind, K. Kowalski, T.P. Straatsma, H.J.J. van Dam, D. Wang, J. Nieplocha, E. Apra, T.L. Windus, W.A. de Jong, Comput. Phys. Commun. **181**, 1477 (2010).

[60] See `http://physics.nist.gov/PhysRefData/DFTdata/Tables/ptable.html` `http://physics.nist.gov/PhysRefData/DFTdata/ref.html` for atomic DFT energies.

[61] G. Kresse and D. Joubert, Phys. Rev. B **59**, 1758 (1999).

[62] P. Blaha, K. Schwarz, G. K. H. Madsen, D. Kvasnicka, and J. Luitz, WIEN2k, *An Augmented Plane WaveLocal Orbitals Program for Calculating Crystal Properties* (Karlheinz Schwarz, TU Vienna, Austria, 2001).

[63] NIST Computational Chemistry Comparison and Benchmark Database, NIST Standard Reference Database Number 101, Release 15b, August 2011, Editor: Russell D. Johnson III. `http://cccbdb.nist.gov/`

[64] J. Paier, R. Hirschl, M. Marsman and G. Kresse, J. Chem. Phys. **122**, 234102 (2005).

[65] W. Kabsch, Acta Crystallographica **32**, 922 (1976).

[66] T. Takatani, E.G. Hohenstein, M. Malagoli, M.S. Marshall, and C.D. Sherrill, J. Chem. Phys. **132**, 144104 (2010).

[67] A. Dal Corso and R. Resta, Phys. Rev. B **50**, 4327-4331 (1994)

[68] A. Willand, M. Gramzow, S. A. Ghasemi, L. Genovese, T. Deutsch, K. Reuter, and S. Goedecker Phys. Rev. B **81**, 201405 (2010)

[69] D. Appel, Nature **419**, 553 (2002).

[70] C.M. Lieber, Nano Lett. **2**, 81 (2002).

[71] G. Zheng, W. Lu, S. Jin, and C.M. Lieber, Adv. Mater. **16**, 1890 (2004).

[72] Y. Cui, Q. Wei, H. Park, and C.M. Lieber, Science **293**, 1289 (2001).

[73] X.T. Zhou *et al.*, Chem. Phys. Lett. **369**, 220 (2003).

[74] T. Rachi, K. Tanigaki, R. Kumashiro, J. Winter, and H. Kuzmany, Chem. Phys. Lett. **409**, 48 (2005).

[75] A. San-Miguel *et al.*, Phys. Rev. Lett. **83**, 5290 (1999).

[76] J.S. Tse *et al.*, Phys. Rev. Lett. **85**, 114 (2000).

[77] J. Gryko *et al.*, Phys. Rev. B **62**, R7707 (2000).

[78] H. Kawaji, H. Horie, S. Yamanaka, and M. Ishikawa, Phys. Rev. Lett. **74**, 1427 (1995).

[79] E. Janssens *et al.*, Phys. Rev. Lett. **99**, 063401 (2007).

[80] K.M. Ho *et al.*, Nature **392**, 582 (1998).

[81] Q. Sun *et al.*, Phys. Rev. B **65**, 235417 (2002).

[82] V. Kumar and Y. Kawazoe, Phys. Rev. B **75**, 155425 (2007).

[83] D. Hossain, F. Hagelberg, C.U. Pittmann, Jr., and S. Saebo , J. Phys. Chem. C **111**, 13864 (2007).

[84] C. Sporea and F. Rabiloud, J. Chem. Phys. **127**, 164306 (2007).

[85] J. Wang, Q.-M. Ma, Z. Xie, Y. Liu, and Y.-C. Lie, Phys. Rev. B **76**, 035406 (2007).

[86] A.D. Zdetsis, Phys. Rev. B **75**, 085409 (2007).

[87] S. Goedecker, J. Chem. Phys. **120**, 9911 (2004).

[88] S. Roy, S. Goedecker, and V. Hellmann, Phys. Rev. E **77**, 056707 (2008).

[89] L. Genovese *et al.*, J. Chem. Phys. **129**, 014109 (2008).

[90] C. Hartwigsen, S. Goedecker, and J. Hutter, Phys. Rev. B **58**, 3641 (1998).

[91] S. Goedecker, W. Hellmann, and T. Lenosky, Phys. Rev. Lett. **95**, 055501 (2005).

[92] S. Goedecker, M. Teter, and J. Hutter, Phys. Rev. B **54**, 1703 (1996).

[93] M. Ernzerhof and G.E. Scuseria, J. Chem. Phys. **110**, 5029 (1999).

[94] P.J. Stephens, F.J. Devlin, C.F. Chabalowski, and M.J. Frisch, J. Phys. Chem. **98**, 11623 (1994).

[95] V. Blum *et al.*, Comp. Phys. Commun. **180**, 2175 (2009).

[96] C. Xiao, F. Hagelberg, I. Ovcharenko, and W.A. Lester Jr., J. Mol. Struct. Theochem **549**, 181 (2001).

[97] K. Koyasu, M. Akutsu, M. Mitsui, and A. Nakajima, J. Am. Chem. Soc. **127**, 4998 (2005).

[98] V. Kumar and Y. Kawazoe, Phys. Rev. Lett. **87**, 045503-1 (2001)

[99] W. Hellmann *et al.*, Phys. Rev. B **75**, 085411 (2007).

[100] *Science of Fullerenes and Carbon Nanotubes: Their Properties and Applications*, M.S. Dresselhaus, G. Dresselhaus, and P. C. Eklund, Academic Press (1996).

[101] A. Heuer, Journal of Physics: Condensed Matter 20, 373101 (2008) ; G. Daldoss, O. Pilla, G. Viliani, C. Brangian and G. Ruocco, Phys. Rev. B **60** 3200 (1999)